ANCR-1129

UC-2

NUCLEAR TECHNOLOGY DIVISION ANNUAL PROGRESS REPORT FOR PERIOD ENDING JUNE 30, 1973

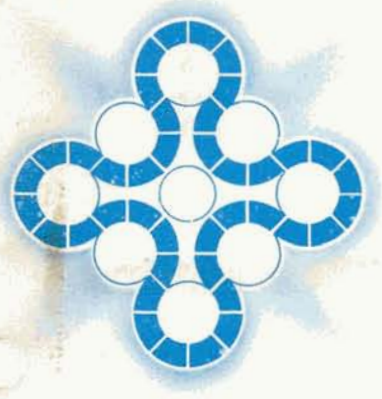

Aerojet Nuclear Company

NATIONAL REACTOR TESTING STATION

Idaho Falls, Idaho — 83401

DATE PUBLISHED—DECEMBER 1973

PREPARED FOR THE

U. S. ATOMIC ENERGY COMMISSION

IDAHO OPERATIONS OFFICE UNDER CONTRACT AT(10-1)-1375

DISCLAIMER

Printed in the United States of America
Available from
National Technical Information Service
U. S. Department of Commerce
5285 Port Royal Road
Springfield, Virginia 22151
Price: Printed Copy $10.60; Microfiche $1.45

ANCR-1129

General, Miscellaneous, and Progress Reports
TID-4500

NUCLEAR TECHNOLOGY DIVISION ANNUAL PROGRESS REPORT FOR PERIOD ENDING JUNE 30, 1973

R. M. Brugger
Manager
Nuclear Technology Division

R. L. Heath
Nuclear Physics Branch

J. F. Kunze
Reactor Technology Branch

E. E. Burdick
Reactor Instruments and Control Systems Branch

G. L. Smith
Instrumentation and Controls Equipment Branch

AEROJET NUCLEAR COMPANY

Date Published - December 1973

PREPARED FOR THE U.S. ATOMIC ENERGY COMMISSION
IDAHO OPERATIONS OFFICE
UNDER CONTRACT NO. AT(10-1)-1375

FOREWORD

This document is a report of progress on technical programs of the Nuclear Technology Division of Aerojet Nuclear Company for FY 73 ending June 30, 1973. It contains abstracts or expansions of abstracts of papers which have been published within the year. In these cases, preprints or reprints of the articles are available. Results of work in progress are also reported; since this work is of a preliminary nature, the authors should be contacted before including any reference to these works in other publications.

Progress reported on projects by the Instrumentation and Control Equipment Branch covers the period January 1, 1972 through June 30, 1973.

THIS PAGE

WAS INTENTIONALLY

LEFT BLANK

CONTENTS

FIGURES

TABLES

A. NUCLEAR PROPERTIES

INTEGRAL CAPTURE CROSS SECTION MEASUREMENTS OF FISSION PRODUCT ISOTOPES (CFRMF)

Y. D. Harker, R. G. Nisle, E. H. Turk, J. R. Berreth[1]

The significant effect of fission products on the economy and design of the Liquid Metal Fast Breeder Reactor (LMFBR) has long been recognized; however there have been and still are serious gaps in neutron data for these nuclides in energy range applicable to the LMFBR. This lack of fundamental physics data in such a critical area creates significant contributions to the uncertainties on the predicted performance parameters such as breeding ratio, doubling time, etc. To fill this need, the Fast Breeder Reactor Physics Constants Program has undertaken and is measuring the capture cross sections of important fission product isotopes in the neutron environment of the Coupled Fast Reactivity Measurement Facility (CFRMF). The neutron spectrum of the CFRMF has been tailored to be representative of that found in an LMFBR and consequently the integral cross section values determined in the CFRMF are useful in applications relating to such a facility.

Because of the identity of the CFRMF with the LMFBR it has been extremely valuable as a fast neutron standard for comparing measured and calculated integral reaction rates. Efforts of the Cross Sections Evaluations Working Group (CSEWG) in the area of evaluations of capture cross sections of fission product isotopes in the energy range from $\sim$ 50 eV to 10 MeV are centered around the use of optical model calculations to generate differential cross section information. As a part of this effort, the CFRMF has been established as a CSEWG benchmark for testing these evaluations against measured integral data. During this past year, the measured cross sections listed in Table I and the CFRMF spectrum[2] have been presented to CSEWG for use in the testing phase of these evaluations.

The reaction cross section values in Table I are the result of not only the measurements of this year but also those of previous years[3-5]. The values reported in Table I may not, however, be the same as those reported earlier; this is because two general aspects have been changed or updated in our measurement program. First, there has been a change in the way the absolute cross section is determined from the reaction rate. In the past, our measurements have been referenced to the gold capture cross section as a standard. At present, this practice is no longer used and the absolute cross section is determined by dividing the reaction rate per atom by the absolute integral flux. This flux has been determined as a by-product of the efforts of the Interlaboratory LMFBR Reaction Rate (ILRR) program.[6] The gold activation determinations which accompany each cross section measurement are now used primarily as flux monitors for the purposes of power normalization to the ILRR irradiations during which the absolute flux level was established.

The second reason for differences results from the updating of the gamma-ray spectrum data used in converting the measured gamma activity to the desired activation cross section. There have been several

advances made recently in obtaining absolute gamma-ray intensities and these have been incorporated in not only the current cross section measurements but also in the past measurements.

Very preliminary comparisons of the results listed in Table I and those calculated from optical model generated data[7] show a general agreement of the order of 20%. Although the more meaningful interpretations are contained in the comparisons for individual nuclides, this generalized agreement represents a rough estimate of the present status of the accuracy of fission product cross section data.

---

[1] Present address: Allied Chemical Corporation, 550 Second Street, Idaho Falls, Idaho 83401.

[2] D. A. Millsap, "Spectrum Calculations for the CFRMF", this report.

[3] J. J. Scoville, R. G. Nisle, B. W. Howes and Y. D. Harker, "Measurements of Fast-Neutron Capture Integrals in the CFRMF", ANS Transactions 13 (1970) 755.

[4] Y. D. Harker, "Fast-Neutron Capture Integral Measurements of ^{99}Tc, ^{109}Ag and Other Fission Products", Proc. of the Third Conf. on Neutron Cross Sections and Technology, U.S. Atomic Energy Commission CONF-710301, Vol. 1 (1971) p. 113.

[5] Y. D. Harker and E. H. Turk, "The Use of CFRMF Integral Data in Cross Section Evaluations", National Topical Meeting on New Developments in Reactor Physics and Shielding, U.S. Atomic Energy Commission CONF-720901 (1972) p. 613.

[6] J. W. Rogers, "Dosimetry Reaction Rate Measurements in CFRMF", this report.

[7] R. E. Schenter, private communication.

TABLE I

MEASURED INTEGRAL DATA FOR PHASE II TESTING OF CAPTURE CROSS SECTIONS OF FISSION-PRODUCT ISOTOPES

Reaction	Chemical* Form	Thickness** (mg/cm^2)	$\bar{\sigma}_m$ † (barns/target atom)
$^{87}Rb(n,\gamma)^{80}Rb$	RbCl	79.7	0.0132 ± .0018
$^{99}Tc(n,\gamma)^{100}Tc$	Tc powder	126.3	0.294 ± .039
$^{102}Ru(n,\gamma)^{103}Ru$	Ru powder	111.4	0.097 ± .011
$^{104}Ru(n,\gamma)^{105}Ru$	Ru powder	96.00	0.0932 ± .0093
$^{115}In(n,\gamma)^{116m}In$	In foil	81.11	0.288 ± .027
$^{121}Sb(n,\gamma)^{122}Sb$	Sb powder	168.2	0.309 ± .028

TABLE I (Cont.)

Reaction	Chemical* Form	Thickness** (mg/cm^2)	$\bar{\sigma}_m$ † (barns/target atom)
$^{123}Sb(n,\gamma)^{124}Sb$	Sb powder	168.2	0.171 ± .024
$^{127}I(n,\gamma)^{128}I$	HIO	249.2	0.216 ± .080
$^{132}Xe(n,\gamma)^{133m}Xe$	^{132}Xe	0.2868	0.00248± .00043
$^{132}Xe(n,\gamma)^{133}Xe$	^{132}Xe	0.2868	0.0401 ± .0040
$^{134}Xe(n,\gamma)^{135}Xe$	^{134}Xe	0.1060	0.0152 ± .0016
$^{133}Cs(n,\gamma)^{134m}Cs$	Cs_2SO_4	88.62	0.0362 ± .0069
$^{133}Cs(n,\gamma)^{134}Cs$	$CsNO_3$	22.94	0.300 ± .026
$^{141}Pr(n,\gamma)^{142}Pr$	Pr powder	101.6	0.080 ± .10
$^{147}Pm(n,\gamma)^{148m}Pm$	$^{147}Pm(NO_3)_3$	13.38	0.379 ± .059
$^{147}Pm(n,\gamma)^{148}Pm$	$^{147}Pm(NO_3)_3$	13.38	0.462 ± .059
$^{148}Nd(n,\gamma)^{149}Nd$	Nd_2O_3	77.44	0.118 ± .015
$^{150}Nd(n,\gamma)^{151}Nd$	Nd_2O_3	77.44	0.107 ± .024
$^{152}Sm(n,\gamma)^{153}Sm$	Sm_2O_3	111.3	0.302 ± .030
$^{154}Sm(n,\gamma)^{155}Sm$	Sm_2O_3	111.3	0.121 ± .012

* Natural abundance elements are used except where the specific isotopes are indicated.

** Mass includes all constituent elements indicated in chemical form. The real thickness for powdered and compound samples is .76 mm and for foils the real thickness can be determined using normal densities.

† $\bar{\sigma}_m$ is determined by dividing the measured reaction rate $\phi_o\sigma_m$ by $\phi_o = 1.205 \times 10^{11}$ $n/cm^2/sec$ (± 8%). ϕ_o is the integral flux as measured using SAND II and the reaction rates measured in the ILRR program. The error assignments are for 67% confidence level and are absolute, i.e., systematic errors have been included.

ACTIVATION CROSS SECTION MEASUREMENTS OF ^{151}Eu AND ^{153}Eu

J. R. Berreth[1], Y. D. Harker, E. H. Turk

The activation cross sections of enriched samples of ^{151}Eu and ^{153}Eu were determined as a part of the Fast Breeder Reactor Physics Constants Program. This program is primarily concerned with measuring integral cross sections of fission products in an LMFBR type neutron spectrum. In this case, the measurements were primarily performed in the interest of determining the possible value of natural europium as a burnable poison for LMFBR type reactor control. The facility used in these measurements was the Coupled Fast Reactor Measurement Facility (CFRMF) which has an LMFBR type neutron spectrum.[2-4]

The enriched samples were obtained from Oak Ridge Isotope Sales. The ^{151}Eu composition was 96.83% ^{151}Eu and 3.17% ^{153}Eu. The ^{153}Eu sample contained 1.24% ^{151}Eu and 98.76% ^{153}Eu. Since it is very important that the Eu be free of other rare earth impurities, a very careful ion exchange column separation was performed prior to neutron irradiation. For details on this separation, see "Techniques and Instrumentation" of this report. Weights of purified materials which were encapsulated for irradiation in small quartz vials were 15.33 mg of $^{151}Eu_2O_3$ and 14.87 mg of $^{153}Eu_2O_3$.

A single irradiation for both samples was performed in the CFRMF at a power level of 10 kW. Gold neutron flux monitor foils were placed with the europium samples on a thin lead foil holder. The activation products of interest for this irradiation were the 9.3-hr $^{152m_1}Eu$, 12.4-y ^{152}Eu and 8.6 y ^{154}Eu. Because the cross sections for materials in the CFRMF flux spectrum are small, the irradiations were done by operating 16 hours per day for a 30-day period with a continuous 48-hour run at the end of the irradiation to optimize the 9.3-hr $^{152m_1}Eu$ activity.

The resultant activities were measured on a 39 mm by 38 mm coaxial Ge(Li) detector coupled to a Nova computer, for data acquisition and storage. Data analysis was done utilizing a Gauss gamma spectrum analysis program.[5] Gamma peaks used for analysis were 841 keV and 963 keV for the 9.3-hr $^{152m_1}Eu$, 778.7, 1085.8, 1112.1, 1408.2 keV for the 12.4-yr ^{152}Eu and 723.3, 1004.8 and 1274.4 keV for the ^{154}Eu. The resultant cross sections are 1.072 ± .086 barns for $^{152}Eu(n,\gamma)^{152m_1}Eu$, 152 ± .13 barns $^{151}Eu(n,\gamma)^{152}Eu$ (after decay of $^{152m_1}Eu$) and 1.51 ± .12 barns $^{153}Eu(n,\gamma)^{154}Eu$. These are considerably higher cross sections than normally encountered (∿ 1.5 barns vs. 0.5 barns per isotope) for most intermediate mass nuclides measured in the CFRMF neutron flux spectrum. Because of its high cross section of ∿ 3 barns, natural $Eu(n,\gamma)$ compares favorably in usefulness with $^{10}B(n,\alpha)$ of ∿ 1.9 barns[6] as a control rod material for LMFBR type reactors.

The cross section of $^{151}Eu(n,\gamma)^{152m_2}Eu$ (97 min) was also measured. The sample size used was 5.49 mg of Eu_2O_3 with the same isotopic ^{151}Eu composition as above and the CFRMF irradiation was for 30 min at 10 KW. The short irradiation minimized the production of 9.3-hr activity but

allowed production of sufficient 97-min activity for easy detection of the 90-keV gamma peak with the Ge(Li) detector. The resulting cross section obtained was $(2.1 \pm 0.2) \times 10^{-3}$ barns.

Although contribution of this isomer as a fission product to gamma heating in reactors is admittedly very small, measurement of the production of short lived isomers is of interest for establishing their contribution to short-term gamma heating effects immediately after reactor shutdown.

---

[1] Present address: Allied Chemical Corporation, 550 Second Street, Idaho Falls, Idaho 83401.

[2] C. L. Beck, et al., Nuclear Technology Branch Annual Progress Report for Period Ending June 30, 1968, IN-1218 (1968) p. 192.

[3] J. J. Scoville, et al., Nuclear Technology Branch Annual Progress Report for Period Ending June 30, 1970, IN-1407 (1970) p. 281.

[4] D. A. Millsap, Nuclear Technology Branch Annual Progress Report for Period Ending June 30, 1970, IN-1407 (1970) p. 286.

[5] R. G. Helmer and M. H. Putnam, GAUSS V - A Computer Program for the Analysis of Gamma-Ray Spectra from Ge(Li) Spectrometers, ANCR-1043 (January 1972).

[6] H. Farrar IV, private communication.

CSEWG THERMAL BENCHMARK CALCULATIONS

F. J. Wheeler, A. W. Brown

Thermal benchmark calculations were performed in conjunction with ENDF/B-III data testing activities at ANC. The results of the calculations were informally transmitted to CSEWG personnel who will tentatively present descriptions of the benchmarks and results of calculations by various CSEWG members at the San Francisco ANS Meeting in November 1973.

The critical lattices for which calculations were performed were designated TRX-1 and TRX-2 and were composed of Al clad, U metal rods at a moderator-to-fuel ratio of 2.35 and 2.40, respectively. The lattices were H_2O moderated with a full H_2O reflector. The values of k-eff obtained are presented in Table I along with a comparison of those computed by other investigators.

Other results of interest were: 1) the ratio of ^{238}U epi-thermal capture to thermal capture (ρ^{28}); 2) the ratio of ^{235}U epi-thermal fission to thermal fission (δ^{25}); and 3) the ratio ^{238}U fission to ^{235}U fission (δ^{28}). These activation ratios are given in Table II.

The spatially and energy weighted cross sections applicable to the unit cell were obtained from transport (S_6) calculations using the SCAMP code with 97 energy groups and a cylindricalized model of the cell. Resonance effects were treated using the RABBLE[1] code*. The k-eff values and activation parameters were obtained from full-core SCAMP calculations using 66 energy groups above 0.625 eV and one energy group (obtained from the SCAMP cell calculations) below this cut-off value.

---

* A self-shielding calculation was also performed using multi-level theory for ^{235}U. The multi-level effect was found to be negligible.

[1] P. H. Keir and A. A. Robba, RABBLE - A Program for Computation of Resonance Absorption in Multiregion Reactor Cells, ANL-7326 (1967).

TABLE I

CRITICALITY CALCULATIONS (ENDF/B-III)

		K_{eff} (exp = 1.0)			
Benchmark	Description	BAPL	ORNL	SRL	ANC
TRX					
-1	Mod/Fuel = 2.35	0.9872	0.9808	0.9766	0.9741
-2	Mod/Fuel = 4.02	0.9913	0.9876	0.9859	0.9823

TABLE II

ACTIVATION PARAMETERS (ENDF/B-III)

	ρ^{28}					δ^{25}					δ^{28}				
Benchmark	EXP	BAPL	ORNL	SRL	ANC	EXP	BAPL	ORNL	SRL	ANC	EXP	BAPL	ORNL	SRL	ANC
TRX-1	1.311 ±0.02	1.422	1.419	1.454	1.438	0.098 ±.001	.1031	.1100	1.024	.1019	0.0914 ±.002	.0894	.0878	.0912	.0901
TRX-2	0.830 ±.015	0.899	0.874	0.890	0.906	0.0608	.0649	.0665	.0621	.0619	.0667 ±.002	.0654	.0627	.0651	.0651

Note: Parameters correspond to a thermal cut-off of 0.625 eV.

THE TOTAL NEUTRON CROSS SECTION OF ^{241}Pu MEASURED AT LIQUID NITROGEN TEMPERATURE FROM 1.0 eV TO 10 keV

F. B. Simpson, H. G. Miller, J. A. Harvey[1], N. W. Hill[1]

Accurate ^{241}Pu cross-section data are important when predicting the growth of Pu in power reactors and to the predicting of heavier transplutonium elements in the production reactors. There have been uncertainties in the ^{241}Pu total cross section data and the relationship of the total to the partial cross sections. For these reasons we were requested and did measure the total neutron cross section of ^{241}Pu on the Oak Ridge Electric Linear Accelerator (ORELA).

These measurements were made at liquid nitrogen temperature using three metal samples of different thicknesses. Table I gives the sample thicknesses and isotopic composition at the time of chemical separation. The operating conditions and neutron energy range for four different sets of measurements are summarized in Table II. The first two sets of data have been converted to cross section vs. energy. However, funding limitations did not permit the completion of the last sets of data covering the higher energy region.

TABLE I

COMPOSITION OF THE PLUTONIUM SAMPLES

Isotope	Wt % Pu	Sample 1 Atoms/cm^2* 10^{20}	Sample 2 Atoms/cm^2* 10^{20}	Sample 3 Atoms/cm^2* 10^{20}
^{238}Pu	0.022	0.00124	0.0050	0.0276
^{239}Pu	0.764	0.04279	0.1901	0.9246
^{240}Pu	3.340	0.1863	0.8277	4.206
^{241}Pu	93.600	5.200	23.10	112.3
^{242}Pu	2.274	0.1258	0.5589	2.693
^{244}Pu	<0.01	<0.00055	<0.00239	<0.0119
^{241}Am		0.0323	0.1413	0.6980

*3/13/73

All of the measurements were made at the 80 meter flight path. The first two sets of data used a Li glass detector and the ^{110}Ne detector was used for the two higher energy measurements. All three samples were contained in the cryostat and a thermocouple attached to the bottom of the sample holder. It does appear, however, from the shape of the resonances, due to the containments, that there was some internal heating in the thick sample. This can only be determined when and if the data are analyzed for resonance parameters.

TABLE II

OPERATING CONDITIONS FOR MEASUREMENTS IN THE DIFFERENT ENERGY REGIONS

Energy Range	Pulse Width (nsec)	Channel Width (nsec)	Pulses/Sec	Detector Thickness (in)	Beam Filter
1.0-100 eV	30	8-2048	80	0.5	Cd (0.035")
30 eV-10 keV	30	8-256	500	0.5	^{10}B
10-200 keV	4	2-2048	800	0.75	^{10}B
100 keV-8 MeV	4	1-2048	800	0.75	^{238}U (0.740")

The raw data has about 2000 to 4000 counts per channel which give counting statistics of approximately 2%. The cross section data look very good and there is good agreement between different runs. The energy resolution $\Delta E/E$ was $0.0007\sqrt{1 + 4E\ (MeV)}$. Backgrounds were approximately 1 to 2%, with a major part of it being a constant room background at low energies, 2.23-MeV gamma rays (with a 16-μsec decay period) from H-capture in the moderator at keV energies with the ^{6}Li glass detector, and a background in the keV measurements with the ^{10}Ne detector due to neutrons being moderated (with a 5-μsec leakage period) by the detector and producing gamma rays from capture in the detector.

---

[1] Oak Ridge National Laboratory.

MULTILEVEL FITTING OF ^{235}U

J. R. Smith

For some years there have been disagreements as to whether or not multilevel effects were important for reactor applications. Comparison of parameters has been hampered by the fact that there can be differences in data interpretation and fitting techniques which obscure the real differences between parameter types. Such comparisons must be based on matched sets of parameters.

Reich-Moore multilevel parameters were fitted to the cross sections of ^{235}U below 82 eV. The multilevel parameters were intended to match closely the single-level parameters previously derived for use in ENDF/B, Version III.[1] The same data were fitted, using the same normalizations and interpretations of resolution. These data sets were as follows:

1. The fission and capture measurements of deSaussure et al.[2]
2. The total cross section measurements of Michaudon.[3]
3. The fission cross section data of Blons.[4]
4. The fission measurements of Cao et al.[5] However, the use of these data in the multilevel program was very limited.
5. The scattering cross section measurements of Poortmans et al.[6] These data were not available at the single-level fitting, but were examined to a certain extent in the multilevel analysis.

The fitting was done using the codes MULTI, ACSAP, and SCORE. MULTI is the only one of the three that automatically adjusts the relative angle between fission vectors of resonances, so its role was to search out the interference patterns in fission. ACSAP was used in final adjustments to insure that the resonance widths would be interpreted as they had been for the single-level analysis, and to prepare detailed plots of calculated versus measured cross sections for the comparison of the effects of adjustments on all data sets. SCORE was used to examine closely the interference effects in some regions where MULTI and ACSAP were both experiencing difficulties deciding on a best fit.

The resonances were divided into two spin states. Spin assignments were made on the basis of measurements where these were available, and on the basis of relative interference where no experimental data existed. For the most part, the spin assignments are not very reliable. The small difference in statistical weight of the two spin states (7/16 and 9/16) makes experimental spin effects small and assignment difficult.

The final parameters are listed in Table I. These parameters generate cross sections very close to those produced by the Version-III parameters. Comparisons between the two sets are discussed in the next section.

---

[1] J. R. Smith and R. C. Young, ^{235}U Resolved Resonance Parameter for ENDF/B, Version III, USAEC Report ANCR-1044 (1971).

[2] G. deSaussure et al., Simultaneous Measurements of the Neutron Fission and Capture Cross Sections for ^{235}U for Incident Neutron Energies from 0.4 eV to 3 keV, USAEC Report ORNL-TM-1804 (1967).

[3] A. Michaudon, Contribution a l'Etude par des Methodes du Temps de Vol de l'Interaction des Neutrons Lents Ave., l'U-235, Report CEA-R2552 (1964).

[4] J. Blons, H. Derrien and A. Michaudon, Measurements and Analysis of the Fission Cross Sections of U-235 and U-235 for Neutron Energies Below 30 KeV, CONF-710301, Vol. 2, (1971) p. 829

[5] M. G. Cao et al., "Fission Cross-Section Measurement of U-235", J. Nucl. Energy 22, (1968) p. 211.

[6] F. Poortmans et al., "Scattering Cross Section of ^{235}U Below 100 eV", 2nd International Conference on Nuclear Data for Reactors, Helsinki, CN-26/20 (1970).

TABLE I

^{235}U MULTILEVEL PARAMETERS

RESONANCE PARAMETERS

RESONANCE ENERGY (EV)	RESONANCE SPIN	GAMMA-N (EV)	GAMMA-N-NOUGHT (EV)	GAMMA-GAMMA (EV)	GAMMA-F1 (EV)	GAMMA-F2 (EV)	
-1.8000E 00	3.0000E 00	4.4274E-03	3.3000E-03	1.0000E-04	-6.2000E-03	-1.9400E-02	1
-1.3500E 00	4.0000E 00	6.9714E-06	6.0000E-06	4.0000E-02	-1.8670E 00	-1.7710E 00	2
-5.2600E-01	4.0000E 00	1.8073E-04	2.4920E-04	5.7633E-02	0.0	-4.0866E-01	3
2.7600E-01	3.0000E 00	4.2029E-06	8.0000E-06	4.3429E-02	4.4101E-02	-6.5043E-02	4
1.1790E 00	4.0000E 00	9.4466E-06	8.7000E-06	3.5851E-02	1.2499E-01	3.8311E-02	5
2.0350E 00	3.0000E 00	1.0271E-05	7.2000E-06	4.2152E-02	1.3428E-02	-3.5800E-04	6
2.7410E 00	3.0000E 00	6.6224E-07	4.0000E-07	6.1575E-02	-3.0361E-02	-6.1992E-02	7
3.1450E 00	3.0000E 00	2.6956E-05	1.5200E-05	4.0857E-02	-4.3513E-02	7.4107E-02	8
3.6120E 00	3.0000E 00	5.8536E-05	3.0800E-05	3.7969E-02	2.9369E-02	3.0256E-02	9
4.8470E 00	3.0000E 00	7.0671E-05	3.2100E-05	3.7211E-02	4.5330E-03	3.8400E-04	10
5.4100E 00	3.0000E 00	1.8608E-05	8.0000E-06	4.0000E-02	-3.6347E-01	1.9212E-02	11
5.7510E 00	4.0000E 00	7.9138E-06	3.3000E-06	3.5605E-02	-1.2280E 00	8.9092E-02	12
6.2200E 00	3.0000E 00	7.6566E-05	3.0700E-05	4.9214E-02	6.2084E-02	1.0226E-01	13
6.3860E 00	4.0000E 00	2.5271E-04	1.0000E-04	3.5653E-02	-6.8240E-03	8.4800E-03	14
7.0770E 00	3.0000E 00	1.4951E-04	5.6200E-05	3.7710E-02	2.8747E-02	2.5770E-03	15
7.7500E 00	3.0000E 00	8.3516E-07	3.0000E-07	4.0000E-02	-2.8000E-05	3.7598E-01	16
8.7750E 00	3.0000E 00	1.3360E-03	4.5100E-04	3.3339E-02	-1.0882E-02	8.8230E-02	17
9.2700E 00	3.0000E 00	1.5345E-04	5.0400E-05	3.4900E-02	7.1897E-02	7.4520E-03	18
9.7550E 00	3.0000E 00	7.7458E-05	2.4800E-05	2.4382E-02	-1.1215E-01	-1.8971E-01	19
1.0166E 01	4.0000E 00	5.1652E-05	1.6200E-05	3.6550E-02	1.6013E-02	-6.1868E-02	20
1.0900E 01	4.0000E 00	5.2824E-05	1.6000E-05	5.0000E-02	2.3173E-01	5.0230E-01	21
1.1380E 01	4.0000E 00	3.3060E-05	9.8000E-06	5.0000E-02	-3.6000E-01	1.8000E-01	22
1.1670E 01	4.0000E 00	4.8304E-04	1.4140E-04	3.5090E-02	2.2300E-03	-7.6800E-03	23
1.2395E 01	3.0000E 00	1.5329E-03	4.3540E-04	3.9672E-02	2.4766E-02	9.2070E-03	24
1.2859E 01	3.0000E 00	9.6462E-05	2.6900E-05	2.8678E-02	3.2141E-02	-1.1384E-01	25
1.3233E 01	3.0000E 00	9.3853E-05	2.5800E-05	2.0583E-02	1.0240E-01	1.3100E-01	26
1.3719E 01	3.0000E 00	1.5668E-04	4.2300E-05	2.3531E-02	9.0000E-06	-2.2247E-01	27
1.3988E 01	3.0000E 00	4.7012E-04	1.2570E-04	2.0000E-02	4.0755E-01	2.1397E-02	28
1.4556E 01	3.0000E 00	1.0950E-04	2.8700E-05	3.4316E-02	-1.3019E-02	4.6250E-03	29
1.5412E 01	3.0000E 00	2.5910E-04	6.6000E-05	3.6914E-02	-1.3000E-04	-4.5699E-02	30
1.6092E 01	3.0000E 00	4.3324E-04	1.0800E-04	3.5399E-02	-1.4281E-02	-7.7780E-03	31
1.6645E 01	3.0000E 00	3.2883E-04	8.0600E-05	3.8200E-02	8.4330E-03	-1.0550E-01	32
1.8045E 01	4.0000E 00	3.4366E-04	8.0900E-05	3.7724E-02	4.2446E-02	8.9880E-02	33
1.8970E 01	3.0000E 00	1.5026E-04	3.4500E-05	6.0000E-02	-7.1658E-02	2.0352E-02	34
1.9298E 01	4.0000E 00	2.9332E-03	6.6770E-04	3.8312E-02	4.7570E-03	-5.8580E-02	35
2.0200E 01	4.0000E 00	7.6405E-05	1.7000E-05	4.3612E-02	-2.5750E-02	1.2103E-01	36
2.0635E 01	3.0000E 00	2.1850E-04	4.8100E-05	3.8685E-02	4.8390E-02	-5.1810E-03	37
2.1057E 01	3.0000E 00	1.8672E-03	4.0690E-04	4.4794E-02	2.5696E-02	9.9200E-03	38
2.2935E 01	3.0000E 00	5.3637E-04	1.1200E-04	3.6000E-02	2.9663E-02	1.7518E-02	39
2.3408E 01	4.0000E 00	6.4299E-04	1.3290E-04	3.7681E-02	-6.1890E-03	-2.9230E-03	40
2.3590E 01	3.0000E 00	1.0316E-03	2.1240E-04	3.2696E-02	1.4447E-02	2.4518E-01	41
2.4221E 01	4.0000E 00	2.8052E-04	5.7000E-05	3.5780E-02	-5.3002E-02	-4.6960E-03	42
2.4360E 01	3.0000E 00	7.3540E-05	1.4900E-05	2.7000E-02	4.0000E-06	-4.4209E-02	43
2.4700E 01	3.0000E 00	1.6252E-04	3.2700E-05	3.0000E-02	2.4373E-02	5.6845E-01	44
2.5592E 01	4.0000E 00	9.8648E-04	1.9500E-04	2.5000E-02	5.5637E-01	3.6068E-02	45
2.6453E 01	4.0000E 00	5.6061E-04	1.0900E-04	3.7853E-02	2.1255E-01	-6.8860E-03	46
2.7147E 01	3.0000E 00	6.3565E-05	1.2200E-05	4.2000E-02	2.0634E-02	2.1858E-02	47
2.7758E 01	3.0000E 00	6.1116E-04	1.1600E-04	2.5571E-02	6.8974E-02	-5.8131E-02	48
2.8120E 01	4.0000E 00	1.6969E-05	3.2000E-06	3.5000E-02	-9.8180E-03	1.4323E-02	49
2.8344E 01	3.0000E 00	2.1828E-04	4.1000E-05	3.0000E-02	-7.4570E-03	1.1663E-01	50

TABLE I (Contd.)

RESONANCE PARAMETERS

RESONANCE ENERGY (EV)	RESONANCE SPIN	GAMMA-N (EV)	GAMMA-N-NOUGHT (EV)	GAMMA-GAMMA (EV)	GAMMA-F1 (EV)	GAMMA-F2 (EV)	
2.8734E 01	3.0000E 00	1.2865E-05	2.4000E-06	5.0000E-02	2.1520E-02	-1.4138E-01	51
2.9150E 01	3.0000E 00	9.1784E-05	1.7000E-05	4.9999E-02	-1.6400E 00	1.6400E-01	52
2.9642E 01	4.0000E 00	1.5244E-04	2.8000E-05	3.7768E-02	6.0510E-03	-1.9928E-02	53
3.0592E 01	4.0000E 00	1.9856E-04	3.5900E-05	5.4164E-02	3.7140E-03	-1.0212E-01	54
3.0868E 01	3.0000E 00	5.9559E-04	1.0720E-04	3.4478E-02	-9.3180E-03	-7.5210E-03	55
3.2073E 01	3.0000E 00	2.1555E-03	3.8060E-04	3.9187E-02	-4.9194E-02	1.4034E-02	56
3.3518E 01	4.0000E 00	1.6743E-03	2.8920E-04	3.5801E-02	-5.7150E-03	-2.1474E-02	57
3.4350E 01	3.0000E 00	2.5788E-03	4.4000E-04	5.0000E-02	-5.1722E-02	-3.2070E-03	58
3.4865E 01	3.0000E 00	1.2400E-03	2.1000E-04	3.5000E-02	8.0000E-02	5.0000E-03	59
3.5179E 01	4.0000E 00	3.9158E-03	6.6020E-04	4.0000E-02	3.1000E-02	7.3000E-02	60
3.5555E 01	4.0000E 00	5.4023E-04	9.0600E-05	3.0000E-02	-7.7551E-01	5.1820E-02	61
3.6400E 01	3.0000E 00	2.7150E-04	4.5000E-05	3.0000E-02	1.0823E 00	-4.6758E-01	62
3.7470E 01	4.0000E 00	1.6527E-04	2.7000E-05	3.0000E-02	3.6821E-01	-4.6178E-01	63
3.8359E 01	4.0000E 00	3.0967E-04	5.0000E-05	4.0000E-02	-3.4000E-01	-8.6000E-05	64
3.9410E 01	4.0000E 00	2.1313E-03	3.3950E-04	2.5513E-02	1.8972E-02	2.5342E-02	65
3.9907E 01	3.0000E 00	4.3589E-04	6.9000E-05	4.8863E-02	-7.6784E-02	1.1813E-01	66
4.0460E 01	3.0000E 00	4.9742E-04	7.8200E-05	4.0783E-02	-1.7439E-01	5.2897E-02	67
4.1350E 01	3.0000E 00	6.6104E-04	1.0280E-04	4.5000E-02	1.5727E-01	-1.3971E-01	68
4.1671E 01	3.0000E 00	1.9108E-04	2.9600E-05	2.0000E-02	-1.2874E-01	1.9054E-02	69
4.1859E 01	4.0000E 00	1.1633E-03	1.7980E-04	2.9540E-02	1.0310E-02	2.6590E-03	70
4.2193E 01	3.0000E 00	5.0406E-04	7.7600E-05	4.8000E-02	3.1686E-02	-6.7057E-02	71
4.2703E 01	4.0000E 00	2.4832E-04	3.8000E-05	5.1135E-02	-6.2320E-03	-4.5380E-03	72
4.3000E 01	3.0000E 00	1.3115E-04	2.0000E-05	2.1407E-02	-2.0442E-01	2.5118E-01	73
4.3390E 01	3.0000E 00	8.1548E-04	1.2380E-04	4.9010E-02	3.6531E-02	-7.2600E-04	74
4.3921E 01	4.0000E 00	4.8379E-04	7.3000E-05	4.5000E-02	3.4003E-02	-1.4081E-01	75
4.4605E 01	4.0000E 00	5.3430E-04	8.0000E-05	3.2000E-02	-4.0782E-02	4.3350E-02	76
4.4957E 01	3.0000E 00	1.2947E-03	1.9310E-04	4.3011E-02	-5.6439E-01	4.8694E-02	77
4.5798E 01	3.0000E 00	2.1250E-04	3.1400E-05	3.6589E-02	3.4615E-02	6.6037E-02	78
4.6781E 01	4.0000E 00	7.8656E-04	1.1500E-04	3.7000E-02	9.4500E-02	-3.9700E-02	79
4.7050E 01	4.0000E 00	5.6246E-04	8.2000E-05	3.7000E-02	-2.8000E-02	6.1000E-02	80
4.7959E 01	3.0000E 00	8.8435E-04	1.2770E-04	4.4056E-02	2.1401E-02	1.3824E-02	81
4.8354E 01	4.0000E 00	9.3875E-04	1.3500E-04	3.8874E-02	-4.9333E-02	-1.7717E-01	82
4.8771E 01	4.0000E 00	8.2546E-04	1.1820E-04	5.1630E-02	-7.5390E-03	-9.6947E-02	83
4.9000E 01	3.0000E 00	8.4000E-05	1.2000E-05	4.0000E-02	6.6486E-02	-5.6647E-01	84
4.9460E 01	4.0000E 00	8.8472E-04	1.2580E-04	5.2716E-02	3.2420E-03	1.9041E-02	85
4.9610E 01	3.0000E 00	1.6904E-04	2.4000E-05	3.9999E-02	5.5200E-01	7.3883E-02	86
5.0108E 01	4.0000E 00	3.1854E-04	4.5000E-05	5.0000E-02	5.0000E-02	-2.1700E-02	87
5.0432E 01	4.0000E 00	8.3230E-04	1.1720E-04	3.5700E-02	1.4880E-03	-3.8214E-02	88
5.1291E 01	4.0000E 00	3.0638E-03	4.2780E-04	5.0846E-02	-7.0908E-02	5.8680E-02	89
5.1630E 01	3.0000E 00	4.7424E-04	6.6000E-05	4.1949E-02	-4.4000E-05	-6.0668E-02	90
5.2275E 01	3.0000E 00	3.2246E-03	4.4600E-04	3.2596E-02	-3.0390E-01	-1.2203E-01	91
5.3413E 01	3.0000E 00	7.9004E-04	1.0810E-04	4.2996E-02	-1.1149E-01	3.3640E-02	92
5.4160E 01	3.0000E 00	2.7965E-04	3.8000E-05	3.5757E-02	1.3120E-01	-2.1800E-02	93
5.5070E 01	3.0000E 00	3.7446E-03	5.0460E-04	4.6496E-02	-9.3950E-03	-4.9954E-02	94
5.5903E 01	3.0000E 00	4.3567E-03	5.8270E-04	3.8000E-02	-3.3282E-01	2.3403E-02	95
5.6506E 01	3.0000E 00	5.1108E-03	6.7990E-04	3.6824E-02	9.4600E-04	-6.8859E-02	96
5.7795E 01	4.0000E 00	9.9210E-04	1.3050E-04	2.4840E-02	-5.4896E-02	1.5309E-01	97
5.8066E 01	4.0000E 00	1.2299E-03	1.6140E-04	3.3364E-02	-1.1841E-02	-2.4751E-02	98
5.8638E 01	3.0000E 00	1.4825E-03	1.9360E-04	3.1106E-02	-1.6260E-03	-1.0923E-01	99
5.9718E 01	4.0000E 00	1.1592E-04	1.5000E-05	4.2000E-02	-1.5000E-01	3.4100E-04	100

TABLE I (Contd.)

RESONANCE PARAMETERS

RESONANCE ENERGY (EV)	RESONANCE SPIN	GAMMA-N (EV)	GAMMA-N-NOUGHT (EV)	GAMMA-GAMMA (EV)	GAMMA-F1 (EV)	GAMMA-F2 (EV)	
6.0196E 01	3.0000E 00	1.4276E-03	1.8400E-04	3.2811E-02	-3.4887E-02	2.0222E-01	101
6.0816E 01	4.0000E 00	4.8116E-04	6.1700E-05	2.8869E-02	-7.5927E-02	5.0699E-02	102
6.1083E 01	3.0000E 00	2.9074E-04	3.7200E-05	2.3836E-02	1.7929E-02	4.1104E-02	103
6.1570E 01	3.0000E 00	4.0332E-04	5.1400E-05	3.0000E-02	-1.8778E-01	-4.0578E-01	104
6.2000E 01	4.0000E 00	7.8740E-07	1.0000E-07	3.0000E-02	3.5662E-01	1.5278E-01	105
6.2470E 01	4.0000E 00	6.4021E-05	8.1000E-06	4.0000E-02	-2.0794E-02	-1.3302E-01	106
6.3759E 01	3.0000E 00	1.1730E-03	1.4690E-04	4.6555E-02	1.8552E-01	4.5781E-01	107
6.4299E 01	4.0000E 00	1.0801E-03	1.3470E-04	4.1261E-02	-7.1950E-03	3.7000E-05	108
6.4693E 01	4.0000E 00	8.8475E-05	1.1000E-05	4.5000E-02	-2.4000E-01	-5.5000E-01	109
6.5757E 01	3.0000E 00	4.2978E-04	5.3000E-05	3.8000E-02	-2.7800E-02	2.0000E-03	110
6.6416E 01	4.0000E 00	3.2598E-04	4.0000E-05	3.1904E-02	2.6439E-02	-3.9580E-03	111
6.7305E 01	4.0000E 00	5.3326E-05	6.5000E-06	4.1000E-02	4.8470E-02	5.3000E-04	112
6.8500E 01	3.0000E 00	2.4829E-04	3.0000E-05	1.4000E-01	-8.5900E-03	1.9530E-01	113
6.9233E 01	3.0000E 00	7.6383E-04	9.1800E-05	3.4611E-02	-1.4780E-03	1.6011E-01	114
7.0420E 01	3.0000E 00	2.6006E-03	3.0990E-04	3.5098E-02	4.0200E-02	-4.7300E-02	115
7.0750E 01	4.0000E 00	2.2971E-03	2.7310E-04	3.6628E-02	-9.0600E-03	1.9809E-01	116
7.1627E 01	4.0000E 00	3.5715E-04	4.2200E-05	3.8000E-02	1.5182E-01	1.2837E-02	117
7.2376E 01	4.0000E 00	2.3055E-03	2.7100E-04	2.9108E-02	3.5724E-02	3.8811E-02	118
7.2821E 01	3.0000E 00	7.7740E-04	9.1100E-05	3.9999E-02	6.8101E-01	2.9846E-02	119
7.4536E 01	4.0000E 00	2.3474E-03	2.7190E-04	3.5949E-02	5.0982E-02	-7.0600E-03	120
7.5208E 01	3.0000E 00	1.0164E-03	1.1720E-04	5.0000E-02	1.7300E-01	-8.1000E-02	121
7.5591E 01	4.0000E 00	1.2372E-03	1.4230E-04	4.5000E-02	-1.7457E-01	-5.1539E-02	122
7.6769E 01	3.0000E 00	2.2430E-04	2.5600E-05	4.1000E-02	1.1852E-01	-6.9576E-02	123
7.7483E 01	3.0000E 00	1.1681E-03	1.3270E-04	3.6095E-02	-5.3300E-04	-8.9099E-02	124
7.8094E 01	3.0000E 00	1.1082E-03	1.2540E-04	4.0000E-02	5.1945E-02	-1.5016E-02	125
7.8400E 01	3.0000E 00	4.8876E-04	5.5200E-05	5.0000E-02	1.1000E-01	2.2000E-01	126
7.9200E 01	4.0000E 00	2.6520E-04	2.9800E-05	4.9995E-02	-6.1700E-01	3.6800E-01	127
7.9694E 01	3.0000E 00	7.5791E-04	8.4900E-05	3.6000E-02	1.6400E-03	-6.1100E-02	128
8.0352E 01	3.0000E 00	8.9639E-04	1.0000E-04	4.0000E-02	-3.3807E-02	-9.8195E-02	129
8.1100E 01	3.0000E 00	3.3321E-05	3.7000E-06	5.5000E-02	3.6267E-02	-5.1917E-02	130
8.1463E 01	4.0000E 00	8.3217E-04	9.2200E-05	4.0000E-02	8.3473E-02	-9.4350E-03	131
8.2688E 01	4.0000E 00	1.7896E-03	1.9680E-04	9.0000E-02	-4.2950E-03	-4.3260E-02	132
8.3582E 01	3.0000E 00	1.9821E-03	2.1680E-04	4.9168E-02	9.0373E-02	6.8100E-04	133
8.6880E 01	3.0000E 00	7.1958E-04	7.7200E-05	5.2000E-02	1.7676E-02	-9.7240E-03	134

COMPARISONS OF SINGLE-LEVEL VS. MULTILEVEL PARAMETERS FOR ^{235}U

J. R. Smith

A current concern to reactor designers is the question of whether or not a multilevel formalism is required for the unresolved region. The availability of matched sets of single-level and multilevel parameters for ^{235}U makes it possible to compare the performances of the two formalisms in terms of various criteria. These included studies of the statistics of the parameters, calculations of cross sections using the parameters projected into the unresolved region, and reactor calculations based on a high temperature lattice having considerable self-shielding.

Statistical studies were made to inquire as to whether there are significant differences in the average values of single-level and multilevel parameters. A least-squares fit to the ladders of $\Sigma\Gamma_n^o$ vs. E gave straight lines where slopes indicate $\bar{\Gamma}_n^o/D = 1.035 \times 10^{-4}$ for the multilevel parameters and 1.025×10^{-4} for the single-level parameter. The distribution of $2g\Gamma_n^o$ for the single-level parameters, assuming 154 levels with $(2g\Gamma_n^o)_{ave} = 0.097$ meV, is shown in Figure 1. The corresponding plot for the multilevel parameters, with $(2g\Gamma_n^o)_{ave} = 0.098$ meV, is shown in Figure 2. The average parameters are shown in Table I. They do not show great differences between the two types of formalization.

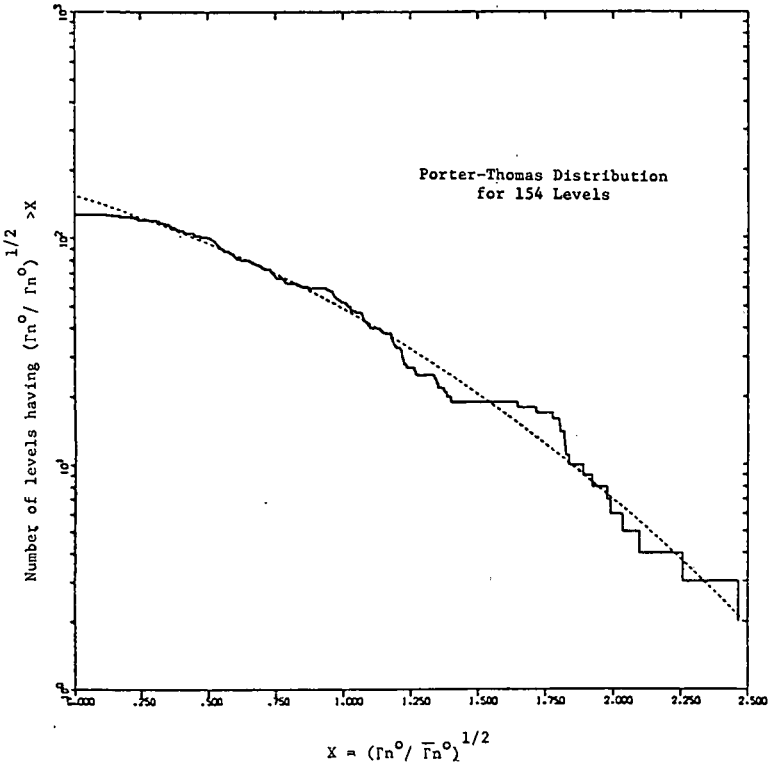

Figure 1 Distribution of neutron widths for single-level resonance parameters of ^{235}U.

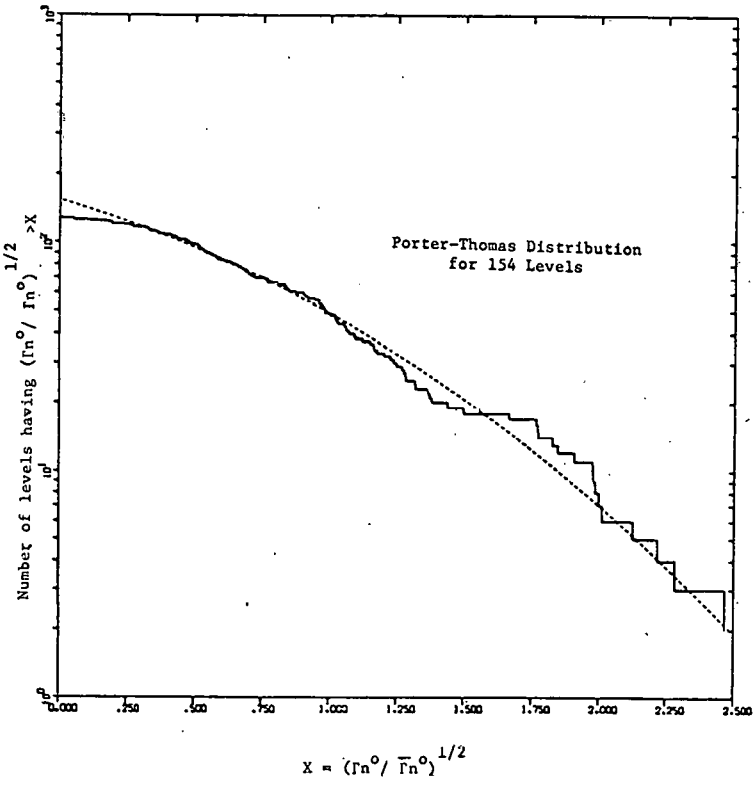

Figure 2 Distribution of neutron widths for the multilevel resonance parameters of ^{235}U.

TABLE I

AVERAGE ^{235}U PARAMETERS

	Single-Level	Multilevel
$2g\Gamma_n^o$ (from fit to distribution)	0.097 meV	0.0977 meV
Γ_f (direct average)	166 meV	218 meV
Γ_f (2 distributions)	87, 400 meV	90 meV, 450 meV
Γ_γ	37.3 meV	39.1 meV
Γ_n^o/D	1.025×10^{-4}	1.035×10^{-4}

The fission widths have the appearance of a double distribution for both sets of parameters. The multilevel parameters appear to include more broad levels, but this is partially due to the fact that a few more broad levels were used to fill in cross sections where necessary. The single-level set used an auxiliary smooth file to accomplish the same thing. The observed multilevel distribution can be approximately fitted by chi-squared distributions utilizing 95 levels having $\bar{\Gamma}_f$ = 90 meV and 45 levels having $\bar{\Gamma}_f$ = 450 meV. A fit to the single-level distribution used 120 levels having $\bar{\Gamma}_f$ = 87 meV, and 25 levels having 400 meV.

Calculations in the unresolved region are often based on mock parameters, generated using observed average values and distribution characteristics observed in the resolved resonance region. Alternatively, we can assume that the observed resolved parameters are typical of the parameters to be found in the present investigation.

A comparison test of the parameter sets was made by bodily projecting the parameters into the unresolved region. Both the neutron width and the Doppler width increase with energy, so calculations of this type make it possible to compare the performances of the parameters under conditions of increasing overlap of the levels.

The single-level and multilevel parameters were projected into the unresolved region by adding 800 eV to each resonance energy. The smooth files for the single-level set were ignored. Unshielded cross sections were calculated between 810 and 874 eV, omitting about 10 eV from each end of the range. In order to make differences due to formalism more apparent, calculations were made for both single-level and multilevel parameters, using both the single-level and multilevel formalisms.

The single-level parameters, when used in the multilevel formula, yielded a fission cross section 35% lower than that produced using the single-level formula. It was suspected that this might be at least partially due to the atypical interference generated by the fact that all the fission widths had the same sign. To investigate this effect, the signs of the fission widths were randomized two ways: by hand (by shuffling cards and assigning negative signs to half the fission widths), and by computer (by assigning signs through use of random numbers). The two randomized sets were then used to calculate cross sections in the region 810-874 eV. The results are shown in Table II, along with the original single-level results. The fission cross sections of the two randomized sets agree well with each other, and fall midway between the single-level and multilevel results previously obtained. It should be noted that the capture cross section changes also, though not so much as the fission cross section.

The final test for differences between parameters formalisms involved reactor calculations using cross sections from the two types of parameters. These calculations were based on the configuration of the Fuel Element Failure Propagation Loop (FEFPL).

TABLE II

AVERAGE CROSS SECTIONS, 810-874 eV, FROM PROJECTED RESONANCE PARAMETERS

A. Multilevel Parameters, T = 300°K

	Calculated as Single-Level	Calculated as Multilevel (Γ_f Signs as Indicated)
Fission	9.075	8.805
Capture	4.333	4.533
Alpha	0.4775	0.5148

B. Single Level Parameters, T = 300°K

	Calculated as Single-Level	Same Sign	Hand-Randomized Signs	Computer-Randomized Signs
Fission	8.739	6.460	7.654	7.629
Capture	4.485	4.726	5.364	5.337
Alpha	0.5132	0.7316	0.7008	0.700

It was suspected that if any differences were observed, they might well be due to differences in the way the resonance cross sections were calculated and the smooth files added in for the single-level parameters. It was further suspected that in heavily shielded cases, it might be better to leave out the smooth file completely. Therefore, calculations were made using resonance cross sections obtained in the following ways: (1) calculated by PHROG-II, the standard reactor cross section code now used by Aerojet Nuclear Company, (2) calculated from multilevel parameters by ACSAP, then passed to PHROG to be self-shielded and formed into group cross sections, (3) calculated from single-level parameters, with smooth files added and Doppler-broadened by ACSAP, then passed to PHROG as above, and (4) calculated from single-level parameters without the smooth file.

The results of these calculations indicate the differences between single-level and multilevel resolved resonance parameters are negligible, even for a high temperature, shielded system such as FEFPL. The failure of PHROG-II to broaden or shield the smooth files cross sections does not seem to effect the reactor calculations appreciably. The smooth files appear to improve the accuracy of the calculations, which are better with than without the smooth files. The differences in treatment of the resonance files by reactor codes can be much larger than the differences between single-level and multilevel parameters themselves.

EVALUATION OF ^{237}Np CROSS SECTIONS FOR ENDF/B, VERSION IV

J. R. Smith

The fission cross section of ^{237}Np is a popular detector for fast neutron dosimetry because of its threshold shape and the completeness with which this isotope can be separated from thermally fissioning isotopes. Enthusiasm for ^{237}Np is nevertheless tempered by uncertainty as to contributions from subthreshold fission, which is appreciable in this isotope, and which may play a part, particularly in spectra having an appreciable low energy component. Re-evaluation of the ENDF/B files for Version IV was therefore concerned principally with getting a good description of the fission cross section, with an updated evaluation normalized to the re-evaluated ^{235}U fission cross section, and a subthreshold fission description that would follow the observed intermediate structure in fission.

The evaluation keeps the Version III low energy file, incorporates the resonance parameters of Paya from 0.3 eV to 130 eV, newly generated energy-dependent unresolved paramaters from 130 eV to 40 keV, and a new evaluation of the fission cross section from 40 keV to 20 MeV by W. E. Stein of Los Alamos. The unresolved parameters were adjusted, using the UR code, to fit triangles whose areas are the fission areas listed by Paya in the region 130 eV-2 keV. From 2 keV to 5 keV, the parameters were adjusted to match isolated measurements near 12, 25 and 10 keV.

The new unresolved parameters, if continued to 120 keV, would tie in closely with recent capture measurements of Nagle et al[1]. The evaluated capture cross section for Version IV matches the calculations using the unresolved resonance parameters at 40 keV and passes through the Nagle data from 120 keV to 3 MeV. The Nagle data are appreciably lower than the Stupegia data[2], on which the capture cross section was based in both previous ENDF/B ^{237}Np evaluations.

Above 1 MeV, the partial cross sections were constrained to produce a total cross section close to the total cross section of ^{239}Pu, as measured recently at RPI. The (n,2n) cross section shape calculated by Pearlstein was normalized to recent measurements by Landrum et al[3]. This gave a curve which falls off more steeply than the Landrum measurements showed, and gave too high a cross section to be consistent with restrictions on the total, scattering and fission cross sections. The (n,2n) shape was modified to use the Landrum shape on its trailing edge, and tie into the Pearlstein[4] shape at a peak value of approximately 0.62 b. The (n,3n) cross section kept the Pearlstein shape, and was normalized to stay within the previously mentioned restrictions on the total cross section.

No real re-evaluation of the inelastic cross section could be made within budget restrictions. The Version III inelastic cross sections were kept, but were lowered above 10 MeV to stay within the limitations on the total cross sections, as (n,2n), (n,3n), and fission cross sections were all increased in this region over the Version III evaluation. The

cross sections for excitation of individual levels were adjusted to they would add up to the total inelastic cross section. The Version III file had some points where the total did not equal the sum of its parts.

The Version IV file for ^{237}Np should prove substantially superior to Version III, particularly the re-evaluated fission cross section that includes improved resonance parameters and an updated high energy resolution.

---

[1] R. J. Nagle, J. H. Landrum and M. Linduer, Neutron Capture Cross Sections in the MeV Range, CONF-710301, Vol. I, p. 259 (1971).

[2] D. C. Stupegia, M. Schmidt and C. R. Keedy, Nucl. Sci. Eng. 29, 218 (1967).

[3] J. H. Landrum, R. J. Nagle and M. Linduer, USAEC Report UCRL-74262 (1972).

[4] S. Pearlstein, Nucl. Sci. Eng. 23, 238 (1965).

EVALUATION OF DECAY SCHEMES FOR ILRR

R. G. Helmer, R. C. Greenwood

The Interlaboratory LMFBR Reaction Rates (ILRR) program has been organized to develop the capability to measure accurately neutron-induced reaction rates. Such measurements are necessary in the development of fuels and other materials for the LMFBR. A goal of the ILRR program is to measure fission and nonfission reaction rates by means of gamma-ray spectroscopy with accuracies of about ± 5% at the 2σ level for fission reactions and ± 10% (2σ) for the non-fission reactions.

In the determination of these reaction rates it is necessary to use certain decay scheme data (i.e., the half-lives and one or two gamma-ray intensities) for the isotopes of interest. It is also necessary that all of the laboratories involved use the same decay scheme data. Therefore, a review of the decay scheme literature has been carried out. The resulting recommended information is given in Tables I and II.

TABLE I

A SET OF RECOMMENDED HALF-LIVES, GAMMA-RAY ENERGIES AND BRANCHING RATIOS FOR THE NONFISSION MEASUREMENTS

Radioisotope	Half-Life[a] $t_{1/2}$		Gamma-Ray Energy[a] (keV)	Gamma-Ray Branching Ratio[a] (%)	
^{27}Mg	9.46(2)	m	843.73(4) 1014.44(5)	71.4(5) 28.6(5)	sum = 100.0
^{24}Na	14.99(2)	h	1368.52(6) 2753.98(10)	99.99(1) 99.85(2)	
^{46}Sc	83.85(10)	d	889.258(18) 1120.516(25)	99.98(1) 99.99(1)	
^{47}Sc	3.39(4)	d	159.39(5)	69.0(25)	
^{48}Sc	43.8(1)	h	983.4(2) 1037.4(3) 1311.9(3)	99.98(1) 97.7(3)[b] 99.99(1)	
^{54}Mn	312.6(3)	d	834.827(21)	99.978(2)	
^{59}Fe	44.6(1)	d	1099.224(25) 1291.564(28)	55.5(17) 44.1(12)	sum = 99.6(1)
^{58}Co	71.3(2)	d	810.757(21)	99.44(2)	
^{60}Co	5.268(5)	y	1173.208(25) 1332.491(41)	99.86(2) 99.985(1)	
^{64}Cu	12.78(5)	h	511.002[c]	36.8(16)	
^{115m}In	4.50(2)	h	336.2(1)	47.0(20)	
^{116m}In	54.10(20)	m	1293.4(3) 2112.1(4)	83.7(15) 16.2(15)	sum = 99.93(2)
^{198}Au	2.696(2)	d	411.794(8)	95.47(10)	
^{239}Np	2.355(4)	d	228.19(1)[d] 277.60(3)[e]	12.5(15)[d] 14.5(15)[e]	

[a] The numbers in parentheses indicate the uncertainty (1 σ) in the last digit(s).

[b] The combined intensity of the 1037-keV gamma ray and a 1212-keV gamma ray is (99.98 ± 0.01)%.

TABLE I (Contd.)

[c] The effective line-energy of this peak may be lower than this energy due to electron binding effects and the finite width of the annihilation radiation energy distribution.

[d] There is also a gamma-ray transition of 226.4 keV which has an intensity of 0.7%.

[e] There are also gamma-ray transitions of 272.8 keV and 280.5 keV, but both have intensities of less than 0.1%.

TABLE II

A SET OF RECOMMENDED HALF-LIVES, GAMMA-RAY ENERGIES AND BRANCHING RATIOS FOR SELECTED FISSION PRODUCT NUCLEI

Radioisotope	Half-Life[a] $t_{1/2}$		Gamma-Ray Energy[a] (keV)	Gamma-Ray Branching Ratio[a] (%)
^{95}Zr	64.6(6)	d	724.184(18) 756.715(19)	43.8(5) 54.4(5)
^{97}Zr	16.85(5)	h	743.35(5)	93.3(4)
^{97}Nb	72.1(7)	m	657.92	98.1(1)
^{103}Ru	39.45(10)	d	497.08(1)	89 (3)
^{132}Te	77.9(5)	h	228.16(6)	88.5(60)
^{137}Cs	29.94(20)	y	661.638(19)	85.0(3)
^{140}Ba	12.79(1)	d[b]		
^{140}La	40.26(2)	h[b]	1596.18(5)	95.33(16)
^{144}Ce	284.4(4)	d	133.53(3)	10.7(4)
^{144}Pr	17.28(5)	m	696.492(19) 2185.608	1.49(15) 0.77(4)

[a] The numbers in parentheses indicate the uncertainty (1 σ) in the last digit(s).

[b] The ratio $t_{1/2}(Ba)/[t_{1/2}(Ba)-t_{1/2}(La)]$, which is the ratio of the ^{140}La to ^{140}Ba activities in a mixed ^{140}Ba-^{140}La source at equilibrium, is therefore 1.15096 ± 0.00012.

GAMMA-RAY ENERGY AND RELATIVE INTENSITY MEASUREMENTS OF SEVERAL FISSION PRODUCT RADIONUCLIDES

R. J. Gehrke, L. D. McIsaac[1], R. L. Heath

This past year we have undertaken the precise measurement of energies and relative intensities of γ rays emitted from the following fission product radionuclides: ^{87}Kr, ^{88}Kr, ^{88}Rb, ^{99}Mo, ^{133}I, ^{134}I and ^{135}I. These data are used in the analysis of Ge(Li) γ-ray spectra resulting from several Nuclear Physics Branch projects including the Assistance to Compliance Program, the GGA gas-cooled reactor experiment in ETR, and the Isotopic Monitoring Program. The energies and intensities of the γ rays emitted from the above radionuclides were determined using the techniques described in Reference [2].

The γ-ray energies and relative intensities obtained from these measurements are listed in Table I.

---

[1] Present address: Allied Chemical Corporation, 550 Second Street, Idaho Falls, Idaho 83401.

[2] R. J. Gehrke, Nuclear Technology Division Annual Report for Period Ending June 30, 1972, ANCR-1088 (1972) 392.

[3] R. G. Helmer, R. C. Greenwood and R. J. Gehrke, Nucl. Instr. and Meth. 96 (1971) 173.

[4] R. C. Greenwood, R. G. Helmer and R. J. Gehrke, "Precise Comparison and Measurement of Gamma-Ray Energies with a Ge(Li) Detector III: 1300-3600 keV", this report.

TABLE I

ENERGIES AND RELATIVE INTENSITIES

76-m ^{87}Kr

Energy (kev)	Intensity (rel.)	Comments
129.4	0.070 ± 0.01	
402.578 ± 0.020	100	
673.871 ± 0.035	4.0 ± 0.2	
814.25 ± 0.08	0.36 ± 0.04	
836.40 ± 0.05	1.48 ± 0.10	
845.45 ± 0.04	15.1 ± 0.9	
893.84 ± 0.20	0.106 ± 0.015	
901.5 ± 0.3	0.071 ± 0.012	Contains ^{125}Xe γ-ray peak
946.82 ± 0.20	0.29 ± 0.04	
976.41 ± 0.25	0.126 ± 0.015	
1175.40 ± 0.08	2.46 ± 0.15	
1337.96 ± 0.08	1.43 ± 0.08	
1382.53 ± 0.07	0.62 ± 0.05	

TABLE I (Contd.)

Energy (kev)	Intensity (rel.)	Comments
1389.86 ± 0.20	0.24 ± 0.03	
1464.5 ± 2.0	0.098 ± 0.014	
1531		Contains DE of 2554 γ ray
1577.98 ± 0.20	0.29 ± 0.03	
1610.94 ± 0.25	0.19 ± 0.03	
1740.52 ± 0.08	4.3 ± 0.2	
1842.32 ± 0.25	0.27 ± 0.03	
2011.81 ± 0.15	6.1 ± 0.3	
2378.9 ± 2.0	0.20 ± 0.03	
2408.8 ± 0.3	0.50 ± 0.07	
2554.88 ± 0.20	20.6 ± 1.6	
2558.20 ± 0.25	7.8 ± 0.7	
2652. ± 2	0.061 ± 0.010	
2811.25 ± 0.20	0.70 ± 0.10	
3054.8 ± 0.3	0.19 ± 0.02	
3308.45 ± 0.18	0.96 ± 0.07	
3704.6 ± 1.0	0.03 ± 0.01	*
2.80-h ^{88}Kr		
122.1 ± 0.3	0.49 ± 0.06	
165.85 ± 0.12	8.9 ± 1.0	
196.288 ± 0.015	74. ± 6.	
240.	0.66 ± 0.07	
311.	0.32 ± 0.03	
334.	0.44 ± 0.05	
362.257 ± 0.040	6.5 ± 0.5	
390.66 ± 0.07	2.01 ± 0.20	
402.8 ± 0.3	0.19 ± 0.02	*
471.86 ± 0.10	1.98 ± 0.15	
490.0 ± 1.5	0.096 ± 0.010	*
499.	0.25 ± 0.03	
517.6 ± 0.3	0.25 ± 0.05	
571.6 ± 1.0	0.32 ± 0.03	
665.	0.22 ± 0.04	
677.5 ± 0.2	0.67 ± 0.06	
742.0 ± 1.0	0.25 ± 0.03	*
774.9 ± 1.0	0.26 ± 0.03	
779.3 ± 1.0	0.36 ± 0.04	
788.55 ± 0.15 790. ± 2	1.86 ± 0.20	
821.	0.24 ± 0.03	
834.820 ± 0.035	35.5 ± 2.5	
850.11 ± 0.25	0.61 ± 0.05	
862.32 ± 0.07	1.94 ± 0.12	
945.11 ± 0.20	0.90 ± 0.09	

* Assignment uncertain

TABLE I (Contd.)

Energy (kev)		Intensity (rel.)		Comments
^{88}Kr (continued)				
950.9	± 1.5	0.23	± 0.03	Doublet
962.1	± 0.3	0.16	± 0.02	
985.88	± 0.20	4.0	± 0.3	
990.3	± 1.0			
1039.57	± 0.15	1.31	± 0.08	
1049.4	± 0.3	0.33	± 0.03	
1053.	± 1	0.05	± 0.03	
1090.0	± 0.3	0.40	± 0.04	
1141.51	± 0.07	3.6	± 0.2	
1179.61	± 0.20	2.79	± 0.18	
1185.12	± 0.20	2.00	± 0.15	
1210.3	± 0.5	1.21	± 0.09	
1214.2	± 1.5			
1246.4	± 0.3	1.17	± 0.08	
1250.70	± 0.10	3.20	± 0.18	
1352.29	± 0.20	0.56	± 0.06	
1369.90	± 0.07	12.1	± 0.8	contains DE of 2392 γ
1407.0	± 0.2	0.56	± 0.06	
1464.90	± 0.25	0.22	± 0.03	
1518.48	± 0.05	5.4	± 0.03	Contains SE of 2030 γ ray
1529.74	± 0.06	30.4	± 1.7	
1603.7	± 0.3	1.29	± 0.12	
1685.31	± 0.15	3.96	± 0.22	Contains SE of 2195 γ ray
1788.5	± 0.5	0.22	± 0.03	
1892.38	± 0.25	0.43	± 0.04	
1908.8	± 0.4	0.39	± 0.04	
2029.82	± 0.08	13.6	± 0.8	
2035.46	± 0.08	10.6	± 0.6	
2186.5	± 0.5	1.2	± 0.2	
2195.76	± 0.07	37.1	± 1.9	
2231.69	± 0.10	9.7	± 0.4	
2258.3	± 1.0	0.27	± 0.04	
2352.03	± 0.10	2.10	± 0.11	
2392.02	± 0.08	100		
2408.9	± 0.4	0.33	± 0.04	
2535.6	± 0.3	0.15	± 0.02	
2548.38	± 0.15	1.95	± 0.17	
2706. 2708.		0.28	± 0.05	
2771.10	± 0.18	0.44	± 0.03	

TABLE I (Cont.)

Energy (keV)	Intensity (rel.)	Comments
^{88}Kr-^{88}Rb IN EQUILIBRIUM		
I (rel.) of stronger ^{88}Rb γ rays with intensity of 2392 keV γ ray of ^{88}Kr normalized to be 100.		
898	44.1	
1836	71.5	
2677	6.5	
3009	0.85	
17.7-m ^{88}Rb		
338.5 ± 1.0	0.25 ± 0.04	
483.3 ± 0.6	0.16 ± 0.02	
898.021 ± 0.019[a]	61.4 ± 4.0	
1027.5 ± 0.3	0.04 ± 0.02	
1217.91 ± 0.12	0.18 ± 0.03	
1366.62 ± 0.12	0.44 ± 0.05	
1382.44 ± 0.08	3.3 ± 0.2	
1679.1 ± 0.4	0.23 ± 0.04	
1779.83 ± 0.08	1.04 ± 0.06	
1799.13 ± 0.12	0.18 ± 0.04	
1836.017 ± 0.040[b]	100	
2111.39 ± 0.15	0.60 ± 0.04	
2118.87 ± 0.08	2.04 ± 0.12	
2390.8 ± 0.3	0.16 ± 0.02	
2577.80 ± 0.10	0.96 ± 0.05	
2677.87 ± 0.10	9.3 ± 0.5	
2734.015 ± 0.060	0.48 ± 0.03	Energy calculated from 898 and 1836
3009.50 ± 0.12	1.24 ± 0.08	
3218.50 ± 0.13	1.07 ± 0.06	
3486.46 ± 0.15	0.65 ± 0.06	
3525. ± 2.	0.024 ± 0.006	
4035.7 ± 0.6	0.057 ± 0.008	
4742.40 ± 0.25	0.78 ± 0.09	
4852.81 ± 0.15	0.054 ± 0.010	
66.0-h ^{99}Mo - 6.0-h ^{99}Tc IN EQUILIBRIUM		
40.576 ± 0.025	0.63 ± 0.25	
140.509 ± 0.020	100	
158.76 ± 0.20	0.013 ± 0.004	
162.34 ± 0.25	0.010 ± 0.003	
181.085 ± 0.016	6.8 ± 0.4	
366.442 ± 0.015	1.37 ± 0.10	

[a] From Reference [3].
[b] From Reference [4].

TABLE I (Cont.)

Energy (kev)	Intensity (rel.)	Comments
^{99}Tc (continued)		
379.9 ± 0.5	0.008 ± 0.002	
411.49 ± 0.12	0.17 ± 0.003	
528.86 ± 0.08	0.050 ± 0.005	
621.93 ± 0.15	0.026 ± 0.008	
739.469 ± 0.025	13.7 ± 0.8	
777.878 ± 0.025	4.9 ± 0.3	
822.979 ± 0.028	0.149 ± 0.009	
859.2 ± 0.5	0.0020± 0.0008	
960.690 ± 0.025	0.110 ± 0.008	
986.7 ± 0.3	0.0022± 0.0006	
1001.4 ± 0.3	0.0037± 0.0006	
	20.8-h ^{133}I	
150.0 ± 0.5	0.018 ± 0.005	
233.18 ± 0.20	0.13 ± 0.02	
245.92 ± 0.20	0.099 ± 0.015	*
262.67 ± 0.08	0.46 ± 0.03	
267.18 ± 0.08	0.16 ± 0.02	
345.7 ± 0.6	0.49 ± 0.08	
360.9 ± 0.3	0.27 ± 0.03	*
381.23 ± 0.25	0.062 ± 0.010	*
386.5 ± 0.3	0.079 ± 0.010	*
417.50 ± 0.2	0.17 ± 0.02	Doublet
422.90 ± 0.06	0.36 ± 0.04	
438.92 ± 0.20	0.046 ± 0.010	*
503.0 ± 0.6	0.025 ± 0.005	
510.565 ± 0.020	2.09 ± 0.15	
529.889 ± 0.018	100	
537.74 ± 0.20	0.036 ± 0.008	*
607.85 ± 0.08	0.063 ± 0.008	
617.94 ± 0.03	0.65 ± 0.06	
642.6 ± 0.5	0.026 ± 0.003	
648.8 ± 0.5	0.055 ± 0.005	
661.9 ± 0.8	0.026 ± 0.003	*Possible Cs^{137} contamination
667.5 ± 0.6 670.0 ± 1.0	0.142 ± 0.018	
680.31 ± 0.04	0.80 ± 0.05	
706.606 ± 0.025	1.71 ± 0.10	
768.36 ± 0.04	0.56 ± 0.04	
772.69 ± 0.10	0.057 ± 0.010	*
789.50 ± 0.10	0.046 ± 0.006	
820.61 ± 0.05	0.19 ± 0.02	
846.4 ± 1.0	0.012 ± 0.007	
856.361 ± 0.025	1.41 ± 0.09	
875.370 ± 0.025	5.1 ± 0.3	

* Assignment uncertain

TABLE I (Cont.)

Energy (kev)	Intensity (rel.)	Comments
909.92 ± 0.10	0.263 ± 0.03	Doublet
911.5 ± 1.0		*
1052.365 ± 0.030	0.65 ± 0.04	
1060.17 ± 0.05	0.18 ± 0.02	+ Accidental summing
1236.525 ± 0.035	1.8 ± 0.2	
1298.329 ± 0.030	2.71 ± 0.14	
1350.54 ± 0.08	0.167 ± 0.020	
	52.6-m ^{134}I	
135.399 ± 0.022	3.94 ± 0.23	
139.030 ± 0.030	0.72 ± 0.05	
151.98 ± 0.15	0.111 ± 0.012	*
162.48 ± 0.07	0.27 ± 0.03	
188.47 ± 0.04	0.73 ± 0.04	
217.0 ± 0.2	0.26 ± 0.03	
235.471 ± 0.026	2.08 ± 0.16	
262.6 ± 0.3	very weak	*
278.80 ± 0.15	0.137 ± 0.015	
319.81 ± 0.06	0.54 ± 0.05	
351.08 ± 0.10	0.52 ± 0.06	
405.451 ± 0.020	7.7 ± 0.4	
411.00 ± 0.08	0.64 ± 0.06	
433.345 ± 0.030	4.39 ± 0.25	
458.92 ± 0.06	1.36 ± 0.09	
465.50 ± 0.10	0.38 ± 0.04	*
488.88 ± 0.04	1.48 ± 0.09	
514.400 ± 0.030	2.45 ± 0.14	
540.825 ± 0.025	8.2 ± 0.5	
565.52 ± 0.04	0.92 ± 0.06	
570.75 ± 0.15	0.22 ± 0.03	
595.362 ± 0.020	11.9 ± 0.6	
621.790 ± 0.025	11.1 ± 0.6	
627.960 ± 0.030	2.48 ± 0.14	
677.338 ± 0.030	8.9 ± 0.5	
706.65 ± 0.10	0.87 ± 0.06	*
730.74 ± 0.04	2.00 ± 0.12	
739.18 ± 0.08	0.80 ± 0.08	
766.675 ± 0.035	4.30 ± 0.28	
784.9 ± 0.3	0.28 ± 0.05	DE
816.38 ± 0.07	0.55 ± 0.05	
847.025 ± 0.025	100	
857.285 ± 0.030	7.3 ± 0.2	
864.0 ± 0.3	0.20 ± 0.03	*
884.090 ± 0.025	68.4 ± 1.0	
922.6 ± 0.3	0.15 ± 0.03	*
947.86 ± 0.04	4.23 ± 0.20	
966.90 ± 0.05	0.37 ± 0.04	

* Assignment uncertain

TABLE I (Cont.)

Energy (kev)	Intensity (rel.)	Comments
52.6-m ^{134}I (continued)		
974.670 ± 0.035	4.88 ± 0.35	
1040.25 ± 0.10	2.0 ± 0.2	
1052.2 ± 0.3	0.07 ± 0.02	*
1058.8 ± 0.3	0.10 ± 0.03	*
1072.547 ± 0.030	16.0 ± 0.8	
1087.0 ± 0.2	0.09 ± 0.02	*
1100.07 ± 0.12	0.72 ± 0.06	
1103.18 ± 0.12	0.76 ± 0.06	
1136.160 ± 0.035	10.2 ± 0.5	
1159.10 ± 0.08	0.37 ± 0.03	
1164.0 ± 0.3	0.14 ± 0.03	*
1183.2 ± 0.5	0.06 ± 0.01	*
1190.03 ± 0.08	0.37 ± 0.03	
1225.5 ± 0.3	0.07 ± 0.02	*
1239.0 ± 0.3	0.22 ± 0.06	*
1243.8 ± 0.3	0.08 ± 0.02	*
1269.49 ± 0.05	0.59 ± 0.04	
1322.4 ± 0.3	0.11 ± 0.04	
1336.0 ± 0.2	0.15 ± 0.03	
1352.62 ± 0.08	0.47 ± 0.04	
1395 ± 1	0.08 ± 0.02	*
1407.4 ± 0.2	0.10 ± 0.02	*
1414.3 ± 0.5	0.23 ± 0.06	*
1428.2 ± 0.3	0.18 ± 0.04	
1431.35 ± 0.25	0.18 ± 0.04	*
1455.24 ± 0.05	2.40 ± 0.15	
1470.00 ± 0.07	0.81 ± 0.05	
1505.5 ± 0.4	0.12 ± 0.04	*
1541.51 ± 0.07	0.53 ± 0.04	
1613.800 ± 0.043	4.57 ± 0.25	
1629.24 ± 0.08	0.27 ± 0.04	
1644.25 ± 0.07	0.42 ± 0.05	
1655.19 ± 0.10	0.24 ± 0.03	
1741.49 ± 0.05	2.8 ± 0.2	
1806.839 ± 0.040	5.95 ± 0.35	
1868.5 ± 0.2	0.07 ± 0.02	*
1893.2 ± 0.3	0.06 ± 0.01	*
1925.88 ± 0.10	0.19 ± 0.02	
1947.3 ± 0.3	0.10 ± 0.02	*
2020.6 ± 0.3	0.18 ± 0.02	
2159.9 ± 0.3	0.22 ± 0.03	
2236.7 ± 0.5	0.056 ± 0.015	*
2262.5 ± 0.3	0.10 ± 0.02	
2312.4 ± 0.2	0.25 ± 0.03	
2409.0 ± 0.3	0.079 ± 0.012	
2452.9 ± 0.3	0.067 ± 0.010	

* Assignment Uncertain

TABLE I (Cont.)

Energy (kev)	Intensity (rel.)	Comments
52.6-m ^{134}I (continued)		
2467.4 ± 0.3	0.16 ± 0.02	
2513.3 ± 0.3	0.073 ± 0.009	
2629.9 ± 0.3	0.070 ± 0.008	
2699.5 ± 0.5	0.034 ± 0.008	*
2840 ± 4	0.02 ± 0.01	*
	6.6-h ^{135}I	
113.0 ± 0.6	0.097 ± 0.025	
158.18 ± 0.05	0.83 ± 0.07	
184 ± 2	0.19 ± 0.03	
196.85 ± 0.30	0.16 ± 0.03	
220.490 ± 0.020	6.4 ± 0.4	
229.680 ± 0.026	0.74 ± 0.05	
264.03 ± 0.25	1.1 ± 0.2	Doublet
288.43 ± 0.03 289.8 ± 0.5	11.7 ± 0.9	
305.52 ± 0.06	0.47 ± 0.04	
333.6 ± 0.3	0.163 ± 0.038	
362.0 ± 0.3	0.43 ± 0.06	
403.10 ± 0.08	1.05 ± 0.10	
415.1 ± 0.3	1.1 ± 0.2	
417.685 ± 0.028	12.5 ± 0.7	
423.0 ± 0.2	0.33 ± 0.05	*
430.026 ± 0.053	1.10 ± 0.09	
433.789 ± 0.035	1.81 ± 0.12	
451.691 ± 0.038	1.03 ± 0.07	
526.581 ± 0.018	45. ± 4	
546.579 ± 0.020	24.8 ± 1.3	
575.8 ± 0.2	0.31 ± 0.04	*
588.37 ± 0.14	0.09 ± 0.04	
649.83 ± 0.05	1.56 ± 0.11	
690.10 ± 0.15	0.58 ± 0.09	
707.53 ± 0.12	2.8 ± 0.4	^{133}I contribution removed
785.63 ± 0.08	0.48 ± 0.05	
797.88 ± 0.15	0.53 ± 0.07	
813.0 ± 0.8	0.23 ± 0.04	*
836.865 ± 0.022	22.5 ± 1.1	
960.98 ± 0.20	0.63 ± 0.08	
972.33 ± 0.04	7.6 ± 0.4	Doublet
995.09 ± 0.20	0.76 ± 0.12	
1038.77 ± 0.04	28.2 ± 1.7	
1097 ± 2	very weak	
1101.60 ± 0.05	5.6 ± 0.3	
1124.020 ± 0.030	12.7 ± 0.8	
1131.561 ± 0.028	76.4 ± 2.0	

* Assignment Uncertain

TABLE I (Cont.)

Energy (kev)	Intensity (rel.)	Comments
1159.95 ± 0.15	0.53 ± 0.06	
1169.12 ± 0.07	3.22 ± 0.26	
1179.8 ± 0.6	0.19 ± 0.04	
1240.52 ± 0.09	3.00 ± 0.29	
1260.462 ± 0.030	100	
1315.5 ± 0.5	0.40 ± 0.04	*
1343.6 ± 0.5	0.31 ± 0.05	*
1367.97 ± 0.05	2.30 ± 0.08	
1448.37 ± 0.09	1.5 ± 0.4	
1457.660 ± 0.035	30.4 ± 1.0	
1502.90 ± 0.05	3.9 ± 0.3	
1566.45 ± 0.06	4.9 ± 0.2	
1678.175 ± 0.038	34.1 ± 1.3	
1706.580 ± 0.045	14.5 ± 0.7	
1791.326 ± 0.038	28.1 ± 1.4	
1830.80 ± 0.05	2.11 ± 0.13	
1927.40 ± 0.07	1.12 ± 0.08	
1948.80 ± 0.12	0.278 ± 0.030	
1968.2 ± 1.5	very weak	
2046.10 ± 0.06	3.13 ± 0.18	
2112.68 ± 0.14	0.27 ± 0.03	
2152.1 ± 1.5	0.11 ± 0.03	
2190	very weak	
2255.51 ± 0.08	2.16 ± 0.20	
2408.77 ± 0.12	3.22 ± 0.19	
2466.25 ± 0.25	0.24 ± 0.3	

* assignment uncertain

STUDIES OF FISSION GASSES AND GROSS FISSION PRODUCTS

E. B. Nieschmidt

The application of on-line real time detection and analysis systems to the monitoring of nuclear reactor systems and effluents requires thorough knowledge of the gamma-ray spectra of fission products as time after fission progresses. The investigation of heat generated by nuclear decay after reactor shutdown also requires this knowledge.

The gamma-ray spectra of fission gasses were accumulated from samples with decay times from 1.1 min from flowing gas samples to 15 min from grab samples. Gamma-ray spectra were obtained from gross fission products with decay times from 5 min to 100 days and irradiation times varying from 5 min to 34 days. Samples were 1, 5 and 100 μgm ^{235}U.

STUDIES OF THE $^{151}Sm(n,\gamma)$ REACTION

R. C. Greenwood, C. W. Reich

The level structure of the deformed even-even nucleus ^{152}Sm has been studied extensively from the decay of ^{152}Eu but not so far by $^{151}Sm(n,\gamma)$ reaction since ^{151}Sm is unstable. Because of the long half-life ($\sim$ 93 y), low β^- associated with the ^{151}Sm decay and the large thermal neutron capture cross section ($\sim$ 15,000 b), we were able to obtain good quality neutron capture spectra from a few-mg sample of this isotope. Figures 1 and 2 illustrate portions of the γ-ray data obtained. Analysis of these data is currently in progress and is expected to reveal new features of the level structure of ^{152}Sm.

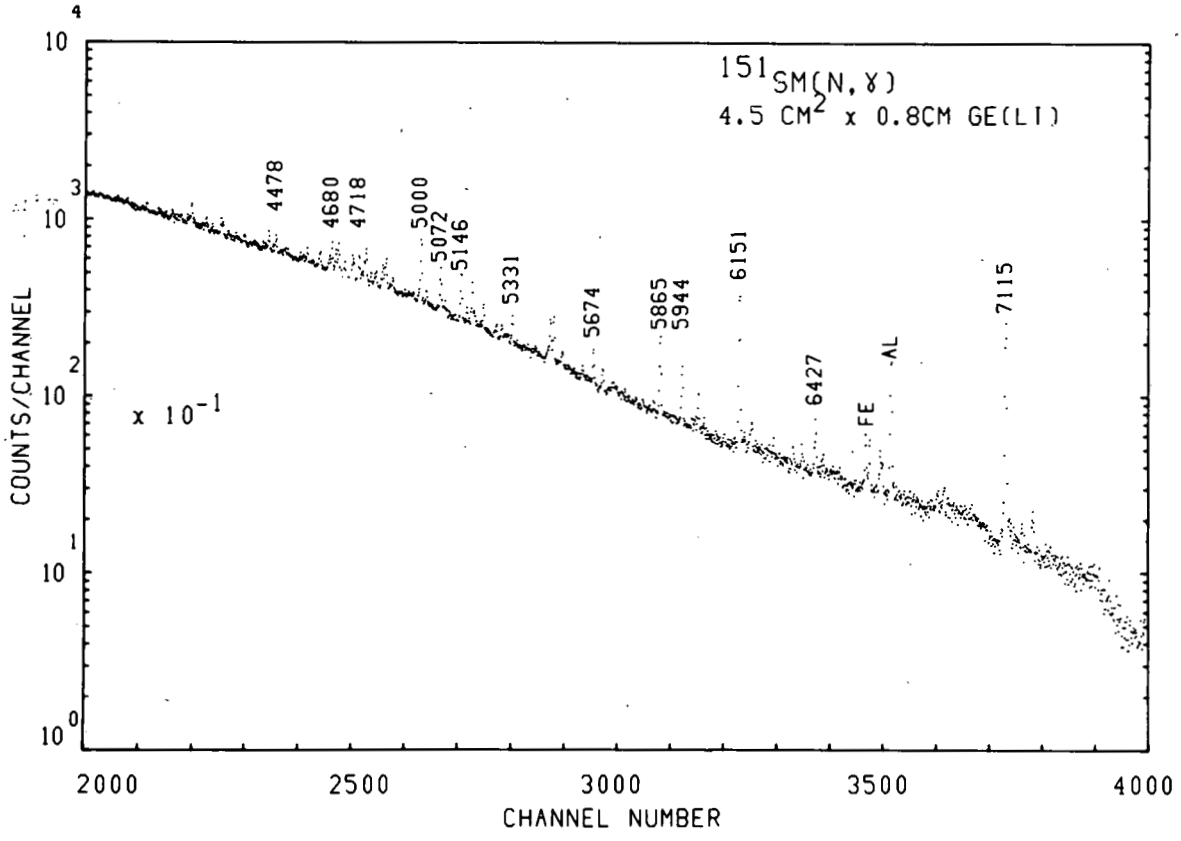

Figure 1 The high-energy portion of the prompt γ-ray spectrum resulting from thermal neutron capture in ^{151}Sm.

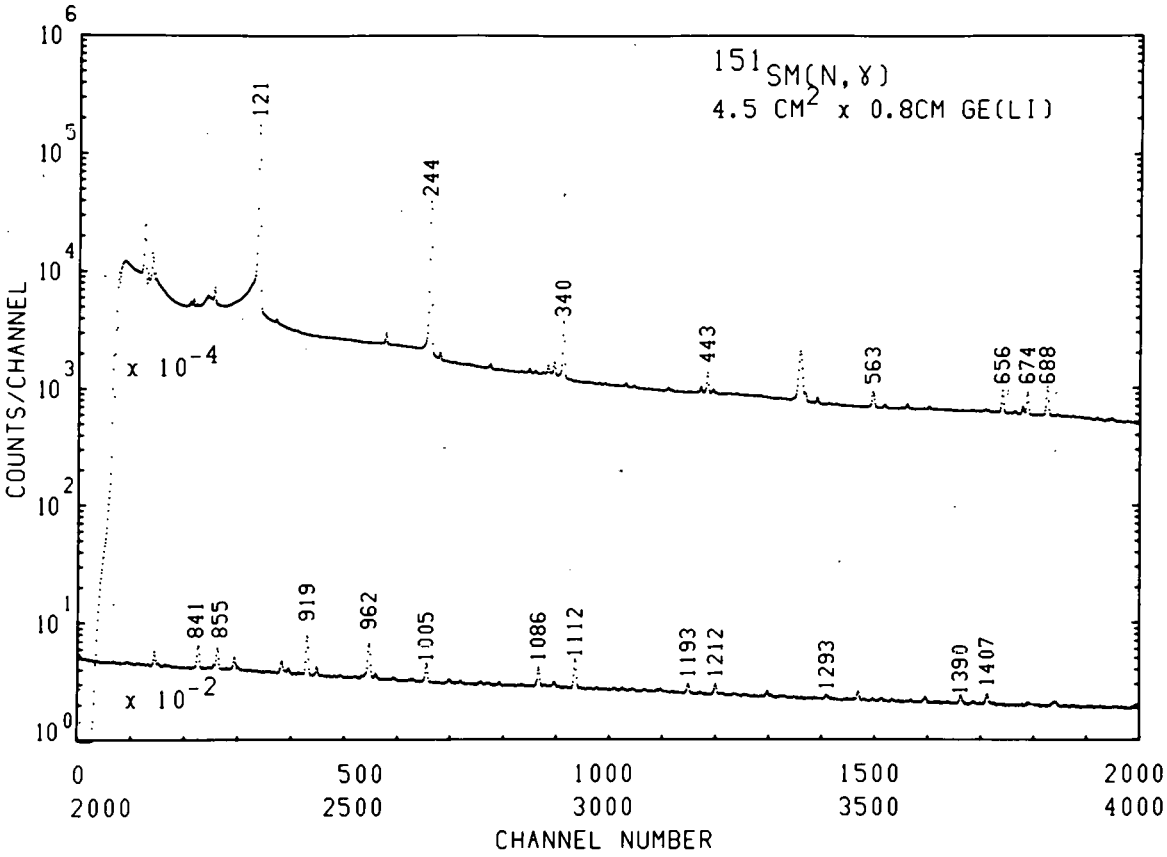

Figure 2 The low-energy portion of the prompt γ-ray spectrum resulting from thermal neutron capture in ^{151}Sm.

EVEN PARITY STATES IN ^{178}Hf FROM THE ^{177}Hf(n,γ) REACTION

R. C. Greenwood, C. W. Reich

Levels in the deformed even-even nucleus ^{178}Hf have been studied extensively through the decay of ^{178}Ta (e.g., References [1,2]) and through the decay of ^{178}Lu[3]. These studies have revealed the existence of four excited 0^+ states below 2 MeV. Further information about the level structure of this nucleus has been obtained from studies of the ^{177}Hf(d,p)[4], ^{179}Hf(d,t)[4], ^{178}Hf(d,d')[4] and ^{180}Hf(p,t)[5] reactions. Noteworthy in these studies has been the establishment of both the $K^\pi = 3^+$ and 4^+ bands resulting from the coupling of the $7/2^-[514]$ and $1/2^-[510]$ neutron orbitals.

The present studies of the prompt γ rays emitted as a result of neutron capture in ^{177}Hf were undertaken to provide further information on the higher spin states in ^{178}Hf. Since the compound nuclear states which result from s-wave neutron capture have $I^\pi = 3^-$ and 4^-, the primary E1 transitions will populate states with $I^\pi = 2^+$-5^+. Several earlier

studies of the neutron capture have been made (e.g., References [6-8]) but the availability of the 2-keV neutron capture data will, we believe, provide more complete information on these final states with spins 2 through 5. Because of the finite energy spread of the 2-keV neutrons ($\sim$ 0.7 keV FWHM) we estimate that the resulting capture γ-ray spectrum of ^{177}Hf represents an average over $\sim$ 200 resonance states, thus providing good averaging of the Porter-Thomas statistical fluctuations in the intensities of the primary transitions. This spectrum is shown in Figure 1. The corresponding portion of the thermal neutron capture spectrum is also included in Figure 1 for comparison. Primary E1 transitions are easily distinguished from M1 transitions (at least for those transitions populating final states with energies < 2 MeV) by comparing their reduced transition intensities, as shown in Figure 2. This plot also provides some distinction between primary E1 transitions to final states with $I^\pi = 3^+$ and 4^+ and those with $I^\pi = 2^+$ and 5^+.

When these primary capture γ-ray data are combined with the extensive data on the low-energy secondary transitions which were also measured we are able to construct the preliminary level scheme shown in Figure 3 for positive parity states in ^{178}Hf. Features of this level scheme which are of special interest include:

- the establishment of the fact that there are no more than four excited $K^\pi = 0^+$ bands below 2 MeV;
- the location of the 4^+ members of each of these excited $K^\pi = 0^+$ bands;
- the location of members of the γ-vibrational band up to spin 6;
- the determination of the modes of decay of the $K^\pi = 3^+$ and 4^+ bands resulting from the coupling of the $7/2^-[514]$ and $1/2^-[510]$ neutron orbitals;
- the establishment of another band with $K^\pi = 3^+$ located at 1758 keV. States in this band decay principally to states in the $K^\pi = 2^-$ octupole vibrational band.

If we now consider specific features of the de-excitations of some of the bands:

γ-vibrational band. While we are in agreement with Fogelberg and Bäcklin[8] on the location of states in this band with $I^\pi \leq 6^+$ we are in substantial disagreement with them on the values of the band-mixing parameters which are necessary to fit the transition intensities from these states to the ground state. While they have proposed that a value of $Z_2 \sim 0.014$ can be used to fit these transition intensities, our data, shown in Table I, would indicate that for states with $I^\pi \leq 4^+$ $Z_2 \sim 0.037$ and for the states with $I^\pi = 5^+$ and 6^+ $Z_2 \sim 0$.

$K^\pi = 0^+$ bands. Relative transition intensities from the 2^+ and 4^+ members of the $K^\pi = 0^+$ bands are shown in Table II. The decay modes from the two lower-lying 2^+ states have been studied in great detail in the decay of ^{178}Ta. Little et al.[1] have shown that the $\Delta I = 0$ transitions have substantial M1 components (86% and 65%, respectively, for the 1183- and 1402-keV transitions). While, as we see from the

final column in Table II, their measured M1 component is actually too large to allow the transition intensities from the 1276-keV level to be fit using a single z_0 parameter, their data are in agreement with the implied M1 component in the decay of the 1496-keV state. Our present data would also imply that there is a significant M1 component in the decay of the 4^+ state at 1450 keV. On the other hand, it is the $\Delta I = 0$ transition which appears to be too weak in the decay from the 1561-keV state, so that an M1 admixture in this transition can only serve to worsen the disparity in the computed z_0 parameters. It is of interest to note that the $\Delta I = +2$ transition is rather weak for both the 1496- and 1636-keV states which might therefore imply a $K^\pi = 2^+$ admixture in this $K^\pi = 0^+$ band.

[1] P. E. Little, J. H. Hamilton, A. V. Ramayya and N. R. Johnson, Phys. Rev. C 5, (1972) 252.
[2] T. A. Siddiqi and G. T. Emery, Phys. Rev. C 6, (1972) 1002.
[3] C. J. Orth, W. R. Daniels, F. O. Lawrence and D. C. Hoffman, Bull. Am. Phys. Soc. 15, (1970) 523.
[4] M. M. Minor, thesis, Florida State University (1968).
[5] M. A. Oothoudt and N. M. Hintz, to be published.
[6] R. K. Smither, Phys. Rev. 129, (1963) 1691.
[7] P. T. Prokofjev and G. L. Rezvaja, Izv. Akad Nauk SSSR 33, (1969) 1655.
[8] B. Fogelberg and A. Bäcklin, Nucl. Phys. A171, (1971) 353.

TABLE I

RATIOS OF REDUCED TRANSITION PROBABILITIES FOR DECAY FROM STATES OF THE γ-VIBRATIONAL BAND TO LEVELS IN THE GROUND-STATE BAND

Initial State		Transition Ratio	Experimental	Alaga Rules	Mixing Parameter
Energy (keV)	I,K^π	$(I_i 2 \to I_f 0)/(I_i 2 \to I_f' 0)$	B(E2) Ratio	(without band mixing)	Z_γ ($\times 10^3$)
1174	$2,2^+$	B(2;22→00)/B(2;22→20)	0.580(26)[a]	0.798	32(10)
		B(2;22→40)/B(2/22→20)	<0.087[a]	0.050	<45
1268	$3,2^+$	B(2;32→40)/B(2;32→20)	0.62(6)	0.400	34(8)
1384	$4,2^+$	B(2;42→20)/B(2;42→40)	0.175(15)	0.340	44(6)
		B(2;42→60)/B(2;42→40)	0.39(6)	0.088	125(53)
1533	$5,2^+$	B(2;52→60)/B(2;52→40)	0.51(9)	0.571	-5(7)
1384	$6,2^+$	B(2;62→40)/B(2;62→60)	0.260(44)	0.269	2(5)
		B(2;62→80)/B(2;62→60)	<7.1	0.107	

[a] Using the γ-ray intensities measured by Little et al. for the ^{178}Ta decay.

TABLE II

RATIOS OF REDUCED E2 TRANSITION PROBABILITIES FOR DECAY FROM MEMBERS OF THE EXCITED $K^{\pi}=0^{+}$ BANDS TO LEVELS IN THE GROUND-STATE BAND

Initial State Energy (keV)	I,K^{π}	Transition Ratio $(I_i 0 \rightarrow I_f 0)/(I_i 0 \rightarrow I_f' 0)$	Experimental B(E2) Ratio	Alaga Rules (without band mixing)	Mixing Parameter Z_o (x 10^3)	%M1 in $\Delta I=0$ Transition[a]
1276	$2,0^+$	B(2;20→00)/B(2;20→20)	0.164(21)	0.700	74(18)	67[b]
		B(2;20→40)/B(2;20→20)	1.13(10)	1.80	-15(2)	
		B(2;20→40)/B(2;20→00)	6.9(9)	2.58	27(4)	
1450	$4,0^+$	B(2;40→20)/B(2;40→40)	0.045(9)	1.10	57(2)	
		B(2;40→60)/B(2;40→40)	0.29(5)	1.75	-27(2)	92
		B(2/40→60)/B(2;40→20)	6.4(16)	1.59	20(4)	
1496	$2,0^+$	B(2;20→00)/B(2;20→20)	0.408(18)[c]	0.700	39(2)	
		B(2;20→40)/B(2;20→20)	0.129(5)[c]	1.80	-52(1)	62[d]
		B(2;20→40)/B(2;20→00)	0.316(13)[c]	2.58	-40(1)	
1636	$4,0^+$	B(2;40→20)/B(2;40→40)	>0.16	1.10	<44	
		B(2;40→60)/B(2;40→20)	<0.47	1.59	< 4	
1561	$2,0^+$	B(2;20→00)/B(2;20→20)	1.11(28)[e]	0.700	-43	
		B(2;20→40)/B(2;20→20)	7.5(12)[e]	1.80	74(12)	
		B(2;20→40)/B(2;20→00)	6.8(14)	2.58	27(6)	
1818	$2,0^+$	B(2;20→00)/B(2;20→20)	<0.21	0.700	>76	
		B(2;20→40)/B(2;20→20)	0.55(10)	1.80	-32(4)	>70
		B(2;20→40)/B(2;20→20)	>2.6	2.58	> 0	

[a] The amount of M1 admixture in the $\Delta I=0$ transition which would be necessary to allow each of the ratios to be fit with the band mixing parameter deduced from the B(2;I0→[I+2]0)/B(2;I0→[I-2]0) ratio.

[b] To be compared to the measured M1 admixture of $(85.6^{+1.1}_{-2.1})\%$.

[c] Using the γ-ray intensities measured by Little *et al.*[1] for the ^{178}Ta decay.

[d] To be compared to the measured M1 admixture of $(65.2 \pm 3.2)\%$.

[e] Since it is the $\Delta I=0$ transition which is too weak, an M1 admixture will only worsen the disparity in the computed Z_o parameters.

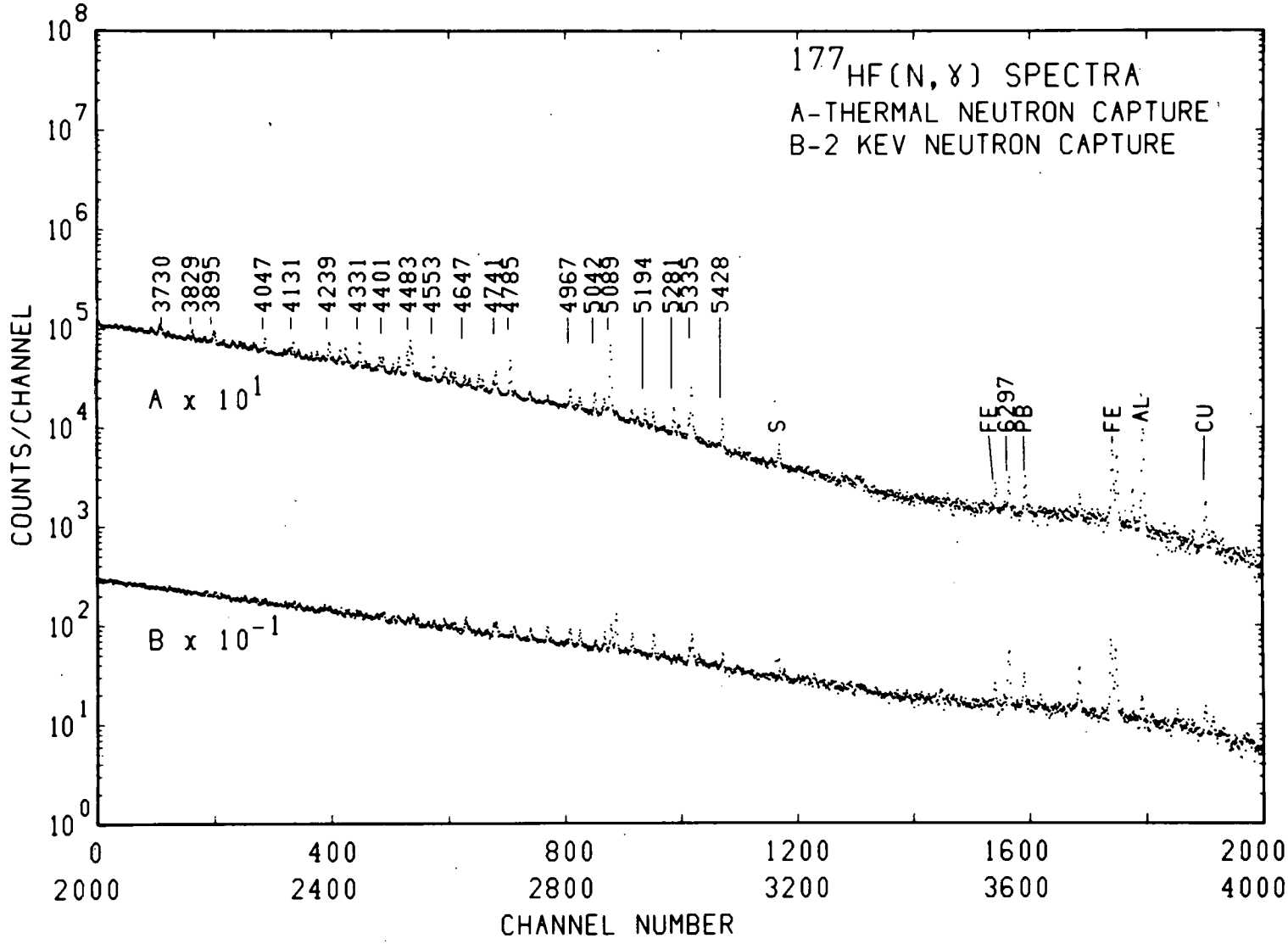

Figure 1 Comparison of the high-energy portions of the prompt γ-ray spectra resulting from 2-keV and thermal neutron capture in ^{177}Hf.

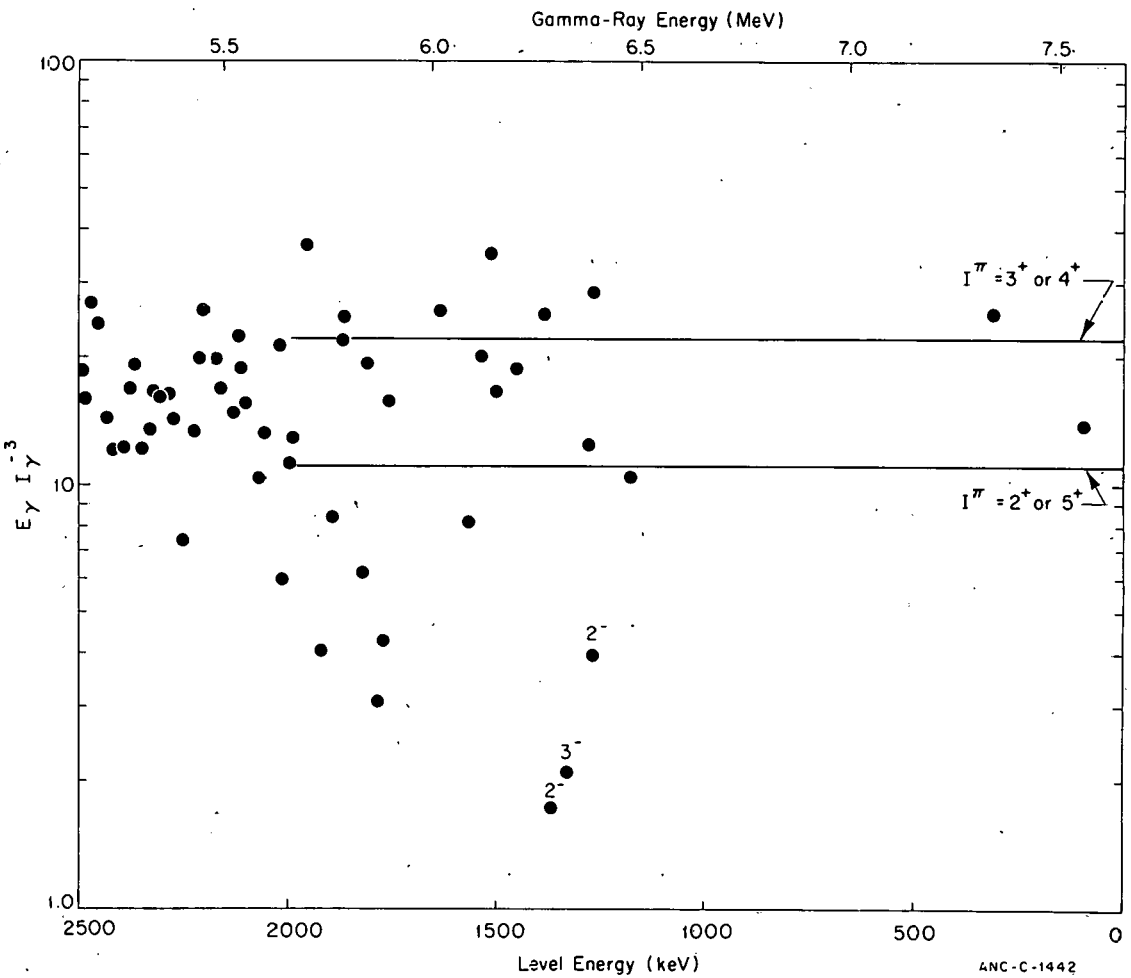

Figure 2 Reduced γ-ray intensities for the 2-keV neutron capture data plotted as a function of transition energy.

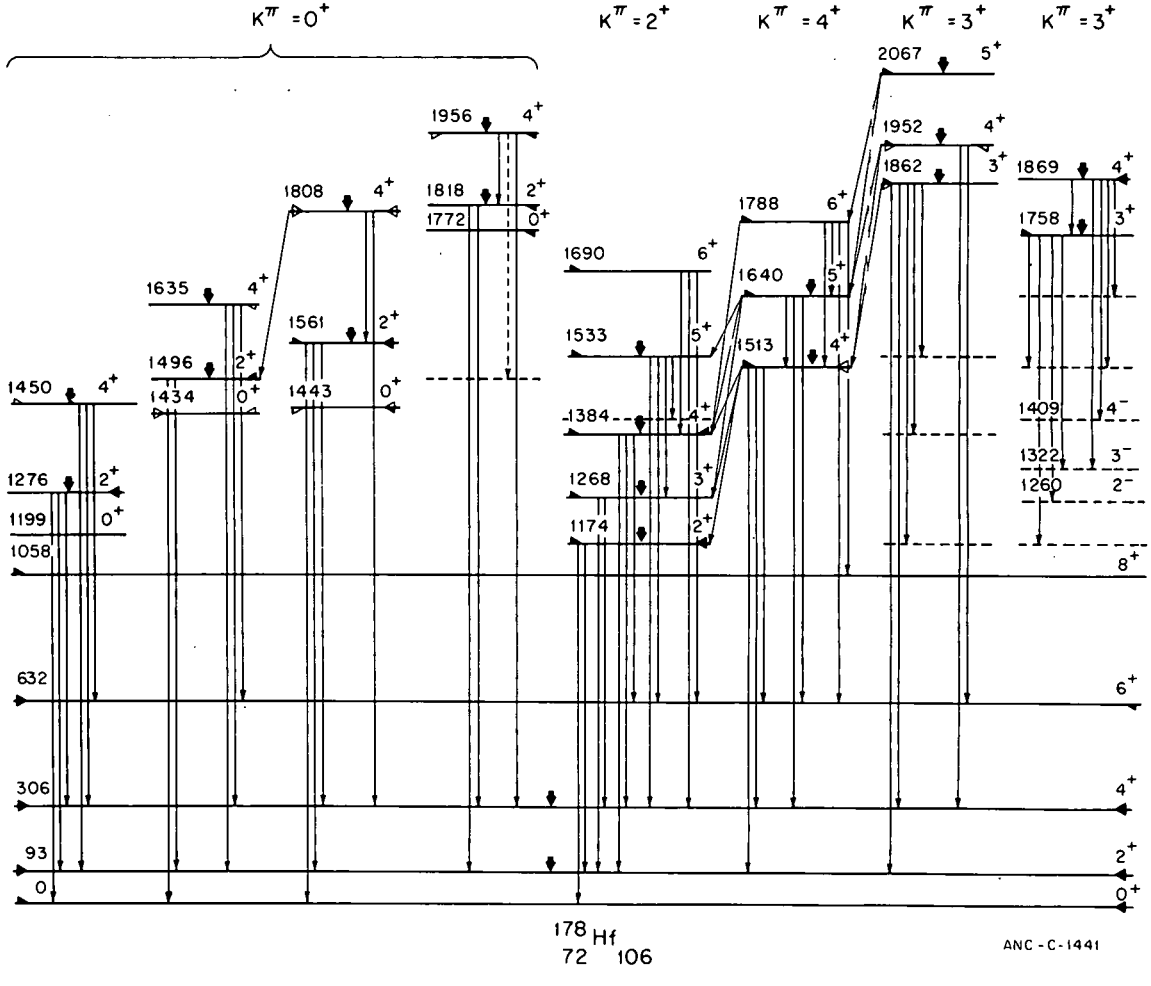

Figure 3 Level scheme for the positive parity states in ^{178}Hf based upon the $^{177}Hf(n,\gamma)$ reaction studies with proposed grouping of states into rotational bands. An arrow into a level indicates population by primary γ-ray transitions. Solid triangles associated with a level indicate that the level is populated by charged particle reactions: upper left indicates (d,p) population, lower left indicates (d,t) population, upper right indicates (d,d') population, and lower right indicates (p,t) population. Open triangles indicate tentative assignments.

STUDIES OF THE $^{168}Yb(n,\gamma)$ REACTION

R. C. Greenwood, C. W. Reich

Analysis of the prompt γ-ray spectra resulting from thermal neutron capture in ^{168}Yb is continuing. These data were obtained using the external neutron beam from the HR-4 facility at the MTR with the γ rays being detected with various Ge(Li) detectors.

This work is being undertaken in a cooperative effort with scientists from Technische Universität München, West Germany (who have made high resolution prompt γ-ray measurements with a bent crystal spectrometer) and Uppsala Universitet, Sweden (who have measured the prompt conversion electron spectrum using a magnetic beta spectrometer) in an effort to improve our understanding of the level structure in the deformed ^{169}Yb nucleus. The energies and relative intensities of the primary prompt γ rays resulting from the $^{168}Yb(n,\gamma)$ reaction are shown in Table I. From the measured energies of those primary γ-ray transitions which populate levels in ^{169}Yb whose energy is previously known, an average value for the neutron binding energy in ^{169}Yb is determined to be 6866.7 ± 0.6 keV. This value for the thermal neutron capturing state energy can then be used in the CAPSPC computer program to compute energies of these states in ^{169}Yb which are populated by primary γ-ray transitions. These final-state energies are also included in Table I. Since the ground state of ^{168}Yb has $I^{\pi} = 0^{+}$ compound-nucleus states in ^{169}Yb with $I^{\pi} = \frac{1}{2}^{+}$ result from s-wave neutron capture. Consequently, primary dipole γ-ray transitions will populate final states in ^{169}Yb with spins $\frac{1}{2}$ and $\frac{3}{2}$, with the more probable E1 transitions populating final states with negative parity.

TABLE I

PRIMARY γ-RAY TRANSITIONS FROM THE $^{168}Yb(n,\gamma)$ REACTION

γ-Ray Energy (keV)	Error (keV)	Relative γ-Ray Intensity	Error (keV)	Level Energy (keV)	Error (keV)
6842.5	0.6	23.0	5	24.201	---
6779.8	0.6	100.0	5	86.93	0.04
6207.1	0.6	15.1	5	659.64	0.05
6146.8	0.7	2.09	10	719.97	0.25
6053.4	0.6	17.8	5	813.31	0.06
6017.7	2.0	0.9	50	849.0	2.0
5832.7	1.0	1.5	15	1034.1	0.7
5706.7	0.8	0.9	20	1160.4	0.5
5664.2	0.8	1.1	15	1202.6	0.5
5643.0	1.2	0.5	30	1223.8	1.1
5633.5	1.2	0.5	30	1233.3	1.1
5595.6	0.6	7.8	7	1271.12	0.15
5517.2	0.7	5.2	10	1349.56	0.25

TABLE I (Cont.)

γ-Ray Energy (keV)	Error (keV)	Relative γ-Ray Intensity	Error (keV)	Level Energy (keV)	Error (keV)
5511.9	0.7	6.1	10	1354.90	0.25
5468.3	0.6	11.1	7	1398.55	0.10
5388.3	0.7	2.5	10	1478.51	0.25
5356.9	0.8	0.9	20	1509.9	0.5
5342.7	0.7	1.9	15	1524.06	0.30
5334.4	0.6	3.2	10	1532.36	0.20
5312.0	0.7	1.8	10	1554.77	0.25
5281.1	0.8	1.2	15	1585.7	0.4
5247.4	0.6	24.5	7	1619.36	0.10
5169.5	0.6	5.8	7	1697.22	0.15
5142.7	0.7	1.9	15	1724.05	0.30
5121.6	0.7	1.9	15	1745.10	0.30
5109.3	0.8	1.1	15	1757.5	0.5
5079.3	0.7	5.4	10	1787.5	0.3
5069.2	0.7	5.3	10	1797.5	0.3
5037.8	0.8	3.1	10	1829.0	0.4
5029.1	0.6	2.8	10	1837.70	0.25
5009.2	0.8	2.9	15	1857.7	0.4
4997.6	1.2	0.9	30	1869.1	1.0
4972.6	0.7	2.4	10	1894.16	0.25
4955.7	1.0	0.7	30	1911.0	0.7
4946.1	0.8	1.6	30	1920.6	0.5
4927.6	0.6	7.9	7	1939.14	0.15
4868.2	0.6	5.0	10	1998.55	0.20
4828.9	0.7	5.5	15	2037.9	0.3
4818.4	1.1	0.9	40	2048.4	0.8
4763.0	0.6	2.7	10	2103.79	0.25
4743.4	1.2	1.0	30	2123.4	1.0
4673.7	0.9	1.3	20	2193.1	0.6
4649.1	1.0	1.4	30	2217.6	1.0
4632.1	0.8	3.0	15	2234.7	0.4
4622.1	0.6	7.1	7	2244.69	0.20
4580.4	1.2	0.8	30	2286.3	1.0
4567.5	0.8	2.1	15	2299.3	0.4
4553.0	0.6	3.5	10	2313.65	0.25
4524.2	0.8	2.4	15	2342.5	0.4
4516.5	0.7	5.4	10	2350.2	0.3
4511.0	0.7	5.2	10	2355.7	0.3
4490.7	1.0	1.0	30	2376.0	0.7
4485.2	1.0	1.2	30	2381.5	0.7
4478.6	0.8	3.5	10	2388.1	0.4
4465.6	0.8	3.0	15	2401.1	0.4
4459.2	0.8	2.1	15	2407.5	0.4
4451.2	0.8	4.0	10	2415.5	0.4
4439.1	1.0	1.0	25	2427.7	0.7
4425.5	0.9	1.5	20	2441.3	0.5
4416.8	0.7	1.7	15	2450.0	0.4
4388.7	1.0	2.5	20	2478.0	0.7

TABLE I (Cont.)

γ-Ray Energy (keV)	Error (keV)	Relative γ-Ray Intensity	Error (keV)	Level Energy (keV)	Error (keV)
4367.9	0.7	2.6	20	2498.9	0.4
4362.2	0.8	1.5	20	2504.6	0.5
4349.5	1.0	1.6	25	2517.2	0.7
4343.8	0.7	3.4	15	2522.9	0.4
4336.3	0.7	1.6	25	2530.4	0.4
4315.5	0.7	2.8	15	2551.2	0.4
4245.7	1.0	2.3	20	2621.0	0.8
4232.6	1.2	0.8	30	2534.2	1.0
4211.2	0.6	8.1	7	2655.58	0.25
4186.9	0.7	4.2	25	2679.8	0.4
4181.8	1.1	1.7	40	2684.9	0.9
4160.7	0.7	4.5	10	2706.0	0.3
4124.8	0.8	2.8	20	2742.0	0.4
4092.1	0.8	3.5	15	2774.7	0.4
4085.6	0.9	2.1	30	2781.2	0.7
4064.7	0.9	3.8	20	2802.0	0.7
4039.4	0.6	6.6	10	2827.5	0.3
4010.6	0.8	2.6	20	2856.2	0.5
3996.7	0.8	1.8	20	2870.1	0.5
3975.0	0.6	7.8	10	2891.7	0.3
3949.3	0.7	2.2	30	2917.4	0.4
3933.8	1.5	1.9	40	2932.9	1.5
3914.6	1.0	2.2	25	2952.3	0.7
3878.0	0.8	4.0	15	2988.8	0.5
3867.7	0.9	1.3	30	2999.1	0.7
3851.4	1.2	2.1	40	3015.3	1.1
3839.2	0.8	3.5	20	3027.6	0.6
3828.2	0.7	4.5	20	3038.6	0.4
3822.8	0.7	3.9	20	3044.0	0.4
3800.5	0.7	2.8	15	3066.3	0.4
3772.1	0.8	2.0	30	3094.6	0.5
3761.0	0.6	6.3	10	3105.8	0.3
3747.7	1.1	2.9	30	3119.0	1.0
3736.3	0.8	2.4	30	3130.5	0.6
3724.0	0.7	5.0	15	3142.9	0.5
3692.8	0.7	3.6	20	3174.0	0.4
3620.1	0.8	2.8	40	3246.6	0.5
3592.6	1.5	3.6	40	3274.1	1.5
3522.2	0.7	4.2	15	3344.6	0.4
3491.2	0.7	2.3	25	3375.6	0.5
3416.6	0.8	3.1	20	3450.1	0.6
3339.9	0.7	6.5	20	3527.0	0.5
3306.7	0.8	4.0	30	3560.1	0.5
3209.6	1.0	1.9	30	3657.1	0.8

HALF-LIFE OF ^{178m_2}Hf AND ITS NEUTRON CAPTURE PRODUCTION

R. G. Helmer, C. W. Reich

In Reference [1], the existence of a long-lived high-spin isomeric state of ^{178}Hf and a study of its decay were reported. In the present work, we report the results of a measurement of the half-life and neutron-capture production cross section of this isomeric state. For the experiments discussed in this paper, four ^{178m_2}Hf samples were used. The irradiation and chemical histories of these samples are given in Table I.

The half-life of ^{178m_2}Hf was determined from 18 gamma-ray spectra for sample #1 (see Table I) measured on one Ge(Li) detector over a period of six years. The first spectra of this set were taken about three years after the neutron irradiation; before that time other activities were too intense to permit observation of the ^{178m_2}Hf lines. For each spectrum, the intensities of six of the gamma rays from ^{178m_2}Hf were determined relative to that of the 270-keV line from ^{182}Hf ($T_{1/2}$ = 9 x 10^6 yr). This comparison method should minimize any error that might result from changes in the detector efficiency over the long period involved. In the analysis the same detector efficiencies were used throughout the six years; therefore, the errors in the relative intensities include only those contributions from the peak areas.

The data for each gamma ray were analyzed by means of a weighted, least-squares fit of a linear function to the logarithm of the observed relative intensity. The resulting values are given in Table II. The normalized χ^2 values

$$\left\{ \text{i.e.,} \quad \frac{1}{n-2} \sum_{i=1}^{n} w_i \left[\ln\left(y_i\right) - a - bx_i \right]^2 \right\}$$

for the six fits averaged 1.9 and ranged from 0.8 to 2.9. This indicates some systematic errors in the data, but this may not be unreasonable considering the long period involved. For example, a change in the relative detector efficiency at the various energies could introduce such an error. For the weighted average of the six half-life values, the normalized χ^2 is $\tilde{\sim}$ 1.0, which indicates excellent agreement. The adopted half-life value is 31 ± 1 y.

The energy and multipolarity of the isomeric transition emitted in the decay of ^{178m_2}Hf have not yet been established. As discussed in Reference [1], we feel that the isomeric transition is most probably a low-energy (< 0.1 MeV) E3 transition, although a 238-keV M4 transition is possible. The latter is the only observed unplaced transition in the ^{178m_2}Hf decay[1].

From the measured half-life, the absolute gamma-ray transition probabilities have been computed for various assumed energies and

multipolarities as shown in Table III. For a 4-times K-forbidden M4 (from $I,K^{\pi} = 17,16^{+}$ to $13,8^{-}$), the hindrance is about 20 per unit of K forbiddenness. For a 5-times K-forbidden E3 (from $I,K^{\pi} = 16,16^{+}$ to $13,8^{-}$), the same factor is about 75 to 110 for the energy range shown. Although this comparison is by no means conclusive, it may lend support to the E3 preference.

A measurement has been made of the cross section for production of this ^{178}Hf isomer in the neutron spectrum of a thermal reactor (i.e., the Materials Testing Reactor). Data from all four samples listed in Table I were used for this measurement. The basic data were the decay rates of samples #3 and #4 after their six-month irradiation in a flux of 5×10^{14} n/cm^2-sec. However, the activity of the ^{178m_2}Hf depends also on its burnup during the irradiation. An upper limit on this burnup cross section was determined from the data from samples #1 and #2.

Because of the large difference in the neutron exposure, a limit on the burnup cross section of ^{178m_2}Hf can be determined from the relative amounts of ^{178m_2}Hf and ^{182}Hf in the two samples, #1 and #2. However, this ratio cannot be used for a quantitative calculation since the burnup cross section for ^{182}Hf itself is not known. From the analysis of the gamma-ray spectra of samples #1 and #2 (Table I), we conclude qualitatively that the ^{178m_2}Hf burnup cross section is less than 20 b.

The production cross section is then found to be 2.3×10^{-7} b. Since the actual integrated flux at the sample may be in error by, say, 25% and there is a 20% uncertainty from the unknown burnup, the final cross section and uncertainty are taken to be $(2 \pm 1) \times 10^{-7}$ b.

The measured cross section for production of ^{178m_2}Hf may be of interest for comparison with models[4-6] used to predict isomeric cross-section ratios. This is especially true since its spin is 12 or more units greater than that of the capturing state. It should be noted that, in some cases, the intensities of gamma rays observed in the (n,γ) reaction give cross sections for production of particular states. Since data of this type exist[7] for ^{177}Hf(n,γ), they have been summarized in Table IV along with the value for the isomer. It is felt that this amount of data, over a large range of final-state spins, may be sufficient to give a much better determination of the several model parameters than is possible for the usual case of only one cross-section ratio per isotope.

---

[1] R. G. Helmer and C. W. Reich, Nucl. Phys. A114, (1968) 649.
[2] R. S. Hager and E. C. Seltzer, Nuclear Data A4, (1968) 1.
[3] S. A. Moszkowski, in Alpha-, Beta- and Gamma-ray Spectroscopy, ed. K. Siegbahn (North-Holland, Amsterdam, 1965) Vol. II, Chapt. XV.
[4] H. K. Vonach, R. Vandenbosch and J. R. Huizenga, Nucl. Phys. 60, (1964) 70.
[5] W. P. Pönitz, Z. Physik 197, (1966) 262.
[6] D. Sperber and J. W. Mandler, Nucl. Phys. A113, (1968) 689.
[7] R. C. Greenwood and C. W. Reich, Nuclear Technology Branch Annual Progress Report for Period Ending June 30, 1970, IN-1407 (1970) 142.
[8] Brookhaven National Laboratory Report BNL-325, Third Edition, to be published.

TABLE I

HISTORY OF ^{178m2}Hf SAMPLES

Sample Number	Mass of Hf (mg)	^{177}Hf Enrichment (atom %)	Neutron Radiation			Chemistry (Element Removed)
			Dates	Flux[a] (10^{14} n/cm^2-sec)	Integrated Flux (10^{20}n/cm^2)	
1	--	18.5 (normal)	7/1961-7/1963	4.6-5.7	264	Ta, rare earths, etc.
2	--	18.5 (normal)	7/1961-1/1962	5.1	66	Ta, rare earths, etc.
3	27.4	84	9/1967-3/1968	5.0	69	Co, rare earths (not Ta)
4	120	84	9/1967-3/1968	5.0	69	None

[a] Unperturbed value.

TABLE II

DETERMINATION OF THE HALF-LIFE OF ^{178m2}Hf FROM GAMMA-RAY INTENSITIES MEASURED RELATIVE TO THAT OF THE 270-keV LINE FROM ^{182}Hf

Gamma-Ray Energy (keV)	Half-life[a] (years)	ε^2[b]
213	29.9 ± 1.4	1.5
216	30.3 ± 1.2	0.8
325	34.6 ± 2.5	1.9
426	40.1 ± 6.4	2.5
495	31.0 ± 3.2	1.8
574	33.4 ± 4.6	2.9
Average (weight = $1/\sigma^2$)	30.9 ± 0.8	1.06
Average (weight = $1/\sigma$)	31.8 ± 1.0	1.3
Adopted value	31 ± 1	

[a] Uncertainty includes a factor $\sqrt{\varepsilon^2}$ if this quantity is >1.0.

[b] Normalized χ^2 value as defined in text.

TABLE III

GAMMA-RAY TRANSITION PROBABILITIES OF THE ISOMERIC TRANSITION FROM ^{178m_2}Hf FOR VARIOUS ENERGIES AND MULTIPOLARITIES (CALCULATED ASSUMING $T_{1/2}$ = 31 y)

E_γ (keV)	Multipolarity	α_T [a]	Deduced Gamma-Ray Transition Probability (sec^{-1})	Hindrance Factor [b]
20	E3	8×10^5	8.9×10^{-16}	1.5×10^9
51	E3	3.5×10^3	2.0×10^{-13}	3.8×10^9
102	E3	67	1.0×10^{-11}	1.2×10^{10}
128	E3	20	3.4×10^{-11}	1.8×10^{10}
238.6	M4	31	2.2×10^{-11}	1.7×10^5

[a] Theoretical values[2].

[b] Hindrance factor of the transition relative to the Moszkowski[3] estimate.

TABLE IV

CROSS SECTIONS FOR (n,γ) POPULATION OF VARIOUS STATES IN ^{178}Hf

Level Energy (keV)	I^π	Cross Section (b)	Reference
0	0^+	365	8
1147	8^-	0.93	7
1364	9^-	0.048	7
1479	8^-	0.25	7
≈ 2450	16^+ (17^+)	$(2 \pm 1) \times 10^{-7}$	This work

LEVEL STRUCTURE OF ^{184}W FROM DECAY OF ^{184g}Re AND ^{184m}Re

R. C. Greenwood, C. W. Reich, R. G. Helmer, D. J. McMillan[1]

The level structure of the doubly even nucleus ^{184}W has previously been investigated using a variety of experimental techniques. In many of these studies, the ^{184}W levels have been populated by the decay of 38-d ^{184g}Re (the ground-state decay) and 165-d ^{184m}Re (the isomer decay). The results of the earliest studies of these nuclear decay modes has been summarized in Reference [2]. Many of the salient features of the decay of the ground and isomeric states of ^{184}Re were established in the work of Harmatz and Handley[3] and in subsequent studies by other investigators[4-10], including a preliminary report[11] of some aspects of the present work. Further details of the level structure of ^{184}W have been obtained from studies of the ^{184}Ta decay[2,12], the prompt γ rays emitted as a result of thermal[13,14], resonance[13,15-17], and 2-keV[14] neutron capture in ^{183}W, Coulomb excitation[18], the ^{183}W(d,p) reaction[19] and the ^{183}W(d,d') reaction[20].

These studies established the following features of the ^{184}W level scheme: the γ-vibrational band at 903 keV; a $K^{\pi}=0^{+}$ band at 1002 keV; the $K^{\pi}=5^{-}$ and 7^{-} bands at 1284 and 1501 keV, respectively; and an octupole band with a 3^{-} state at 1221 keV and an associated 2^{-} state tentatively proposed as the level at 1129 keV.

The present work was undertaken to obtain more complete information on the decay of the isomeric and the ground states of ^{184}Re. In a parallel effort, measurements were made of the prompt γ rays emitted as a result of neutron capture in ^{183}W. These latter results are discussed in a following report[21]. Together these studies provide a more complete level scheme for the ^{184}W nucleus and information about the make-up of many of these states.

Several publications have recently appeared giving results of additional studies of the ^{184}W level structures. These studies involve investigations of the decay of ^{184m}Re[22,23], the decay of ^{184}Ta[24], the prompt γ rays emitted as a result of neutron capture in the 7.8-eV resonance of ^{183}W[25], and the ^{182}W(t,p)[26] and ^{183}W(d,p)[27] reactions. The study of the ^{184m}Re decay by Canty *et al.*[23], while not providing as complete information on the levels populated or on their decay modes, is in essential agreement with this present work, as are the results of the ^{184}Ta decay[24] for those levels which are observed in both decay modes. From γ-ray angular distribution measurements from a source of aligned ^{184}Re nuclei, Krane *et al.*[22] measured multipole mixing ratios for many of the stronger γ-ray transitions. The recent particle transfer reaction studies[26,27] also provide additional valuable insights into the make-up of several of the ^{184}W levels.

The ^{184}Re source which was principally used in the present work was produced $\sim$ 3-1/2 years ago by irradiating natural tungsten (with a low rhenium impurity level) with 22-MeV protons in the internal beam of the 218-cm cyclotron at Oak Ridge National Laboratory. Specific measurements

which have been made with this source include:

- γ-ray spectrum measurements with various Ge(Li) and Si(Li) detectors soon after source production and at frequent intervals thereafter up to the present time. At short times (a few months) after source production the dominant activities were ^{184g}Re and ^{183}Re while at the present time the dominant activity is ^{184m}Re with only a trace of ^{183}Re remaining. Portions of the ^{184m}Re spectra are shown in Figures 1 and 2; and the energies and intensities of the γ-ray transitions associated with the ^{184g}Re and ^{184m}Re decays are summarized in Table I.

- γ-γ coincidence measurements conducted soon after source production (as described in Reference [11]).

- conversion electron measurements using a 35-cm radius iron-free $\pi\sqrt{2}$ electron spectrometer made soon after source production (as described in Reference [11]) and ∿ 1.5 years later. Internal-conversion coefficients derived from these data together with the γ-ray data are summarized in Table II. These conversion coefficients are quite consistent with those which can be computed from the conversion-electron intensities reported by Ageev et al.[6,7] and the γ-ray intensities for ^{184m}Re listed in Table I. Conversion coefficients computed in this way for several of the transitions not measured in the present work are shown in Table III.

The ^{184}Re decay scheme which was constructed using these data is shown in Figure 3. The "best" set of level energies, given in Table IV, was determined for ^{184}W utilizing a linear least-squares fitting program. The electron-capture branching ratios and log ft values which have been computed from these branching ratios for a ^{184}Re decay energy of 1496 ± 6 keV† are shown in Table V.

While many of the features of this scheme are in substantial agreement with those proposed by earlier investigators[3,4,6-10], the present data provide a more complete characterization of the ^{184}W level scheme. These additional features include:

- new levels at 1425 and 1431 keV with $I^{\pi}=3^{+}$ and 2^{+}, respectively;

- establishment of $I^{\pi}=2^{-}$ for the 1130-keV state;

- placement of transitions from the 5^{-} state at 1284 keV to the 2^{+} and 4^{+} members of the γ-vibrational band;

† From measurements of Q values of (^{3}He,d), (α,t) and (d,t) reactions on various tungsten and rhenium isotopes, D. Elmore obtained two determinations of the ^{184}Re-^{184}W mass difference, 1491 ± 5 keV and 1502 ± 17 keV. The value given is just an average of these two numbers.

- placement of a transition between the 1130-keV state and the 3^+ member of the γ-vibrational band; and

- placement of the $4^+ \rightarrow 2^+$ intraband transition within the γ-vibrational band.

Of special note also is the fact that the $\Delta I=0$ transitions from the states at 1386 and 1431 keV to the ground-state band are both established to contain E0 components thus indicating either pure $K^\pi=0^+$ states or admixtures of $K^\pi=0^+$ in these states. Further discussion of these two states is contained in a following report[21].

The 3^- state at 1221 keV is observed to be Coulomb excited; and, from its B(E3)↑ value[18], absolute transition probabilities can be deduced for the de-exciting γ-ray transitions. This analysis reveals, among other things, that the E1 transitions between the $K^\pi=2^-$ octupole-vibrational band and the γ-vibrational band are reasonably "fast" [$F_M(E1) \sim 10^4$]. This fact can be readily understood in terms of unhindered "single-particle" E1 transitions involving small-amplitude two-quasiparticle components in the wave functions of the vibrational states. An unexpected result is the observation of a relatively large M2 transition strength between these two bands [$F_M(M2) \sim 1.4$]. We have as yet found no explanation for this interband M2 transition strength.

Comparison, using a Mikhailov plot, of the E2 transition probabilities to the ground-state band from the 4^+_γ state with those from the 2^+_γ state suggests that the intraband $(4^+_\gamma \rightarrow 2^+_\gamma)$ transition may be somewhat slower than expected for a pure rotational E2 transition. This deviation can be explained as a result of mixing with the other low-lying ($\lesssim$ 1.5 MeV) positive-parity bands (primarily the 2^+ band at 1386 keV). These conclusions are discussed in more detail in a forthcoming paper[30].

---

[1] U.S. Atomic Energy Commission Postdoctoral Fellow, 1969-70. Present address: University of Wisconsion - Stevens Point, Wisconsin, 54481.
[2] M. J. Martin, Nucl. Data B1 (1966) 63.
[3] B. Harmatz and T. H. Handley, Nucl. Phys. 56 (1964) 1.
[4] B. S. Dzelepow, P. A. Tischkin and I. Z. Schischelow, Nucl. Phys. 89 (1966) 359.
[5] V. A. Ageev, A. S. Klimenko, V. K. Maidanyuk and A. I. Feoktistov, Izv. Akad Nauk SSSR (ser. fiz.) 30 (1966) 2037.
[6] V. A. Ageev, V. V. Babenko, J. Vrzal, J. Liptak, V. K. Maidanyuk, J. Urbanets and A. I. Feoktistov, Izv. Akad. Nauk SSSR (ser. fiz.) 32 (1968) 119.
[7] V. A. Ageev, V. I. Gavrilyuk, V. I. Kupryashkin, G. D. Latyshev, I. N. Lyutyi, V. K. Maidanyuk, Yu. A. Makovetskii and A. I. Feoktistov, Izv. Akad. Nauk SSSR (ser. fiz.) 34 (1970) 2121.
[8] J. Glatz, K. E. G. Löbner and F. Oppermann, Z. Phys. 227 (1969) 83.
[9] A. H. Kukoc, B. Singh, J. D. King and H. W. Taylor, Nucl. Phys. A143 (1970) 545.

[10] H. W. Taylor, J. D. King and B. Singh, Can. J. Phys. 49 (1971) 2614.
[11] D. J. McMillan, R. G. Helmer, L. D. McIsaac and C. W. Reich, Nuclear Technology Branch Annual Progress Report for Period Ending June 30, 1970, IN-1407 (1970) p. 114.
[12] N. R. Johnson and N. K. Aras, Oak Ridge National Laboratory report ORNL-3394 (1966) p. 19.
[13] R. R. Spencer and K. T. Faler, Phys. Rev. 155 (1967) 1368.
[14] R. C. Greenwood and C. W. Reich, Nuclear Technology Division Annual Progress Report for Period Ending June 30, 1971, ANCR-1016 (1971) p. 59; R. C. Greenwood and C. W. Reich, Bull. Am. Phys. Soc. 17 (1972) 889.
[15] K. T. Faler, R. R. Spencer and R. A. Harlan, Phys. Rev. 175 (1968) 1495.
[16] M. Beer, M. Bhat, R. E. Chrien, M. A. Lone and O. A. Wasson, Proceedings of Conference on Slow-neutron-capture Gamma-ray Spectroscopy, Argonne National Laboratory report ANL-7282 (1968) p. 459.
[17] C. Samour, J. Julien, R. N. Alves, S. deBarros and J. Morgenstern, Nucl. Phys. A123 (1969) 581.
[18] W. T. Milner, F. K. McGowan, R. L. Robinson, P. H. Stelson and R. O. Sayer, Nucl. Phys. A177 (1971) 1; and private communication.
[19] A. Isoya, T. Maki, T. Nakashima, N. Kato, Y. Kumamoto, T. Sugimitsu and K. Kimara, J. Phys. Soc. Japan 32 (1972) 886.
[20] C. Günther, P. Kleinheinz, R. F. Casten and B. Elbek, Nucl. Phys. A172 (1971) 273.
[21] R. C. Greenwood and C. W. Reich, "Level Structure of ^{184}W from the ^{183}W(n,γ) Reaction", this report.
[22] K. S. Krane, C. E. Olsen and W. A. Stayert, Phys. Rev. C 7 (1973) 263.
[23] M. J. Canty, C. Günther, P. Herzog and B. Richter, Nucl. Phys. A203 (1973) 421.
[24] S. W. Yates, P. J. Daly, N. R. Johnson and N. K. Aras, Nucl. Phys. A204 (1973) 33.
[25] R. F. Casten and W. R. Kane, Phys. Rev. C 7 (1973) 419.
[26] R. F. Casten and O. Hansen, Bull. Am. Phys. Soc. 18 (1973) 37; and private communication.
[27] P. Kleinheinz, P. J. Daly and R. F. Casten (submitted for publication in Nucl. Phys.).
[28] R. S. Hager and E. C. Seltzer, Nucl. Data 4 (1968) 1.
[29] M. E. Rose, Internal Conversion Coefficients (North-Holland Publishing Co., Amsterdam, 1958).
[30] D. J. McMillan, R. C. Greenwood, C. W. Reich and R. G. Helmer (to be submitted for publication in Nucl. Phys.).

TABLE I

GAMMA-RAY ENERGIES AND INTENSITIES MEASURED FOR THE DECAY OF 38-d ^{184g}Re AND 165-d ^{184m}Re

Gamma-ray Energy (keV)	Relative γ-ray intensity	
	^{184g}Re[a]	^{184m}Re
55.278 ± 0.005		5.9 ± 0.6
63.715 ± 0.015		0.95 ± 0.15
87.452 ± 0.010		0.61 ± 0.03
91.270 ± 0.010		0.65 ± 0.03
104.729 ± 0.007		34.4 ± 1.0
111.207 ± 0.007	38.4 ± 4.0	55.7 ± 1.7
124.060 ± 0.020		0.38 ± 0.02
151.134 ± 0.020		0.124 ± 0.012
161.269 ± 0.015		16.6 ± 0.3
215.326 ± 0.012		7.1 ± 0.2
216.547 ± 0.012		24.1 ± 0.5
226.748 ± 0.010		3.81 ± 0.10
230.45 ± 0.06		0.049 ± 0.008
252.845 ± 0.010	6.7 ± 0.4	34.5 ± 0.5
295.01 ± 0.07		0.052 ± 0.010
318.008 ± 0.010		14.7 ± 0.2
382.82 ± 0.014		0.16 ± 0.2
384.250 ± 0.012		8.01 ± 0.12
482.98 ± 0.116	0.037 ± 0.010	0.044 ± 0.008
536.674 ± 0.015		8.44 ± 0.13
539.220 ± 0.025	0.60 ± 0.07	0.86 ± 0.04
641.915 ± 0.020	5.04 ± 0.25	5.50 ± 0.09
757.362 ± 0.035	0.142 ± 0.017	0.147 ± 0.010
769.778 ± 0.017	1.77 ± 0.010	2.19 ± 0.05
792.067 ± 0.022	97.5 ± 5.0	98.8 ± 1.5
857.247 ± 0.027		0.415 ± 0.012
894.760 ± 0.019	41.9 ± 2.0	44.2 ± 0.7
903.282 ± 0.019	100.0 ± 5.0	100.0 ± 1.5
920.933 ± 0.021		20.8 ± 0.3
1010.240 ± 0.030	0.219 ± 0.012	0.218 ± 0.015
1018.93 ± 0.05		0.243 ± 0.025
1022.630 ± 0.030	1.37 ± 0.07	1.69 ± 0.09
1061.04 ± 0.14		0.0062 ± 0.0012
1110.082 ± 0.026		1.49 ± 0.08
1121.437 ± 0.035	0.080 ± 0.007	0.084 ± 0.006
1173.771 ± 0.028		3.10 ± 0.16
1221.286 ± 0.035		0.051 ± 0.004
1274.109 ± 0.030	0.289 ± 0.017	0.285 ± 0.014
1313.786 ± 0.035	0.025 ± 0.002	0.0266 ± 0.0020
1319.94 ± 0.14		0.0054 ± 0.0006
1386.329 ± 0.032	0.257 ± 0.017	0.245 ± 0.012
1408.49 ± 0.42 (?)		0.0022 ± 0.0004
1430.96 ± 0.08		0.0057 ± 0.0008

[a] A more complete characterization of the ^{184g}Re decay γ rays is derived from the ^{184m}Re in secular equilibrium decay and is given in Table VII. Therefore, it is this latter set which should be used in any consideration of the ^{184g}Re decay modes.

TABLE II

K-ELECTRON INTENSITIES AND INTERNAL CONVERSION COEFFICIENTS FOR TRANSITIONS RESULTING FROM THE DECAY OF ^{184}Re. UNCERTAINTIES IN THE LEAST SIGNIFICANT FIGURES OF THE EXPERIMENTAL VALUES ARE INDICATED IN PARENTHESIS.

Transition Energy (keV)	K-Electron Intensity[a]	Gamma-Ray Intensity[a]	Experimental $10^3\,\alpha_k$[b]	E1	E2	E3	M1	M2	Inferred Multipolarity
83[c]									
215			41.7 (7)[d]	43.4	140	416	464	2100	M4 (≤ 1.0% E5)
216	34 (4)	1.32 (12)	118 (18)[d]	42.8	138	410	456	2060	E1
226			42.3 (12)[d]	38.1	122	360	402	1760	E1 + M2 + E3
252	153	8.2 (5)	85 (8)[e]	29.1	91	265	299	1230	E2
318	3.1 (2)	0.82 (7)	27.3 (20)	16.7	49.2	139	151	580	E1
384	2.9 (2)	0.46 (4)	28 (3)	10.7	30.4	82	97	320	E2
536	0.62 (13)	0.44 (4)	6.4 (14)	5.1	13.7	34.0	40.4	116	E1 + (M2+E3)
539	2.4 (2)	0.85 (8)	12.9 (16)	5.1	13.6	33.6	39.9	114	E2
641	9.8 (5)	5.0 (3)	8.9 (6)	3.54	9.2	21.8	25.5	69	E2
769	2.55 (17)	1.79 (10)	6.5 (6)	2.47	6.3	14.2	16.1	41.3	E2
792	125 (3)	97 (5)	5.8 (3)	2.33	5.9	13.3	15.0	38.1	E2
894	42.8 (9)	42 (2)	4.6 (2)	1.85	4.62	10.1	11.0	27.3	E2
903	≡100	≡100	4.54	1.82	4.54	9.9	10.8	26.6	E2
920	0.71 (4)	1.15 (8)	2.8 (3)	1.74	4.37	9.5	10.3	25.3	E1 + M2 + E3
1010	0.53 (4)	0.219 (11)	11.0 (10)	1.48	3.64	7.7	8.2	19.7	E2 + M1 + E0
1022	1.14 (5)	1.39 (7)	3.7 (3)	1.45	3.56	7.5	719	19.1	E2
1110	<0.035	0.082 (6)	<2.1	1.25	3.04	6.3	6.5	15.4	E1
1121	0.065 (3)	0.079 (8)	3.7 (19)	1.23	2.98	6.2	6.3	15.0	E2
1173	0.24 (3)	0.173 (14)	6.3 (10)	1.13	2.73	5.6	5.6	13.3	E3
1275	0.23 (4)	0.289 (17)	3.6 (6)	0.98	2.33	4.7	4.6	10.7	E2 + M1 + E0
1386	0.12 (4)	0.255 (17)	2.1 (8)	0.85	1.99	4.0	3.8	8.7	E2

[a] Intensities of the mixed ^{184}Re source at the beginning of the internal conversion electron experiments.

[b] Conversion coefficients are computed on the assumption that the 903 keV transition is pure E2.

[c] The $L_1/L_2/L_3$ conversion electron ratio was measured to be (0.275 ± 0.019)/(0.053 ± 0.010)/1.000 which can be compared to theoretical ratios of 0.253/0.0494/1.000 for an M4 transition[28] and 0.374/1.30/1.000 for an E5 transition[29].

[d] Determined in the later series of measurements with the ^{184m}Re secular-equilibrium source, with the conversion coefficients computed on the assumption that the 252-keV transition is pure E2.

[e] A conversion coefficients of $(1.55 \pm 0.06) \times 10^{-2}$ was determined in the later series of measurements with the ^{184m}Re secular-equilibrium source, based upon the assumption that the 252- and 384-keV transitions are pure E2.

TABLE III

ADDITIONAL (TO TABLE II) K-CONVERSION COEFFICIENTS COMPUTED USING CONVERSION-ELECTRON INTENSITIES MEASURED BY AGEEV *et al.*,[6,7] FOR ^{184m}Re IN SECULAR EQUILIBRIUM AND OUR γ-RAY INTENSITIES FROM TABLE I

Transition Energy (keV)	K-Electron Intensity	Gamma-Ray Intensity	Experimental $10^3\ \alpha_k$	Theoretical $10^3\ \alpha_k$					Inferred Multipolarity
				E1	E2	E3	M1	M2	
104	24000	34.4	3170	280	792	1720	3870	27800	M1
111	7800	55.7	640	235	731	1810	2990	21000	E2
161	2500	16.6	680	90.8	302	892	1040	5660	M1 + E2
483			>11[a]	6.44	17.5	44.6	53.1	159	
769	2.7	2.19	5.6	2.47	6.28	14.2	16.1	41.3	E2
903	100	100	4.54		4.54				E2
1018	∿0.15	0.243	∿2.8	1.46	3.58	7.59	7.99	19.3	E1+(M2+E3)
1313	0.015	0.0266	2.6	0.93	2.21	4.42	4.28	9.93	E2+(M1)
1319	0.03	0.0054	25	0.92	2.19	4.38	4.23	9.81	E2+M1+E0

[a] No K-electron intensity is given for the 483-keV transition in Reference [7]. There is only a lower limit given on this coefficient.

TABLE IV

BEST ENERGIES DETERMINED FOR THE LEVELS IN ^{184}W POPULATED IN THE ^{184}Re DECAY

Level Energy (keV)
0.0
111.207 ± 0.006
364.055 ± 0.012
748.309 ± 0.019
903.283 ± 0.020
1005.968 ± 0.022
1121.438 ± 0.029
1130.029 ± 0.024
1133.840 ± 0.024
1221.292 ± 0.025
1284.991 ± 0.027
1386.327 ± 0.034
1425.011 ± 0.041
1431.02 ± 0.07
1446.260 ± 0.032
1501.538 ± 0.032

TABLE V

ELECTRON-CAPTURE BRANCHING RATIOS AND log ft VALUES DETERMINED FOR THE ^{184}Re DECAY, USING A VALUE OF 1496 ± 6 keV FOR THE ^{184g}Re-^{184}W MASS DIFFERENCE

Level Energy (keV)	Branching Ratio[a] (%)	Log ft
^{184g}Re decay		
111	4.6 ± 2.6	$9.4^{+0.4}_{-0.2}$
364	0.37 ± 0.25	$10.3^{+0.5}_{-0.2}$
903	75.4	7.38
1005	17.5	7.83
1121	0.189 ± 0.009	9.53 ± 0.03
1130	< 0.2	9.5
1133	1.20 ± 0.05	8.69 ± 0.02
1221	< 4	< 7.9
1284	< 0.4	< 8.6
1386	0.243 ± 0.010	7.91 ± 0.08
1424	0.038 ± 0.005	8.04 ± 0.10
1431	0.0046± 0.0004	8.87 ± 0.09
^{184m}Re decay		
1501	24.9 ± 0.6	7.25 ± 0.03

[a] An uncertainty is placed on these branching ratios only for those cases when the percentage uncertainty is greater than the percentage change which might occur from any reasonable renormalization; for example, if there were in fact essentially zero branching to the 2^+ and 4^+ members of the ground-state band (which would not be unreasonable since the uncertainties which are quoted represent 1σ values).

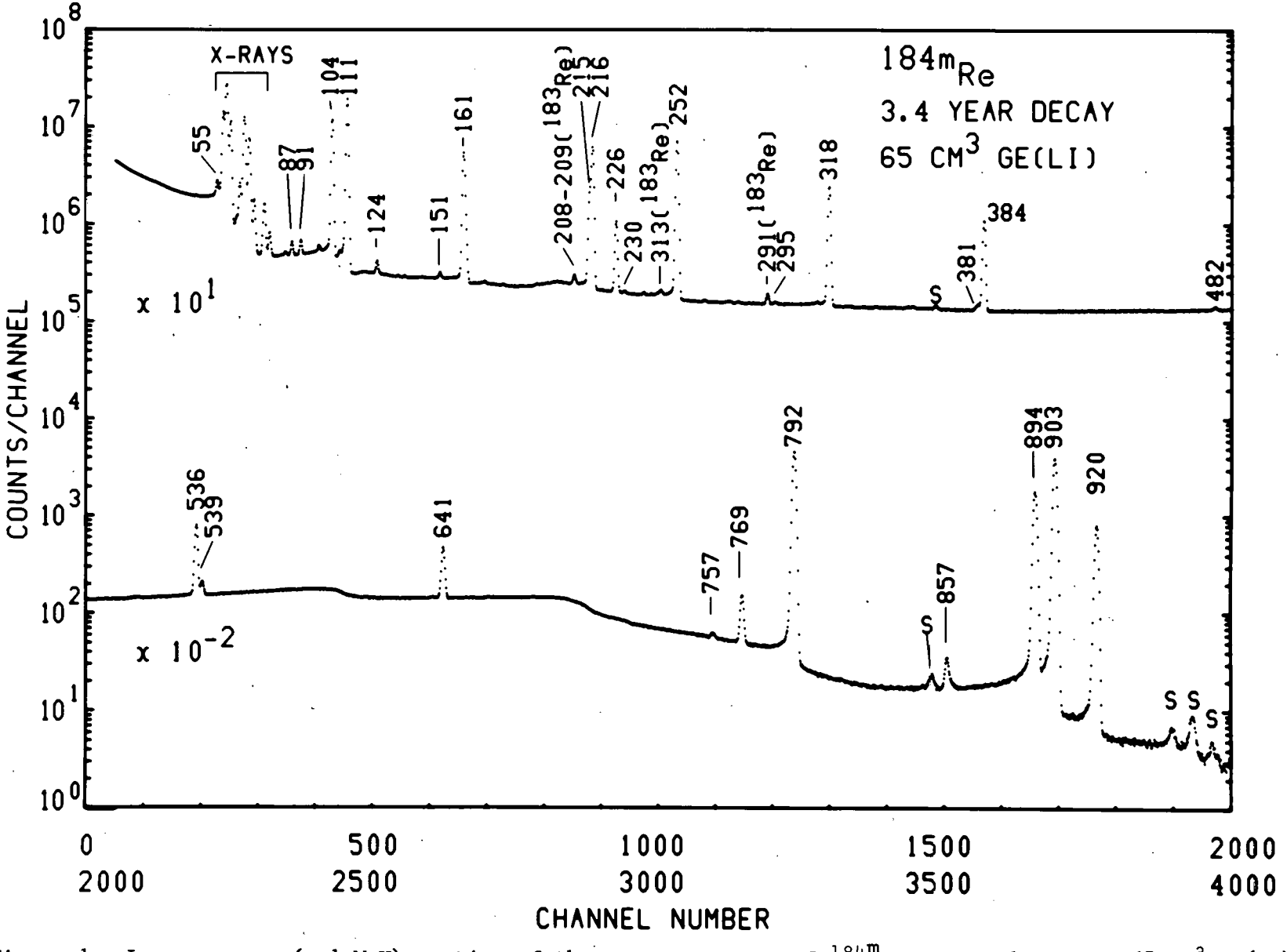

Figure 1 Lower energy (< 1 MeV) portion of the γ-ray spectrum of ^{184m}Re measured using a 65-cm^3 Ge(Li) detector at a source-to-detector distance of 10 cm. The spectrum was obtained 3.4 years after source production. Platinum K x-rays, resulting from fluorescent excitation in the backing material, are also present in the spectrum.

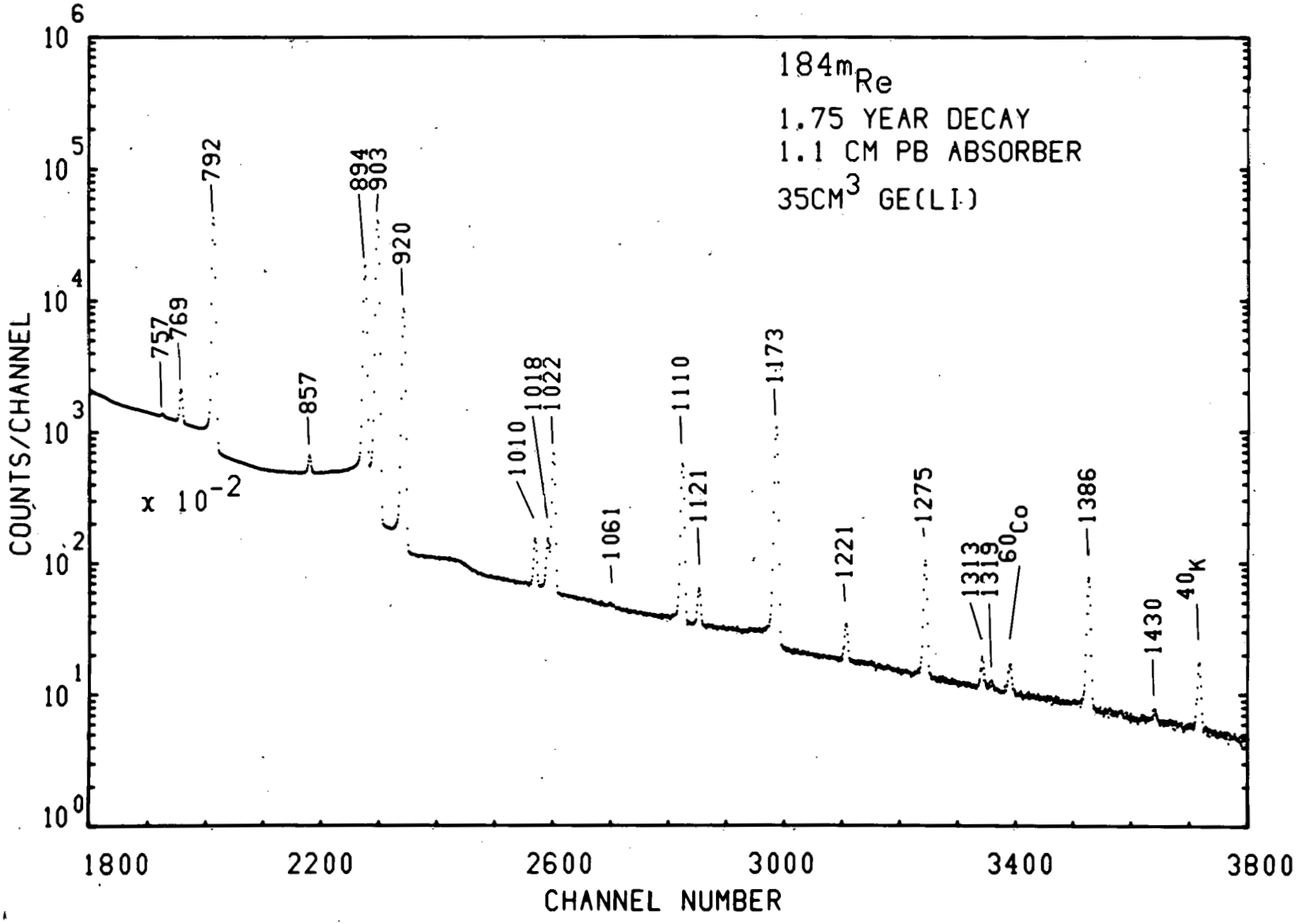

Figure 2 Higher energy (> 0.7 MeV) portion of the γ-ray spectrum of ^{184m}Re obtained 1.75 years after source production with a 35-cm^3 Ge(Li) detector. An ≈ 0.8-cm lead absorber was interposed between the source and the detector.

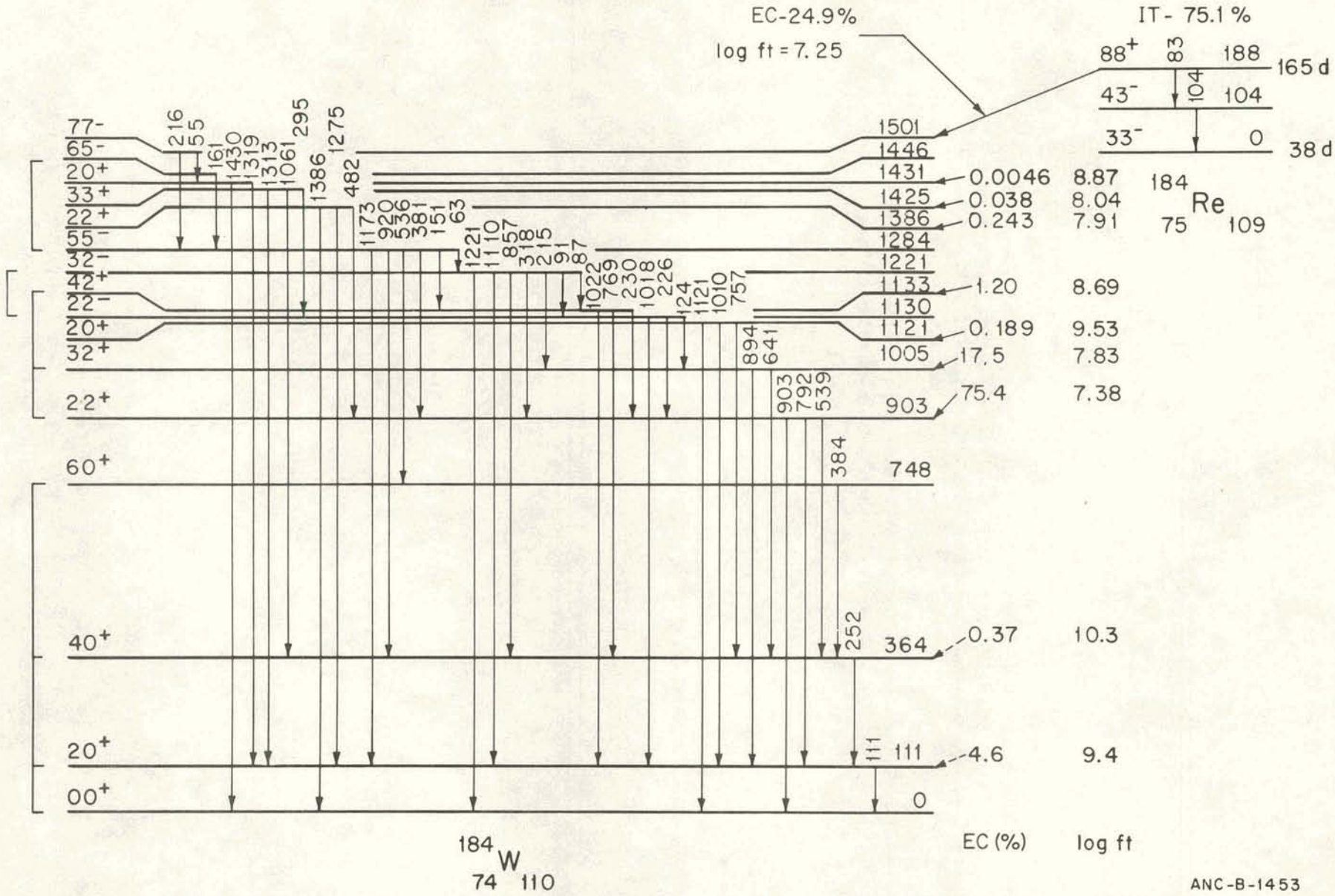

Figure 3 Decay scheme of ^{184g}Re and ^{184m}Re. The brackets at the left of the figure indicate the grouping of states into rotational bands.

E3 TRANSITION PROBABILITIES AND QUASIPARTICLE-PHONON MIXING IN ^{184}W

C. W. Reich

The decay-scheme studies of ^{184g}Re and ^{184m}Re summarized in the preceding report[1] have provided a much more complete picture of the decay patterns of many of the levels in ^{184}W than has previously been available. Of interest for this present note are the γ-ray transitions from the 8.33-μsec, I,$K^{\pi}=5,5^-$ state at $\sim$ 1284 keV, in particular those which proceed to various members of the ground-state rotational band. From the γ-ray relative intensities and the E1/M2/E3 mixing-ratio data of Krane et al.[2] for these transitions, we obtain the B(E3)$\downarrow$ values given in column 7 of Table I. These E3 transitions are twice-K-forbidden and hence may be treated as arising from admixed configurations of other K-values in the initial and/or the final state. As discussed in detail in a forthcoming publication[3], the known admixture of the γ vibration ($K^{\pi}=2^+$) in the ground-state band cannot by itself account for the observed E3 transitions, since the predicted transition probabilities are roughly two orders of magnitude low and have an incorrect final-state spin dependence. It seems natural, therefore, to assume that these transitions result primarily from K-admixtures in the initial state. In the following, we show that the observed E3 transitions can be accounted for quite satisfactorily in terms of $K^{\pi}=2^-$ and 3^- admixtures in the initial state and discuss briefly the relative contribution of collective (i.e., octupole vibrational) and two-quasiparticle components to these deduced admixtures.

In this case (K-admixtures in the initial state only), the B(E3) values to the ground-state band can be expressed in terms of two transition-amplitude parameters, X_2 and X_3, which describe the E3 transitions with $\Delta K=2$ and 3, respectively, as follows:

$$B(E3;5^-\rightarrow I^+) = 2\left[\langle 523\text{-}2|I0\rangle X_2 + \langle 533\text{-}3|I0\rangle X_3\right]^2 e^2\cdot b^3 \quad . \qquad (1)$$

From Equation (1), it is seen that the square roots of the B(E3) values depend linearly on X_2 and X_3. If the relationships obtained from taking the square root of both sides of Equation (1) for each final-state spin are plotted on an X_3 vs X_2 graph, a series of straight lines results. Those (X_2, X_3) "points" (if any) at which lines corresponding to the three different final-state spins intersect represent "solutions" which fit all three B(E3) values. Such a plot is shown in Figure 1. Inspection of Figure 1 reveals three different roots consistent with the B(E3) data. The properties of these roots are summarized in Table I.

There are two sources of $K^{\pi}=2^-$ and 3^- admixtures in the 1284-keV, 5^- state which may have a significant influence on the E3 transition probabilities. These are (1) the respective octupole-vibrational components, which although possibly present with small amplitudes nonetheless possess enhanced E3 matrix elements to the ground-state band and

TABLE I

SUMMARY OF TRANSITION-AMPLITUDE VALUES WHICH ARE CONSISTENT WITH THE OBSERVED B(E3) VALUES OF THE TRANSITIONS FROM THE 1284-keV STATE TO THE 2^+, 4^+ AND 6^+ MEMBERS OF THE GROUND-STATE BAND IN ^{184}W

Root	X_2 ($e \cdot f^3$)	X_3 ($e \cdot f^3$)	Transition $5^- \rightarrow I^\pi$; E_γ(keV)	$10^6 B(E3)\downarrow$ ($e^2 \cdot b^3$) Calculated	Experimental
I	+6.1	+4.7	$5^- \rightarrow 2^+$; 1173.8	2.38	2.36 ± 0.15
			$5^- \rightarrow 4^+$; 920.9	4.50	4.7 $^{+\ 2.1}_{-\ 1.8}$ [a]
			$5^- \rightarrow 6^+$; 536.7	46.5	43. $^{+23.}_{-18.}$ [a]
II	2.28	-1.06	$5^- \rightarrow 2^+$; 1173.8	2.43	2.36 ± 0.15
			$5^- \rightarrow 4^+$; 920.9	2.08	3.0 ± 1.0 [b]
			$5^- \rightarrow 6^+$; 536.7	1.35	7.4 $^{+10.6}_{-\ 6.0}$ [b]
III	-0.65	+3.2	$5^- \rightarrow 2^+$; 1173.8	2.11	2.36 ± 0.15
			$5^- \rightarrow 4^+$; 920.9	7.35	4.7 $^{+\ 2.1}_{-\ 1.8}$ [a]
			$5^- \rightarrow 6^+$; 536.7	1.20	7.4 $^{+10.6}_{-\ 6.0}$ [b]

[a] Set 1 of Reference [2].

[b] Set 2 of Reference [2].

(2) two-quasiparticle states, which although having somewhat smaller E3 matrix elements to the ground-state band might be present with larger amplitudes because of Coriolis-mixing effects. The transition-amplitude parameters, X_K, may be expressed in terms of the collective and two-quasiparticle E3 matrix elements by the relation

$$X_K = \left[C_K P_K \langle K^- | M'(E3;K) | 0^+ \rangle + \frac{(\overset{0}{\omega}_0/\omega_0)^{3/2}}{1,314} A^{1/2} a_K P'_{K,K'} G_{E3}(\Delta K) \right] e \cdot b^{3/2}, \quad (2)$$

where A is the mass number (=184), P and P' are the pairing factors, and $\overset{0}{\omega}_0, \omega_0$ and G_{E3} are as defined by Nilsson[4], it being understood that the G_{E3} is that appropriate to the single-particle (Nilsson) states involved in the transition of the odd particle. (See, for example, Reference [5].) The C_K and a_K are the admixed amplitudes of the

collective and the two-quasiparticle components, respectively. Equation (2) as written treats the effect of only one two-quasiparticle component; if several such terms are assumed to be present, their effect can be included by incorporating additional terms.

The parameters which influence the B(E3) values of the transitions to the ground-state band affect other transition probabilities as well. Therefore, knowledge of these other transition probabilities helps in the parameter determination. The interrelationship of these various quantities is illustrated in Figure 2. There it is seen that the C_2 and C_3 amplitudes (which influence the E3 transitions to the ground-state band), together with the b_K, have a very important effect on the transition probability of the 63-keV E2 transition. These b_K are, in turn, related to both the B(E3)↑ value of the 1221-keV state and the B(E2) value of the intraband ($3^-\rightarrow 2^-$) transition. In addition, the B(E3)↑ value depends on the two collective E3 matrix elements, which themselves also influence the transition probabilities of the E3 transitions from the 1284-keV state to the ground-state rotational band.

The X_K values provide, through Equation (2), one set of relationships among the relevant parameters. Additional such relationships are provided by the B(E2) values of the $5^-\rightarrow 3^-$ and $3^-\rightarrow 2^-$ transitions and by the B(E3) value of the transition from the ground state to the 3^- state at 1221 keV. In terms of the notation given in Figure 2, these relations can be written:

$$B(E2;5^-\rightarrow 3^-) = \frac{5}{16\pi}\left[\sum_{K=2,3} b_K C_K \langle 5K20|3K\rangle Q_o(K^-)\right]^2 e^2\cdot b^2 \quad ; \qquad (3)$$

$$B(E2;3^-\rightarrow 2^-) = \frac{5}{16\pi}\left|b_2\langle 3220|22\rangle Q_o(2^-)\right|^2 e^2\cdot b^2 \quad ; \qquad (4)$$

$$B(E3;0^+\rightarrow 3^-) = 2\left[\sum_{K=2,3} b_K \langle K^-|M'(E3;K)|0\rangle\right]^2 e^2\cdot b^3 \quad . \qquad (5)$$

The following procedure was used to extract parameter values from the transition-probability data. For each allowed (X_2,X_3) root in Table I, the products $C_K\langle K^-|M'(E3;K)|0^+\rangle$ were obtained from Equation (2), after correction for the assumed two-quasiparticle contribution. These E3 matrix elements were then substituted into Equation (5). This equation, together with Equation (3), provides two relations involving the products b_2C_2 and b_3C_3. For "reasonable" [i.e., consistent with the B(E2) value of the $3^-\rightarrow 2^-$ transition] choices of b_2 (and hence b_3), consistent values of C_2 and C_3 were then obtained through graphical solution of Equations (3) and (5). For convenience, it was assumed

that the two intrinsic quadrupole moments were equal to that of the ground-state band.

The contributions of the admixed two-quasiparticle states which are needed for these calculations could not be determined experimentally. Instead, their magnitude was estimated assuming that the admixtures result from Coriolis coupling with the dominant component in the 5^- state, namely[6] $\{1/2^-[510]_n, 11/2^+[615]_n\}_{5^-}$. We expect that the Coriolis-mixed $K^\pi=3^-$ and 2^- two-quasiparticle states with the largest amplitudes will be $\{1/2^-[510]_n, 7/2^+[633]_n\}_{3^-}$ and $\{1/2^-[510]_n, 5/2^+[642]_n\}_{2^-}$, owing to the expected strong Coriolis coupling among these $i_{13/2}$-related orbitals. These calculations indicated that the magnitude of the contribution of these two-quasiparticle components to the X_K amplitudes might be of the order of 0.6 $e\cdot f^3$ and 1.0 $e\cdot f^3$ for K=2 and 3, respectively. With these estimates, calculations were carried out for three different situations. In the first and second of these, the above estimated two-quasiparticle contribution to the X_K was assumed to interfere constructively and destructively, respectively, with the collective component. In the third, this contribution was assumed to vanish (i.e., a_2 and a_3 were set equal to zero).

From the available data, it is not possible to obtain unique values for all the parameters involved in the analysis. However, the fact that all the relevant data (see Figure 2) can be fit quite well using "reasonable" parameter values suggests that the interpretation is fundamentally correct. In spite of the lack of uniqueness of the results obtained, some conclusions can nonetheless be drawn from the analysis. For example, although Root I gives the best overall fit to the B(E3)↓ data (see Figure 1), it is probably not a realistic solution. The reason for this is that, while the deduced E3 matrix elements for this case do indeed fit the observed $B(E3;0^+\rightarrow 3^-)$ value, the K=2 and K=3 contributions interfere destructively. One might expect, and the calculations of Neergård and Vogel[7] indicate, that the enhanced B(E3) value to the lowest collective 3^- state in these nuclei would result from a constructive, not destructive, interference of the various components.

In Table II are presented the results of two of the calculations. The cases summarized there are those where the contribution of the two-quasiparticle components to the X_K amplitudes has been assumed to be zero. In general, for each of these cases, there are, for a given choice of (b_2, b_3), four (C_2, C_3) solution sets. We have listed in Table II only those sets for which the two E3 matrix elements are predicted to have the same sign [so that constructive interference in $B(E3;0^+\rightarrow 3^-)$ is predicted]. From these calculations there is little basis for choosing between Roots II and III, although a slight preference for the former might exist simply because the two E3 matrix elements are of more nearly equal magnitude. A preference for Root II is also indicated by the quite recent γ-γ directional-correlation data of Canty et al.[8]. Of the two E3/E1 mixing-ratio parameters which they obtained for the 920-keV γ ray, the one corresponding to Root II had the smaller χ^2 value.

TABLE II

SELECTED RESULTS OF THE PARAMETER VALUES OBTAINED FROM A CONSISTENT FITTING OF THE EXPERIMENTAL TRANSITION-PROBABILITY DATA SUMMARIZED IN FIGURE 2

The calculations included here were carried out neglecting the possible contribution of the two-quasiparticle states to the E3 transition matrix element from the 1284-keV state. Only those (C_2,C_3) roots which lead to E3 matrix elements of the same sign are included.

Root[a]	b_2	b_3	$B(E2;3^-\rightarrow 2^-)^b$ $(e^2\cdot b^2)$	C_2	C_3	$\langle 2^-\|M'(E3;2)\|0^+\rangle$ $(e\cdot b^{3/2})$	$\langle 3^-\|M'(E3;3)\|0^+\rangle$ $(e\cdot b^{3/2})$
II	0.707	0.707	0.69	0.0214	-0.0059	0.106	0.180
				0.0088	-0.0400	0.258	0.027
	0.96	0.27	1.27	0.0141	-0.0060	0.162	0.177
				0.0110	-0.128	0.207	0.0083
	0.995	0.10	1.36	0.0127	-0.0045	0.180	0.235
				0.0113	-0.354	0.202	0.003
	1.0	0	1.37	0.0124[c]	d	0.184[e]	d
				0.0113[f]	d	0.202	d
III	0.707	0.707	0.69	-0.0253	+0.0123	0.026	0.26
				-0.0035	+0.0325	0.187	0.098
	0.96	0.27	1.27	-0.0139	+0.0055	0.047	0.572
				-0.0033	+0.0864	0.200	0.037
	0.995	0.10	1.36	-0.0128	+0.0021	0.050	1.52
				-0.0032	+0.234	0.202	0.013
	1.0	0	1.37	-0.0124[c]	d	0.052[e]	d
				-0.0032[f]	d	0.202	d

[a] For the associated (X_2,X_3) values, see Table I and Figure 1.

[b] Calculated using Equation (4) (see text). The experimental value is $(1.27\pm0.21)\ e^2\cdot b^2$.

[c] Obtained from fitting the observed $B(E2;5^-\rightarrow 3^-)$ value.

[d] Quantity indeterminate in this case.

[e] Obtained from X_2 and deduced C_2 values, but does not give the correct $B(E3)\uparrow$.

[f] Consistent with X_2 value and $\langle 2^-|M'(E3;2)|0^+\rangle$ obtained from $B(E3)\uparrow$.

It should be noted that the "order-of-magnitude" estimates of the two-quasiparticle contribution to the transition amplitudes, X_K, are quite close to the value of X_3 for Root II and X_2 for Root III. Once it has become possible to establish which of these roots is the proper one, serious consideration will have to be given to the possibility that the relevant K-admixture may be due entirely to two-quasiparticle states, the corresponding collective component being essentially absent in the 5^- state. Taking Root II as an example, we would conclude in such a case (cf. Figure 2) that the contribution of the collective term to the K=3 transition amplitude was zero and that, consequently, the collective K=2 admixture in this state is much larger than that from K=3.

---

[1] R. C. Greenwood, C. W. Reich, R. G. Helmer and D. J. McMillan, "Level Structure of ^{184}W from Decay of ^{184g}Re and ^{184m}Re", this report.

[2] K. S. Krane, C. E. Olsen and W. A. Steyert, Phys. Rev. C 7, (1973) 263.

[3] D. J. McMillan, R. C. Greenwood, C. W. Reich and R. G. Helmer (to be submitted for publication in Nucl. Phys.).

[4] S. G. Nilsson, Mat. Fys. Medd. Dan. Vid. Selsk. 29, no. 16 (1955).

[5] C. W. Reich, R. G. Helmer and R. C. Greenwood, Nucl. Phys. A168, (1971) 487.

[6] P. Kleinheinz, P. J. Daly and R. F. Casten (to be published).

[7] K. Neergård and P. Vogel, Nucl. Phys. A145, (1970) 33.

[8] M. J. Canty, C. Günther, P. Herzog and B. Richter, Nucl. Phys. A203, (1973) 421.

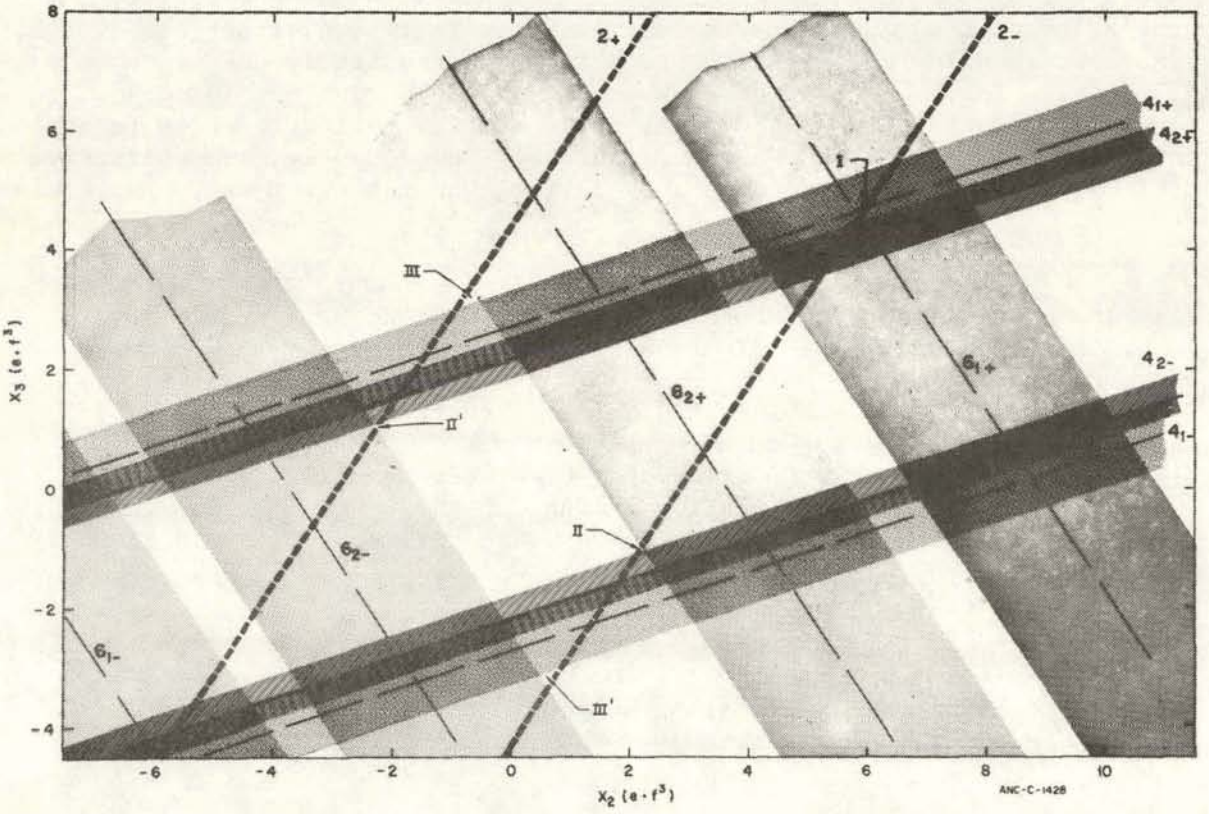

Figure 1 X_3 vs X_2 plot summarizing the B(E3) data from the 5^- state at 1284-keV to the 2^+, 4^+ and 6^+ members of the ground-state band. The dashed lines and the shaded areas surrounding them represent the experimental values and their associated uncertainties, respectively. Each such line is labeled by the spin of the final state with a subscript denoting whether it corresponds to the positive or negative square root (in Equation 1). For the transitions to the 4^+ and 6^+ states, the data of Krane et al.[2] yield two solution sets for the E3/E1 mixing ratio (and hence for the B(E3) value). In these cases, an additional subscript is included, denoting which set (in the notation of Ref. [2]) is involved. Those points at which lines corresponding to three different final-state spin values intersect are labeled by Roman numerals. It should be noted that for each such point (X_2,X_3), there is a corresponding point $(-X_2,-X_3)$ which is also a solution.

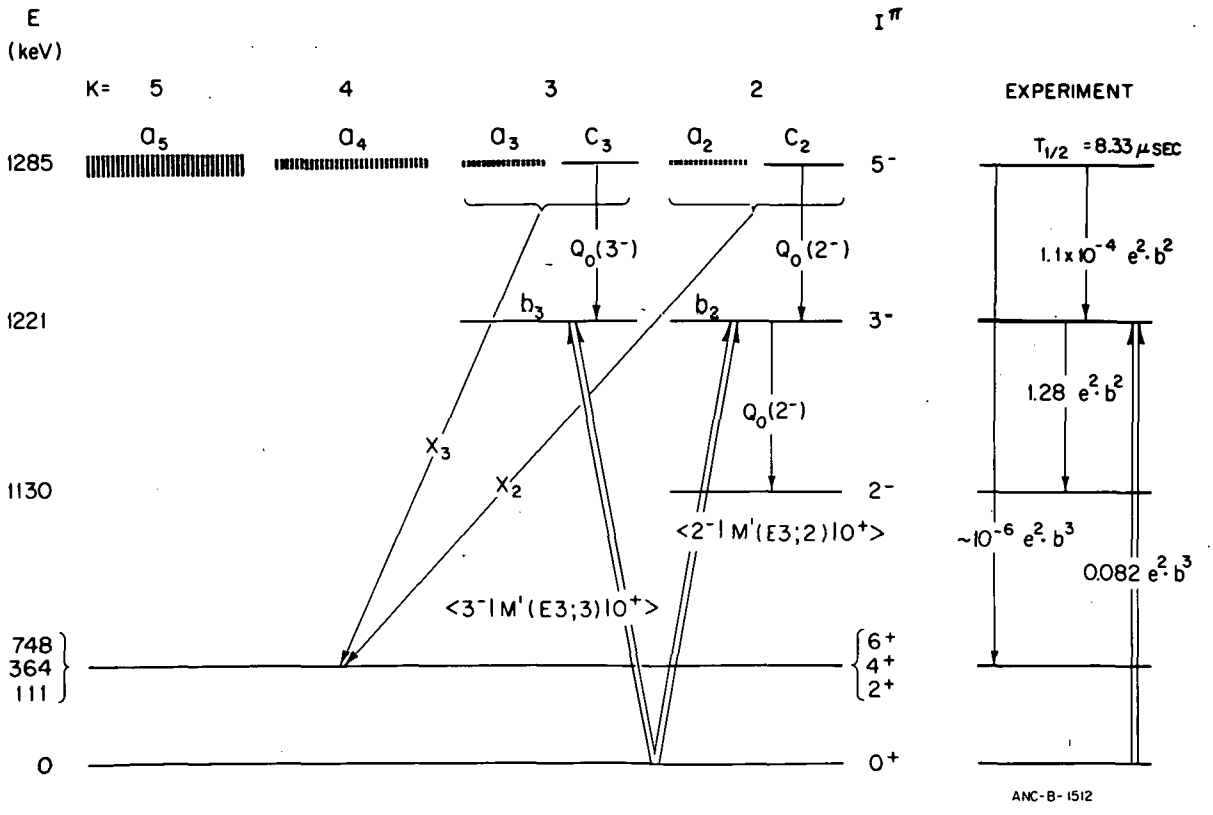

Figure 2 Representation of the relation of the various quantities considered in treating the 1284-keV state in ^{184}W. The a_K denote the amplitudes of the various two-quasiparticle states in the wave function of the 1284-keV state, the widths of the associated lines indicating their expected relative magnitudes. The amplitudes of the admixed 2^- and 3^- octupole-vibrational states in the 1284-keV state are C_2 and C_3, respectively, while the corresponding quantities in the 1221-keV, $I^\pi=3^-$, state are b_2 and b_3. (It is assumed that the 2^- state at 1130 keV is pure K=2, i.e., the amplitude of the $K^\pi=2^-$ octupole-vibrational component is unity.) The E2 and E3 matrix elements considered in this analysis are indicated by arrows between those components of the wave functions which they are assumed to connect. The effect of possible direct E2 matrix elements between the 2^- and 3^- octupole vibrations has been neglected. At the right in the figure are shown the relative experimental quantities.

LEVEL STRUCTURE OF ^{184}W FROM THE ^{183}W(n,γ) REACTION

R. C. Greenwood, C. W. Reich

Studies of the decay of 38-d ^{184g}Re and 165-d ^{184m}Re, described in a preceding report[1], have provided detailed spectroscopic information about a number of levels in doubly-even ^{184}W. In order to obtain further insights into the level structure of ^{184}W we have undertaken a complementary study of the prompt γ rays associated with the ^{183}W(n,γ) reaction. Prompt γ rays resulting from capture of both thermal and 2-keV neutrons were measured. These additional studies have allowed us to obtain a more complete picture of the level structure of ^{184}W, especially with regard to the occurrence and distribution of states having $I^{\pi}=0^{+}$, 1^{+} and 2^{+} up to an excitation energy $\sim$ 2 MeV. Preliminary reports of some aspects of this work have been presented previously[2].

Earlier studies of the ^{183}W(n,γ) reaction have principally involved measurements of the primary prompt γ rays resulting from resonance-neutron capture in ^{183}W[3-6]. Faler *et al.*[7] did, however, make neutron capture measurements specifically to establish the lowest excited $K^{\pi}=0^{+}$ band in ^{184}W and to determine the decay modes from this band. Recently, Casten and Kane[8] have reported on their measurements of both primary and secondary prompt γ rays which were undertaken to obtain information about the lower (< 2.5 MeV) lying levels in ^{184}W.

Details of the specific γ-ray measurements made were reported in Reference [2]. By combining the primary capture γ-ray data (thermal and 2-keV neutron) with the extensive data on the low-energy secondary transitions which were also measured, we were able to construct the level scheme shown in Figure 1 for those states in ^{184}W populated in the ^{183}W(n,γ) reaction. The levels have been grouped into rotational bands whenever such assignments can be made with a high degree of confidence. The energies of the levels are also listed in Table I, together with their de-exciting γ-ray transitions (including the energies of these transitions which for clarity are not included in Figure 1). The level energies represent a "best" set determined both in this work and in that of a preceding report[1]. Features of this level scheme which are of interest include:

- establishment of the 1130-keV state as being the band head of a $K^{\pi}=2^{-}$ octupole vibrational band;

- establishment of admixed $K^{\pi}=0^{+}$ and 2^{+} bands at 1322 and 1386 keV, respectively. Based upon the ratios of absolute E0 transition probabilities in the $\Delta I=0$ transitions de-exciting the 2^{+} states and upon the ratio of ft values of the electron-capture transitions from ^{184g}Re decay, we estimate a $\sim$ 12% mixing of the 1386- and 1431-keV 2^{+} states.

- establishment of a higher lying $K^{\pi}=0^{+}$ band at 1614 keV and $K^{\pi}=1^{+}$ bands at 1613 keV and 1713 keV.

A phenomenological five-band mixing analysis involving the $K^{\pi}=0^{+}$ and 2^{+} bands below $\sim$ 1.5 MeV has been carried out. While this analysis is not unique, in that values of several of the matrix elements entering the calculation cannot be precisely determined, it does nontheless reveal certain features of the ^{184}W level scheme. Among these are the following.

Explanation of the decay properties of the 0^{+} band at 1322 keV appears to require a nonzero E2 matrix element between this band and the γ-vibrational band. If the proposed assignment of the 425-keV γ ray as the $2,0^{+} \rightarrow 3,2^{+}_{\gamma}$ transition is correct and if it has a pure (or at least dominant) E2 multipolarity, then the magnitude of this interband E2 matrix element can be inferred. It is found that this matrix element and the coupling strength between these two bands are comparable in magnitude with those connecting the ground-state and γ-vibrational bands. This behavior and the strong preference of the 1322-keV state for decay to the γ band rather than to the ground-state band [$B(E2;0^{+}\rightarrow 2^{+}_{g})/B(E2;0^{+}\rightarrow 2^{+}_{\gamma}) < 10^{-3}$] are properties expected for a "2-phonon" vibration with $K^{\pi} = {}^{\gamma}0^{+}$, although several properties of this 0^{+} band are apparently not consistent with such an interpretation.

The γ-band is not found to be strongly mixed with any of the 0^{+} bands. This conclusion contradicts the calculations of Kumar and Baranger[9], which predict strong mixing between the γ-vibrational band and the lowest excited 0^{+} band in ^{184}W.

The $4,0^{+}$ state at 1358 keV, reported in (d,d') and (d,p) studies, lies $\sim$ 40 keV lower than predicted by our analysis. No reasonable parameter choice can fit the energies of all three members of this band.

The smallness of the E2 matrix elements connecting the ground-state band and the excited 0^{+} bands suggests that neither of them can be regarded as being predominantly "β vibrations".

A more detailed discussion of the features of the ^{184}W level scheme which have been found as a result of the present data is given in a forthcoming paper[10].

---

[1] R. C. Greenwood, C. W. Reich, R. G. Helmer and D. J. McMillan, "Level Structure of ^{184}W from Decay of ^{184g}Re and ^{184m}Re", this report.

[2] R. C. Greenwood and C. W. Reich, Nuclear Technology Division Annual Progress Report for Period Ending June 30, 1971, ANCR-1016 (1971) p. 59; and R. C. Greenwood and C. W. Reich, Bull. Am. Phys. Soc. 17 (1972) 889.

[3] E. R. Rae, W. R. Moyer, R. R. Fullwood and J. L. Andrews, Phys. Rev. 155 (1967) 1301.

[4] R. R. Spencer and K. T. Faler, Phys. Rev. 155 (1967) 1368.

[5] M. Beer, M. Bhat, R. E. Chrien, M. A. Lone and O. A. Wasson, Proc. of Conf. on Slow-neutron-capture gamma-ray spectroscopy, Argonne National Laboratory report ANL-7282 (1968) 459.

[6] C. Samour, J. Julien, R. N. Alves, S. deBarros and J. Morgenstern, Nucl. Phys. A123 (1969) 581.

[7] K. T. Faler, R. R. Spencer and R. A. Harlan, Phys. Rev. 175 (1968) 1495.
[8] R. F. Casten and W. R. Kane, Phys. Rev. C 7 (1973) 419.
[9] K. Kumar and M. Baranger, Nucl. Phys. A122 (1968) 273.
[10] R. C. Greenwood and C. W. Reich (to be submitted for publication in Nucl. Phys.).

TABLE I

LEVELS IN ^{184}W AND THEIR MODES OF DE-EXCITATION DETERMINED FROM STUDIES OF THE $^{183}W(n,\gamma)$ REACTION

Initial State		De-exciting Transition		Final State	
Level energy[a,b] (keV)	I,K^{π}[c]	Gamma-ray energy[b] (keV)	Relative gamma-ray intensity[a]	Level energy (keV)	I,K^{π}
111.207(6)	$2,0^+$	111.218	163(11)	0	$0,0^+$
364.055(12)	$4,0^+$	252.850	59.5(30)	111	$2,0^+$
748.309(19)	$6,0^+$	(383.98)	2.0(2)	364	$4,0^+$
903.283(20)	$2,2^+$	903.262	103(5)	0	$0,0^+$
		792.056	100(5)	111	$2,0^+$
		539.38	1.3(3)	364	$4,0^+$
1002.49(4)	$0,0^+$	891.271	50.6(25)	111	$2,0^+$
1005.968(22)	$3,2^+$	894.748	57.3(29)	111	$2,0^+$
		641.874	6.9(3)	364	$4,0^+$
1121.438(29)	$2,0^+$	1121.390	11.2(8)	0	$0,0^+$
		1010.247	28.9(14)	111	$2,0^+$
		757.314	21.9(11)	364	$4,0^+$
1130.029(24)	$2,2^-$	1018.63	2.9(3)	111	$2,0^+$
		226.743	58.6(41)	903	$2,2^+$
		124.071	5.7(6)	1005	$3,2^+$
1133.840(24)	$4,2^+$	1022.57	4.7(5)	111	$2,0^+$
		769.44	8.1(6)[d]	364	$4,0^+$
1221.292(25)	$3,2^-$	1109.88	1.5(2)	111	$2,0^+$
		318.017	16.7(8)	903	$2,2^+$
		215.332	8.7(6)	1005	$3,2^+$
		91.31	0.55(8)	1130	$2,2^-$
1284.991(27)	$5,5^-$	920.81	2.8(4)	364	$4,0^+$
		536.67	0.8(2)	748	$6,0^+$
1294.06(25)	$5,2^+$	930.00	2.0(3)	364	$4,0^+$
1322.13(40)	$0,0^+$	418.847	7.1(5)	903	$2,2^+$
1345.35(10)	$4,2^-$	339.34	3.0(6)	1005	$3,2^+$
		211.63	0.8(2)	1133	$4,2^+$
1386.327(34)	$2,2^+$	1386.36	20.5(10)	0	$0,0^+$
		1275.07	25.6(13)	111	$2,0^+$
		482.925	5.0(5)	903	$2,2^+$
		380.24	$1.0(2_5)$	1005	$3,2^+$
1425.011(41)	$3,3^+$	1313.72	6.2(6)	111	$2,0^+$
		1060.85	2.0(3)	364	$4,0^+$
		294.962	8.4(4)	1130	$2,2^-$
		203.56	1.1(2)	1221	$3,2^-$

TABLE I (Cont.)

Initial State		De-exciting Transition		Final State	
Level energy[a,b] (keV)	I,K^{π}[c]	Gamma-ray energy[b] (keV)	Relative gamma-ray intensity[a]	Level energy (keV)	I,K^{π}
1431.01(5)	$2,0^+$	1430.97	8.5(6)	0	$0,0^+$
		1319.84	10.8(7)	111	$2,0^+$
		(424.36)	0.9(2)	1431	$3,2^+$
1523.26(8)	$3,2^+$	1412.05	7.3(5)	111	$2,0^+$
1536.88(8)	$4,3^+$	1424.6	$1.0(2_5)$	111	$2,0^+$
		315.59	1.3(3)	1221	$3,2^-$
1613.46(8)	$1,1^+$	710.08	8.5(9)	903	$2,2^+$
		607.620	9.0(5)	1005	$3,2^+$
1614.90(8)	$0,0^+$	1503.74	6.9(5)	111	$2,0^+$
		711.58	8.8(9)	903	$2,2^+$
1627.69(8)	$2,1^+$	724.388	14.4(7)	903	$2,2^+$
		241.46	$0.7(1_4)$	1386	$2,2^+$
1713.42(12)	$1,1^+$	810.16	2.5(4)	903	$2,2^+$
1774.82	$2,1^+$	871.56	3.4(7)	903	$2,2^+$
		(769.44)	8.1(6)[d]	1005	$3,2^+$
1808.50(15)	$2,0^+$	1808.54	2.3(5)	0	$0,0^+$
		1697.49	3.1(5)	111	$2,0^+$
		1444.50	2.7(7)	364	$4,0^+$
		802.53	1.4(3)	1005	$3,2^+$
		(678.17)	3.4(3)	1130	$2,2^-$
		(586.94)	$1.5(1_5)$	1221	$3,2^-$
1877.0(2)	$2,2^+$	1877.3	3.5(7)	0	$0,0^+$
		1765.6	3.8(11)	111	$2,0^+$
		746.59	1.8(4)	1130	$2,2^-$
		655.38	1.0(2)	1221	$3,2^-$
[1995.3(3)]	$(0\text{-}2),K^-$	(1995.33)	8.6(17)	0	$0,0^+$
2012.8(3)	$(1,2),K^+$	(1007.03)[e]	2.8(3)	1005	$3,2^+$
		(882.75)[e]	2.0(4)	1130	$2,2^-$
2031.3(3)	$(0\text{-}2),K^+$	1920.07	3.1(8)	111	$2,0^+$
2035.3(3)	$(1,2),K^+$	2035.05	8.7(17)	0	$0,0^+$
		1132.36	1.5(3)	903	$2,2^+$
2061.1(4)	$(0\text{-}2),K^+$	1949.60	7.8(12)	111	$2,0^+$
		(635.92)	2.1(3)	1425	$3,3^+$
2097.7(4)	$(1,2),K^+$	2097.65	4.2(6)	0	$0,0^+$
		1986.6	3.4(7)	111	$2,0^+$
2104.2(5)	$(0\text{-}2),K^+$	(1098.28)[e]	3.4(3)	1005	$3,2^+$
		(982.44)[e]	1.4(3)	1121	$2,0^+$
		(782.19)[e]	0.9(3)	1322	$0,0^+$

TABLE I (Cont.)

Initial State		De-exciting Transition		Final State	
Level energy[a,b] (keV)	I,K^{π}[c]	Gamma-ray energy[b] (keV)	Relative gamma-ray intensity[a]	Level energy (keV)	I,K^{π}
2112.5(10)	$(0\text{-}2),K^{+}$	(982.44)[e]	1.4(3)	1130	$2,2^{-}$
2126.00(15)	$(0,2),K^{+}$	2015.32	8.4(8)	111	$2,0^{+}$
		1004.47	3.7(4)	1121	$2,0^{+}$
		996.06	4.4(4)	1130	$2,2^{-}$
2167.80(20)	$1,K^{+}$	2056.34	7.3(11)	111	$2,0^{+}$
		1046.42	1.5(5)	1121	$2,0^{+}$
		846.21	1.5(5)	1322	$0,0^{+}$
		(782.19)[e]	0.9(4)	1386	$2,2^{+}$
		743.19	4.2(4)	1425	$3,3^{+}$
[2194.7(10)]	$(0\text{-}2),K^{-}$				
2221.3(4)	$1,K^{+}$	2109.99	3.4(9)	111	$2,0^{+}$
		446.64	0.7(2)	1774	$2,1^{+}$
2228.2(6)	$(2,K^{-})$	(1098.28)[e]	3.4(3)	1130	$2,2^{-}$
		(1007.03)[e]	2.8(3)	1221	$3,2^{-}$
		(882.75)[e]	2.0(4)	1345	$4,2^{-}$
2246.4(3)	$(1),K^{+}$	2135.12	3.1(9)	111	$2,0^{+}$
2294.7(3)	$(0,0)^{+}$	2183.62	7.8(12)	111	$2,0^{+}$
		1391.23	3.6(4)	903	$2,2^{+}$
2352.1(8)	$(0\text{-}2),K^{+}$				
2370.3(3)	$(1,2),K^{+}$	2370.37	4.0(6)	0	$0,0^{+}$
		2258.6	4.3(11)	111	$2,0^{+}$
2395.3(4)	$(0,1),K^{+}$	2284.2	9.2(14)	111	$2,0^{+}$
		(782.19)[e]	0.9(4)	1613	$1,1^{+}$

[a] The uncertainties in the least significant figures are indicated in parentheses.

[b] Parentheses around a level energy, or a γ-ray energy, indicates a tentative assignment.

[c] Parentheses are used to indicate probable spin values or probable limits on the spin values, and the use of the symbol K indicates that the K quantum number is unknown.

[d] Based upon the ^{184}Re decay data[1] we would estimate that only (74±7)% of this intensity results from decay of the 1133-keV level, with the balance, (26±7)%, being emitted in decay from the 1774-keV level.

[e] This γ-ray transition can be assigned as de-exciting one or more additional states in ^{184}W.

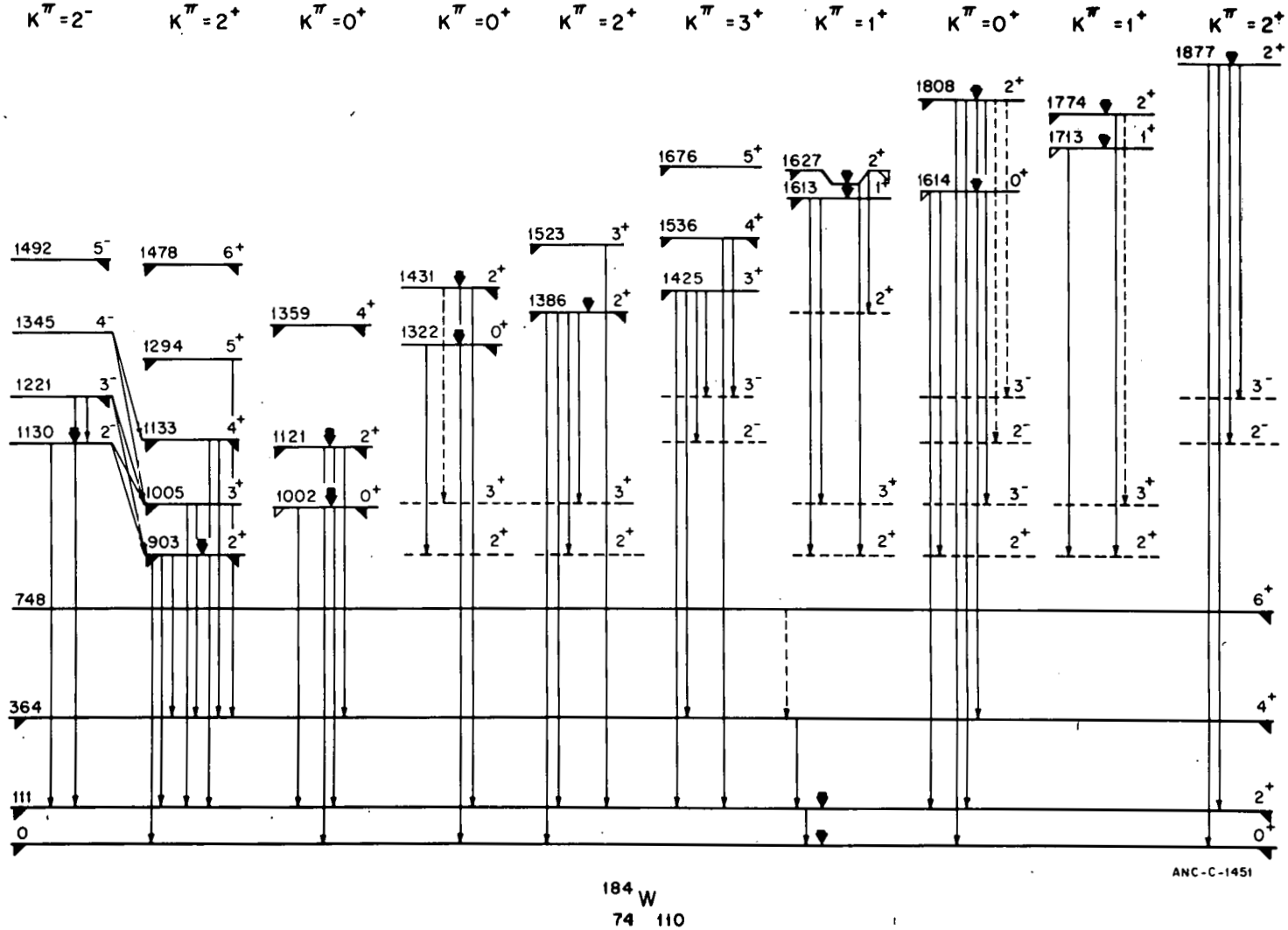

Figure 1 Level scheme for ^{184}W based upon the $^{183}W(n,\gamma)$ reaction studies with proposed grouping of states into rotational bands. An arrow into a level indicates population by primary γ-ray transitions. Solid triangles associated with a level indicate that the level is populated by charged particle reactions: lower left indicates (d,p) population, and lower right indicates (d,d') population. Open triangles indicate tentative assignments.

NUCLEAR STRUCTURE STUDIES USING THE 25-keV NEUTRON BEAM FACILITY ON HFBR

R. C. Greenwood

The iron-aluminum filter which has been installed in the H-1B beam of the HFBR provides an intense ($\sim 10^6$ neutrons/cm^2-sec) beam of 25-keV neutrons. Furthermore, the beam is quite monoenergetic, containing a < 3% component of higher energy neutrons. Of specific import to us, for nuclear structure studies, is the finite energy spread in the 25-keV neutrons. The 25-keV neutron distribution will have a FWHM ranging from 1.1-2.0 keV depending upon the thickness of the filter. Hence, for the higher-Z nuclei not close to closed shells, we expect the resultant capture γ-ray spectra to represent an average over many compound resonance states. Such averaging will thus tend to smooth out the Porter-Thomas statistical fluctuations in the intensities of the primary transitions, thus allowing these transition intensities to be related to the I^{π} of the final states.

Measurements which have been undertaken to date with this facility have been exploratory in nature and hence have intentionally duplicated measurements we have previously undertaken with the 2-keV neutron beam of the MTR. The purpose of these measurements have in the main been to determine sensitivity; that is, what sample sizes are needed to obtain spectra of suitable quality to extract useful nuclear structure information. To this end, we have measured 25-keV neutron capture spectra from targets of natural gadolinium oxide ($\sim$ 100 g), 8.8 g each of $^{182}WO_3$ and $^{183}WO_3$, and natural tantalum. Figure 1 shows a portion of the spectrum of $^{182}W(n,\gamma)$ obtained in a $\sim$ 36-hr run using a $\sim$ 10 cm^3 intrinsic Ge detector. This spectrum can be compared with that obtained using 2-keV neutrons shown in Reference [1]. After allowing for the different running times we conclude that the spectra are of fairly comparable quality. The prompt γ-ray spectrum resulting from capture of these 25-keV neutrons in the gadolinium sample is also shown in Figure 2. This spectrum, while it was obtained with only a $\sim$ 4 cm^3 Ge(Li) detector having poor resolution (it had been significantly neutron damaged), shows considerable line structure.

---

[1] R. C. Greenwood and C. W. Reich, Nuclear Technology Division Annual Progress Report for Period Ending June 30, 1971, ANCR-1016 (1971) 54.

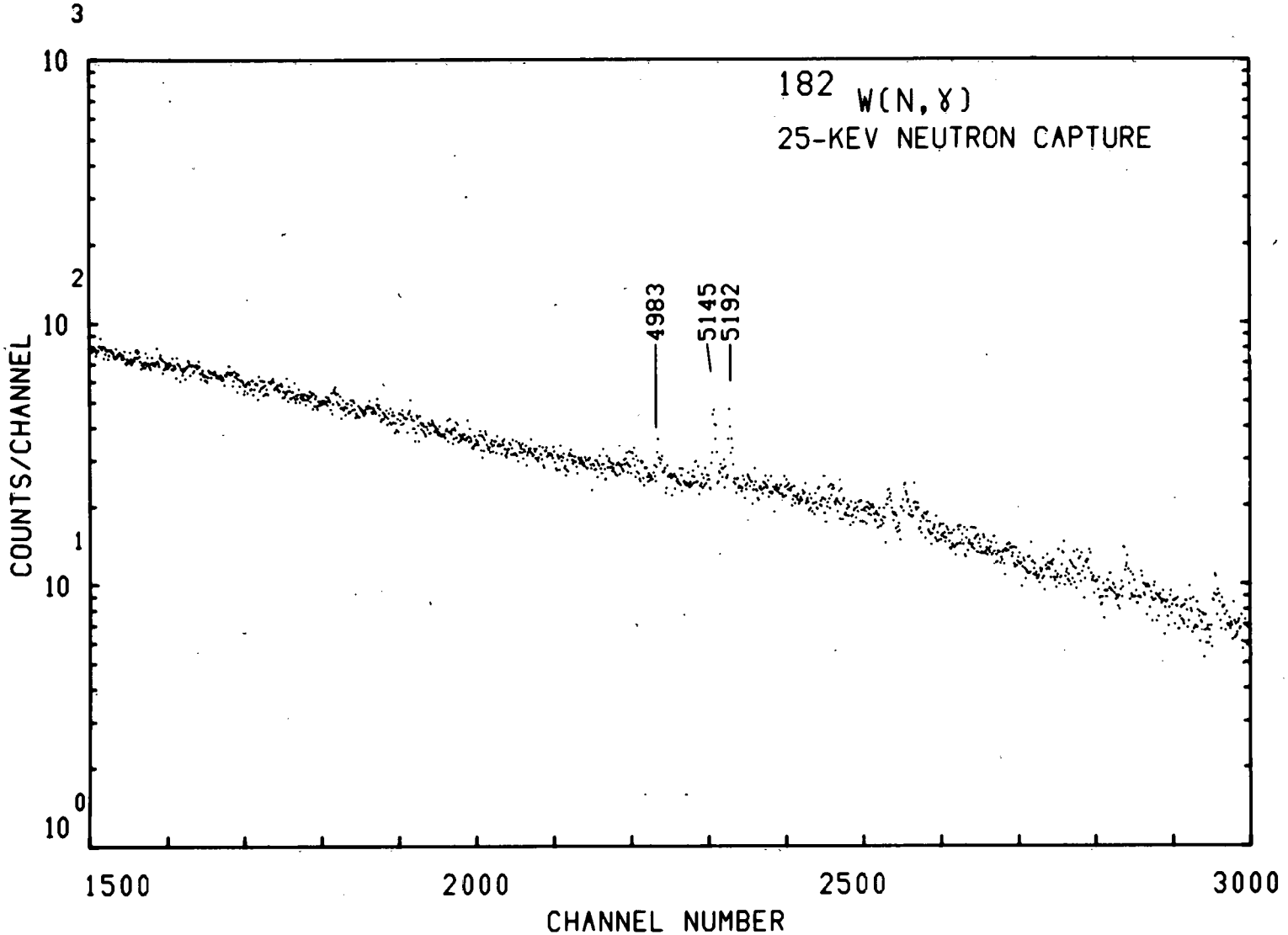

Figure 1. Higher energy portion of the prompt γ-ray spectrum resulting from 25-keV neutron capture on ^{182}W.

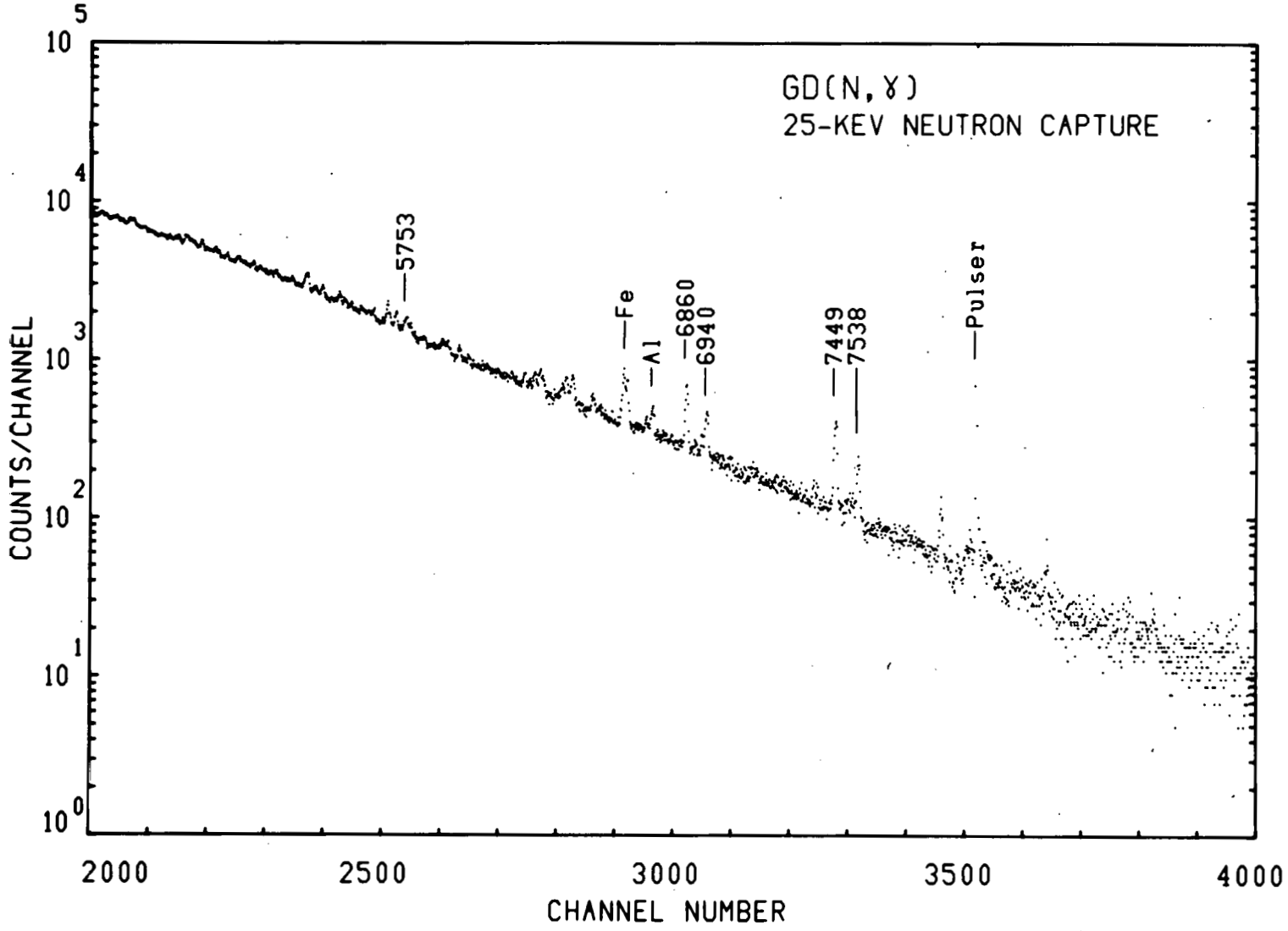

Figure 2 Higher energy portion of the prompt γ-ray spectrum resulting from 25-keV neutron capture on a natural gadolinium target.

^{182}Ta CONVERSION ELECTRON STUDIES

R. G. Helmer

The internal-conversion-electron spectrum above 800 keV from the decay of ^{182}Ta (115 d) has been measured with the $\pi\sqrt{2}$ electron spectrometer. A list of the lines observed and the resolutions used is given in Table I.

The ^{182}Ta source used was made by vacuum evaporation of stable tantalum onto an 0.0003-in. thick aluminum backing with subsequent irradiation in a flux of $\sim 4 \times 10^{14}$ n/cm^2-sec for $\sim$ 30 days. The electron data were accumulated over a period of four months of almost continuous operation.

The ^{182}Ta source is quite thick. Several low-energy (i.e., < 200 keV) lines were measured in order to provide information on the source thickness. An attempt will be made to take this thickness into account in the analysis of the data.

TABLE I

INTERNAL-CONVERSION-ELECTRON LINES MEASURED IN DECAY OF ^{182}Ta (Lines for transitions below 300 keV are for information on source thickness.)

Resolution	Gamma-Ray Energy (keV)	Lines	Resolution	Gamma-Ray Energy (keV)	Lines
0.075%	100	L_1 L_2 L_3	0.10% (Cont.)	1221	K L_1 L_2 L_3
	264	K		1223	K
	1113	K		1231	K
	1121	K L_1 L_2 L_3		1257	K
	1157, 1158	K		1273	K
	1189	K L_1 L_2 L_3		1289	K L_1 L_2 L_3
	1221	K L_1 L_2 L_3		1342	K
	1223	K		1374	K
	1231	K		1387	K
	1257	K		1410	K
	1273	K		1453	K
	1289	K			
			0.20%	891	K
0.10%	100	L_1 L_2 L_3		927	K
	264	K		959	K
	891	K		1002	K
	927	K		1121	K
	959	K		1139	K
	1002	K L_1 L_2 L_3		1157	K
	1039	K		1221	K
	1044	K		1231	K
	1113	K		1373	K
	1121	K L_1 L_2 L_3		1387	K
	1139	K		1410	K
	1157, 1158	K		1453	K
	1189	K L_1 L_2 L_3			

STUDIES OF CONTINUOUS ELECTRON SPECTRA

R. G. Hughes[1], R. G. Helmer

In the beta decay process, a continuous spectrum of electrons is emitted. These spectra are often composed of several components, with each one populating a different state in the daughter nucleus. The analysis of such spectra involves for each component, the determination of (1) the relative intensity and (2) the shape (i.e., the energy dependent shape factor). An analysis of these continuous spectra is often important for the determination of absolute gamma-ray intensities as well as the study of certain nuclear structure properties.

Continuous electron spectra measurements have been made for ^{32}P, ^{86}Rb and ^{124}Sb on the iron-free $\pi\sqrt{2}$ spectrometer. The positron spectrum from ^{84}Rb has also been measured. The ^{32}P sources were made both by vacuum evaporation and by drying the solution. Comparison of the spectra of these different sources yields information on the electron scattering in the sources. The spectrum was also measured with various source arrangements to determine the magnitude of the electron scattering from material in the vicinity of the source, including the source backing.

The $^{84,86}Rb$ sources were also made both by drying the solution and by vacuum evaporation. The spectra were measured at a resolution of 0.3%. Sources of ^{124}Sb were made by vacuum evaporation of a ^{123}Sb sample irradiated $\sim$ 15 days in the ETR. Sources of different thickness were made as a check on the electron scattering in the source. These sources were mounted on 0.00003-in. thick aluminum foil. For this thin backing, the electron scattering from the backing should be negligible.

The analysis of these data is in progress.

---

[1] Graduate student from Utah State University, Logan, Utah on AWU program. Current address: Naval Research Lab, Ocean Technology Division, Washington, D.C.

THIS PAGE

WAS INTENTIONALLY

LEFT BLANK

B. GENERAL REACTOR DEVELOPMENT AND SUPPORT

THIS PAGE

WAS INTENTIONALLY

LEFT BLANK

FISSION AND ACTIVATION PRODUCT INVENTORIES IN COMMERCIAL POWER REACTOR COOLANT, OFF-GAS AND WASTE SYSTEMS

N. C. Dyer, J. E. Cline[1], R. L. Heath

In conjunction with the Directorate of Regulatory Operations of the USAEC, measurements have been made of the radionuclides present in the coolant, off-gas and waste systems of six boiling water reactors. Preliminary measurements have been done at one pressurized water reactor. These plants are being operated in commercial power productions. The inventories were taken as a portion of the independent measurements program of Regulatory Operations to determine the behavior and levels of radionuclides in the reactor coolant and effluent systems.

A list of the typical samples taken from each BWR is presented in Table I. The gamma rays emitted by these samples were measured over a period of several weeks to obtain information on radionuclides with both short and long half-lives. A high-resolution, large volume, 4096-channel Ge(Li) gamma-ray spectrometer was transported to each reactor site for the week during which samples were collected. This enables the collection of gamma-ray spectra for the measurement of the short-lived radionuclides. The samples and spectrometer were then returned to NRTS in order to acquire data on the longer-lived species. About 100 to 130 gamma-ray spectra were acquired from the samples for each BWR. These were analyzed in the batch process mode using the computer analysis program Gauss VI[2] that was developed at this laboratory. Without the use of an automated batch processing analysis package, measurements such as these would be very difficult and time consuming.

Some 40 fission and activation-product radionuclides were quantitatively inventoried in the measurements of each BWR. The results are being used by Regulatory to evaluate the hazards and the release rates of boiling water reactors. For the next fiscal year, measurements are planned for six operating PWR plants designed by three different manufacturers.

---

[1] Present address: Nuclear Environmental Services, Div. of JRB Associates, 455 W. 17th Street, P. O. Box 831, Idaho Falls, Idaho 83401.

[2] J. E. Cline, M. H. Putnam and R. G. Helmer, Gauss VI, A Computer Program for the Automatic Batch Analysis of Gamma-Ray Spectra from Ge(Li) Spectrometers, ANCR-1113 (1973).

TABLE I

SAMPLES FROM A TYPICAL BWR

1)	50-ml samples of primary coolant water	7
2)	100-ml sample of primary coolant water taken just after start-up of following refueling - for "crud" analysis	1
3)	500-ml samples of steam (condensed in the sampling line)	4
4)	500-ml samples of condensate water	4
5)	50-ml samples of water taken at the inlet to the bypass or clean-up demineralizer	4
6)	500-ml samples of water taken at the outlet of the bypass demineralizer	4
7)	500-ml samples of water from the outlet of the full-flow demineralizer	4
8)	500-ml samples of reactor feed water	4
9)	1000-ml samples of water tank effluent	2
10)	15-ml samples of off-gas from the steam-jet air ejector	3
11)	15-ml samples of off-gas after delay line	1
12)	60.5-gm samples of by-pass demineralizer resin bed - just prior to regeneration	2
	Total Samples	40

ASSISTANCE TO REGIONAL OFFICES OF AEC REGULATORY OPERATIONS

N. C. Dyer, R. G. Helmer, J. E. Cline[1], E. W. Killian[2], R. J. Gehrke, R. C. Davies[2], R. L. Heath

Regulatory Operations of the USAEC have felt it would be advantageous if their regional offices could have the capability to make in-field radionuclide inventories at nuclear plant sites similar to an ongoing project at this laboratory[3]. As a pilot project, ANC and Brookhaven National Laboratory have been assisting the Region I Office of AEC Regulatory Operations in the implementation of a gamma-ray spectral analysis system which will be housed in a mobile van. Our part of the project has been to provide the software programming for an existing computer-analyzer system (HP 2114), purchase and calibrate the Ge(Li) detector and linear amplifier, integrate the different components into a working gamma-ray spectrometer, provide instruction to Region I personnel in the use of the system and provide batch process analysis for some of the spectra collected through use of Gauss VI[4].

During this past fiscal year, the Ge(Li) detector has been obtained and calibrated plus the software packages have been written and partially tested. It is anticipated that the complete gamma-ray measurement and analysis system will be made operational and instruction of Region I personnel will be completed during this next year. An analysis and measurement system such as this should prove very useful to the regional Regulatory offices.

---

[1] Present address: Nuclear Environmental Services, Division of JRB Associates, 455 W. 17th Street, P. O. Box 831, Idaho Falls, Idaho 83401

[2] Members of Analysis and Programming Branch, Technical Services Division, ANC.

[3] N. C. Dyer, J. E. Cline, R. L. Heath, "Fission and Activation Product Inventories in Commercial Power Reactor Coolant, Off-Gas and Waste Systems", this report.

[4] J. E. Cline, M. H. Putnam and R. G. Helmer, Gauss VI, A Computer Program for the Automatic Batch Analysis of Gamma-Ray Spectra from Ge(Li) Spectrometers, ANCR-1113 (1973).

NUCLEAR DATA GENERATION FOR FISSION-PRODUCT DECAY-HEAT STUDIES

C. W. Reich, R. G. Helmer, R. C. Greenwood

In recognition of the pressing need for such data in a variety of reactor-related applications, the scope of ENDF/B has been expanded to include information on the decay properties of radioactive nuclides. Through our participation in the Decay-Heat Task Force of the Fission-Product Subcommittee of CSEWG, we have a major involvement in this

project. The first task was to decide upon the data content of this file. After consideration of the potential user applications of radioactive decay data,a file content was proposed which should have applicability in a wide range of practical problems. This proposed content was adopted by CSEWG during its May, 1973 meeting at Brookhaven National Laboratory.

The current phase of this effort is the preparation for inclusion in ENDF/B-IV of certain nuclide decay data for a selected group of fission-product nuclides relevant to decay-heat calculations in reactor cores. These data include fission yields, half-lives, decay energies and average β- and γ-ray energies. A list of 338 "priority" nuclides for which these data are necessary has been drawn up by the Decay-Heat Task Force.

At present, we have completed a compilation of the total decay energies (i.e., Q_β values) for these nuclides. Experimental values have been taken primarily from the 1973 revision of the Wapstra-Gove atomic-mass tables[1] although, where such data have appeared sufficiently recently as not to be included in this compilation, these later data have been used. For those nuclides for which no experimental data exist, the Q_β values have been taken from the predictions of Garvey et al.[2]

It has been found that $\langle E_\beta \rangle$ and $\langle E_\gamma \rangle$ values can be derived from experimental data for $\sim$ 180 of these "priority" nuclides, and this data compilation effort is currently under way. For the remaining $\sim$ 150 nuclei, it will be necessary to use theoretical considerations to estimate the $\langle E_\beta \rangle$ and $\langle E_\gamma \rangle$ values. The major responsibility for this portion of the task has been assumed by HEDL, although some suggestions of possible approaches to this problem have been made by ANC personnel.

The major responsibility for the preparation of the fission-yield and half-life data for these nuclides has been taken by personnel at other laboratories, although ANC personnel will have some involvement in the half-life data. The present schedule calls for these data, in a form suitable for preliminary file-evaluation purposes, to be ready by the latter part of September, 1973.

---

[1] A. H. Wapstra and N. B. Gove, private communication from N. B. Gove (1973).

[2] G. T. Garvey, W. J. Gerace, R. L. Jaffe, I. Talmi and I. Kelson, Reviews of Modern Physics 41, No. 4, part II (1969).

SPECTRUM CALCULATIONS FOR THE CFRMF

D. A. Millsap

There has been a continuing effort to improve knowledge of the neutron spectrum of the Coupled Fast Reactivity Measurement Facility (CFRMF) by way of calculations. Recent investigations have employed three different computer codes to calculate the CFRMF spectrum. These were: SCAMP[1], a one-dimensional transport code covering the entire energy range; RAFFLE[2], a Monte Carlo code; and RABBLE[3], a multi-region resonance absorption cross section code. The latter codes were limited to distinct energy ranges.

SCAMP, a one-dimensional S_n neutron transport code was used to calculate the CFRMF spectrum over the full energy range from thermal to 10 MeV. Since this code is quite versatile with many useful options and a relatively short computation time, it was used as the principal tool for the spectrum investigations presented here. A special 69-group library was prepared for use with SCAMP, using the cross section code PHROG[4]. All cross sections were derived from ENDF/B, Version III data except for those of iron which came from Version II. The group structure used for the calculations is given in Table I. A wide variety of calculations was performed both to refine the geometric representation of the model and to evaluate the effects of the various assumptions made for the codes being used. Details of the model found to give the best possible representation of the CFRMF within the limitations of the codes are given in Table II. The SCAMP calculation using this model was an eigenvalue problem with a semi-isotropic reflective boundary condition at the outer boundary. A constant axial buckling of $B^2 = 0.001769$ was used for all regions. The full core loading for the CFRMF could not be represented by SCAMP due to computer core storage limitations. The particular dimension of the outer boundary given in Table II was an arbitrary choice, selected only because it gave an eigenvalue close to 1.0. A series of outer boundary dimensions was tested and gave eigenvalues ranging from 0.96 to 1.07; however, the central flux spectrum was not significantly effected by such changes.

The Monte Carlo Code RAFFLE was used to calculate fluxes over the energy range 15.0 keV to 10 MeV. The purpose of the RAFFLE calculation was to examine as carefully as feasible the residual effects of the resonances of the aluminum and oxygen contained in the thermal driver on the central fluxes of the CFRMF. The basic geometric model used for the RAFFLE calculation is identical to that of the SCAMP calculations whose details are given in Table II. Certain possible deficiencies of the calculational model or of the code itself were examined using SCAMP in order to evaluate their approximate effect on the RAFFLE generated spectrum. A previous RAFFLE calculation[5] used a spatially constant fixed source in the reactor fuel region. It was found that a SCAMP problem with a uniform fixed source gave significantly different fluxes from those of the eigenvalue problem. It was for this reason that the fuel regions were split into several subregions. Suitable volume-averaged sources for the fuel containing regions were determined from

SCAMP and used in the corresponding regions in the RAFFLE problem. The relative volume-integrated sources used are given in Table III. Other deficiencies were found to be of relatively minor importance. The previous RAFFLE problem used pointwise elastic scatter cross sections for aluminum and oxygen. For this calculation, pointwise absorption cross sections for ^{10}B were added to eliminate any possible flux smoothing effect due to the group-averaged cross section of this isotope. Also, the source spectrum was input using a 0.125 lethargy group structure.

A special version of the computer code RABBLE was used to calculate fluxes over the energy range from 0.876 eV to 52.5 keV. Among other features, this code gives group-averaged cross sections for the resonance energy range using space and lethargy dependent slowing down sources. Extremely fine group fluxes are calculated in order to represent the resonance absorption properly. Modifications were made to the code which allowed a greater number of broad groups and regions, unresolved resonance subroutines were added, and a provision to output the fine group fluxes on magnetic tape was incorporated. A routine was then programmed to plot the fine group fluxes from tape. Examination of fine group flux plots could then presumably show the presence of "holes" or "windows" not seen by the SCAMP calculation with its much broader group structure.

A calculation was performed using the revised RABBLE code and a geometric representation which incorporated the identical major material boundaries and atom densities of the SCAMP problems described above. Details of this model are given in Table IV. The broad group structure used is the same as that of the SCAMP (see Table I) for groups 22 through 65. Each broad group had 250 fine groups of equal lethargy width, making a total of 1000 fine groups per unit lethargy.

The results of the various calculations using SCAMP, RAFFLE and RABBLE are presented in Figures 1-6. Figure 1 gives the CFRMF flux calculated using an S_8 SCAMP for the energy range 3.06 eV to 10 MeV. For energies below 3.06 eV (group 60), the flux continues to drop off very steeply and appears to be of little significance for activation calculations. Figure 2 compares this transport calculation with a previous 44-group diffusion theory calculation which used the computer code MONA[6]. The significantly higher fluxes of the transport calculation at energies below 1.0 keV result largely from a change in the PHROG code which prepares the group-averaged cross sections. No resonance calculation was made for the elastic scatter cross sections in the earlier calculation. Thus, the elastic scatter cross sections were infinite dilute and the diffusion constants for the uranium block were greatly distorted. The SCAMP cross section library was prepared by the revised PHROG code and the spectrum change in the SCAMP calculation relative to the older calculation is, at least in part, a direct result of this change. Figure 3 compares the SCAMP spectrum with the proton-recoil measurement coalesced to a similar lethargy structure. As in previous work, there are significant differences between the measurement and the calculation, particularly at the groups corresponding to energies of 1.0 MeV, 225 keV, and 90 keV. For some time it has been suspected that

these differences might result because of the smoothing effect of the cross section processing codes on the resonances of aluminum and oxygen. However, the Monte Carlo approach, with pointwise cross sections for most of the materials expected to be contributing to a flux-smoothing effect (aluminum and oxygen elastic scatter, ^{10}B absorption), shows only minor differences from the SCAMP calculation (Figure 4, SCAMP vs. RAFFLE). The low energy broad-group flux spectrum calculated by RABBLE is plotted with that of SCAMP in Figure 5. The general profile of the broad-group central fluxes of the two calculations compare very well over the energy range from 3.93 eV to 15.0 keV. It is therefore plausible to assume that the fine-group fluxes of the RABBLE calculation (shown in Figure 6) present a fairly reasonable picture of the flux distribution of the CFRMF over this energy range. The structure in Figure 6 clearly indicates the effects of the resolved resonances present in the ENDF/B Version III data. Below 80 keV, the influence of the ^{235}U resolved resonances are superimposed on the much broader flux structure produced by the ^{238}U. The fine-group flux calculation shows that there are no important windows in the flux.

Because of the general agreement between the results of the widely varying approaches one can conclude that the 69-group flux spectrum given by SCAMP is as good a representation of the CFRMF spectrum as can be calculated with the existing cross section sets. Any further improvements in the calculated flux spectrum will probably originate primarily from changes in cross sections rather than from modifications of the calculation procedures.

---

[1] C. E. Beck, "S_n Codes for the Analysis of Multigroup Problems", Beck-2-68A, Idaho Nuclear interoffice correspondence.

[2] W. E. Vesley, F. J. Wheeler, R. S. Marsden, The RAFFLE General Purpose Monte Carlo Code, ANCR-1022 (April 1973).

[3] P. H. Kier and A. A. Robba, RABBLE, A Program for Computation of Resonance Absorption in Multiregion Reactor Cells, ANL-7326 (April 1973).

[4] R. L. Curtis, F. J. Wheeler, G. L. Singer, R. A. Grimesey, PHROG - A Fortran IV Program to Generate Fast Neutron Spectra and Average Multigroup Constants, IN-1435 (April 1971).

[5] D. A. Millsap, Nuclear Technology Division Annual Progress Report for Period Ending June 30, 1972, ANCR-1088 (1972) p. 302.

[6] G. E. Putnam, MONA, A Multigroup One-Dimensional Neutronics Analysis Code, ANCR-1051 (March 1972).

TABLE I

BASIC GROUP STRUCTURE

Group Number	Lower Lethargy	Lower Energy (eV)	Group Number	Lower Lethargy	Lower Energy (eV)
1	0.25	7.79×10^6	36	9.00	1.23×10^3
2	0.50	6.07	37	9.25	961.1
3	0.75	4.72	38	9.50	748.5
4	1.00	3.68	39	9.75	582.9
5	1.25	2.87	40	10.00	454.0
6	1.50	2.23	41	10.25	353.6
7	1.75	1.74	42	10.50	275.4
8	2.00	1.35	43	10.75	214.5
9	2.25	1.05	44	11.00	167.0
10	2.50	8.21×10^5	45	11.25	130.1
11	2.75	6.39	46	11.50	101.3
12	3.00	4.98	47	11.75	78.9
13	3.25	3.88	48	12.00	61.4
14	3.50	3.02	49	12.25	47.9
15	3.75	2.35	50	12.50	37.3
16	4.00	1.83	51	12.75	29.0
17	4.25	1.43	52	13.00	22.6
18	4.50	1.11	53	13.25	17.6
19	4.75	8.65×10^4	54	13.50	13.7
20	5.00	6.74	55	13.75	10.68
21	5.25	5.25	56	14.00	8.32
22	5.50	4.09	57	14.25	6.48
23	5.75	3.18	58	14.50	5.04
24	6.00	2.48	59	14.75	3.93
25	6.25	1.93	60	15.00	3.06
26	6.50	1.50	61	15.25	2.38
27	6.75	1.17	62	15.50	1.86
28	7.00	9.12×10^3	63	15.75	1.44
29	7.25	7.10	64	16.00	1.125
30	7.50	5.53	65	16.25	0.876
31	7.75	4.31	66	16.50	0.683
32	8.00	3.36	67	16.75	0.532
33	8.25	2.61	68	17.00	0.414
34	8.50	2.04	69	∞	0.0
35	8.75	1.59			

TABLE II

DETAILS OF MODEL USED FOR SCAMP AND RAFFLE CALCULATIONS

Region Number	Outer Radius (cm)	Material Description	Isotopes Contained	Atom Densities ($cm^{-3} \times 10^{-24}$)
1	1.95393	Void	--	--
2	2.12344	Stainless Steel Type 304 Dry Tube and Cladding	Chromium	0.0174285
			Manganese	0.0017947
			Iron	0.0580747
			Nickel	0.0081239
3	2.21996	Uranium Sleeve	^{235}Uranium	0.0453606
			^{238}Uranium	0.0026310
4	2.29997	Stainless Steel Type 304 Cladding	Same as Region 2	
5	2.65049	Enriched Boron Sleeve	^{10}Boron	0.0732773
			^{11}Boron	0.0068255
6	2.69748	Stainless Steel Type 304 Cladding	Same as Region 2	
7	3.796236	Uranium Block	^{235}Uranium	0.9334×10^{-4}
			^{238}Uranium	0.0476476
8	4.894992	Uranium Block	Same as Region 7	
9	5.993748	Uranium Block	Same as Region 7	
10	7.092504	Uranium Block	Same as Region 7	
11	8.19126	Uranium Block	Same as Region 7	
12	8.97083	Boral Thermal Neutron Filter	Carbon	0.0087848
			Aluminum	0.0361511
			^{10}Boron	0.0069505
			^{11}Boron	0.0281886
13	9.32910	Stainless Steel Type 304 Assembly Housing	Same as Region 2	
14	9.649385	Water Annulus Side Plates and Reactor Fuel	Hydrogen	0.0274447
			Oxygen	0.0137223
			Aluminum	0.0354132
			^{235}Uranium	4.76406×10^{-5}
			^{238}Uranium	2.82833×10^{-6}

TABLE II (Cont.)

Region Number	Outer Radius (cm)	Material Description	Isotopes Contained	Atom Densities ($cm^{-3} \times 10^{-24}$)
15	9.96967	Water Annulus Side Plates and Reactor Fuel	Same as Region 14	
16	10.4221975	Homogenized Reactor Fuel	Hydrogen	0.0430022
			Oxygen	0.0215001
			Aluminum	0.0212863
			^{235}Uranium	1.14407×10^{-7}
			^{238}Uranium	6.79208×10^{-6}
17	10.984725	Homogenized Reactor Fuel	Same as Region 16	
18	11.77978	Homogenized Reactor Fuel	Same as Region 16	
19	12.684835	Homogenized Reactor Fuel	Same as Region 16	
20	15.40	Homogenized Reactor Fuel	Same as Region 16	

THIS PAGE

WAS INTENTIONALLY

LEFT BLANK

TABLE III

RELATIVE VOLUME INTEGRATED SOURCES

By Region

Region Number	Description	Relative Source
1		
2		
3	Uranium Sleeve	6.8461×10^{-3}
4		
5		
6		
7	Uranium Block	5.8416×10^{-3}
8	Uranium Block	8.1378×10^{-3}
9	Uranium Block	1.1242×10^{-2}
10	Uranium Block	1.5517×10^{-2}
11	Uranium Block	2.1728×10^{-2}
12		
13		
14	Water Annulus,	6.2259×10^{-3}
15	Side Plates, Reactor Fuel	7.9352×10^{-3}
16	Homogenized Reactor Fuel	3.4659×10^{-2}
17	Homogenized Reactor Fuel	4.4424×10^{-2}
18	Homogenized Reactor Fuel	0.11518
19	Homogenized Reactor Fuel	0.14592
20	Homogenized Reactor Fuel	0.57636

TABLE IV

DETAILS OF MODEL USED FOR RABBLE CALCULATION*

Region Number	Outer Radius (cm)	Material Description
1	1.95393	Void
2	2.12344	Stainless Steel
3	2.21996	Uranium Sleeve
4	2.29997	Stainless Steel
5	2.65049	Enriched Boron Sleeve
6	2.69748	Stainless Steel
7	4.894992	Uranium Block
8	7.092504	Uranium Block
9	8.19126	Uranium Block
10	8.97083	Boral
11	9.3291	Stainless Steel
12	9.96967	Water Annulus, Side Plates and Reactor Fuel
13	15.40	Homogenized Reactor Fuel

* Isotopes contained in the various materials and their atom densities are the same as for SCAMP and RAFFLE, shown in Table II.

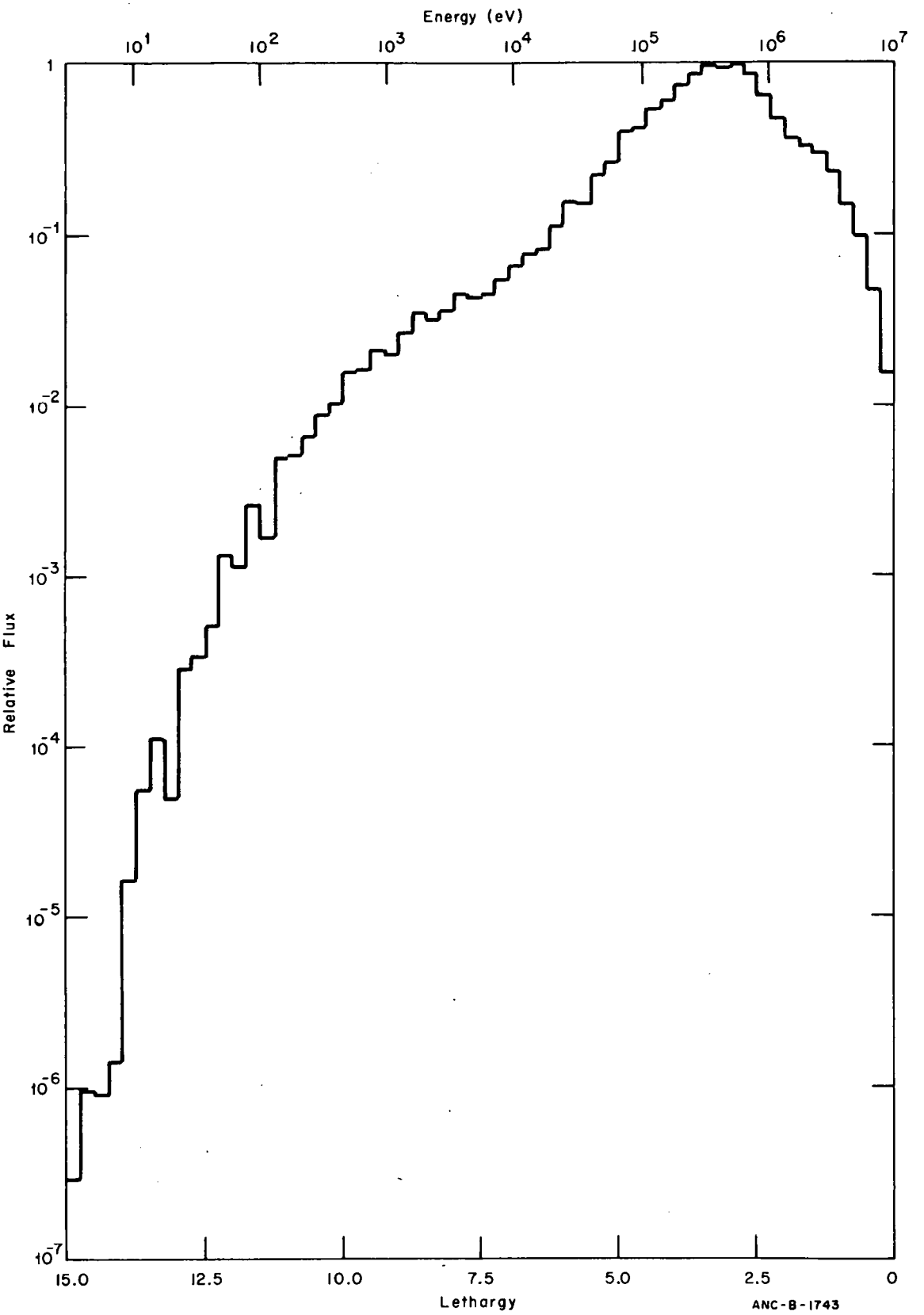

Figure 1 CFRMF Central Flux as Calculated by SCAMP.

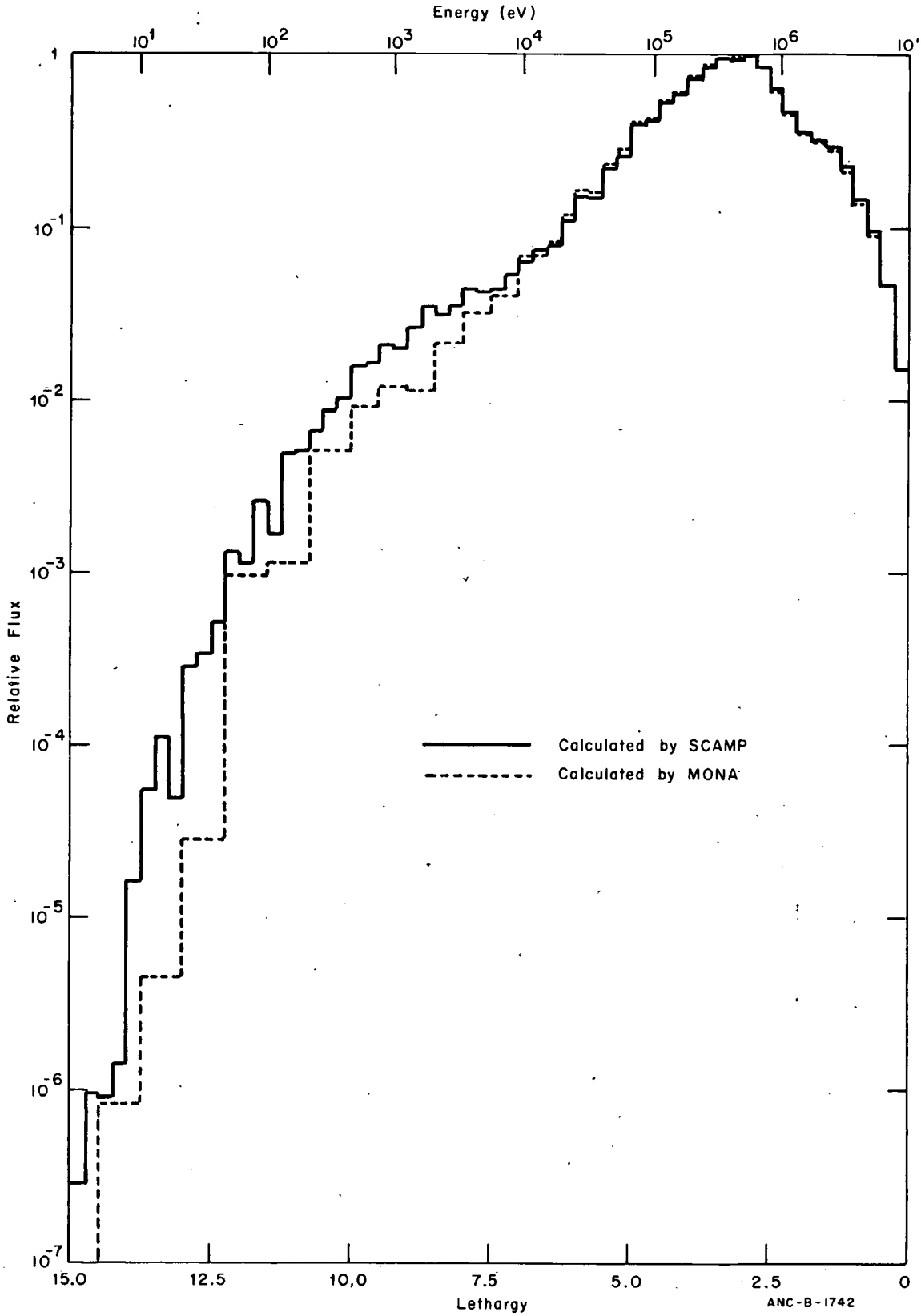

Figure 2 CFRMF Central Flux: A comparison of calculations by SCAMP and MONA.

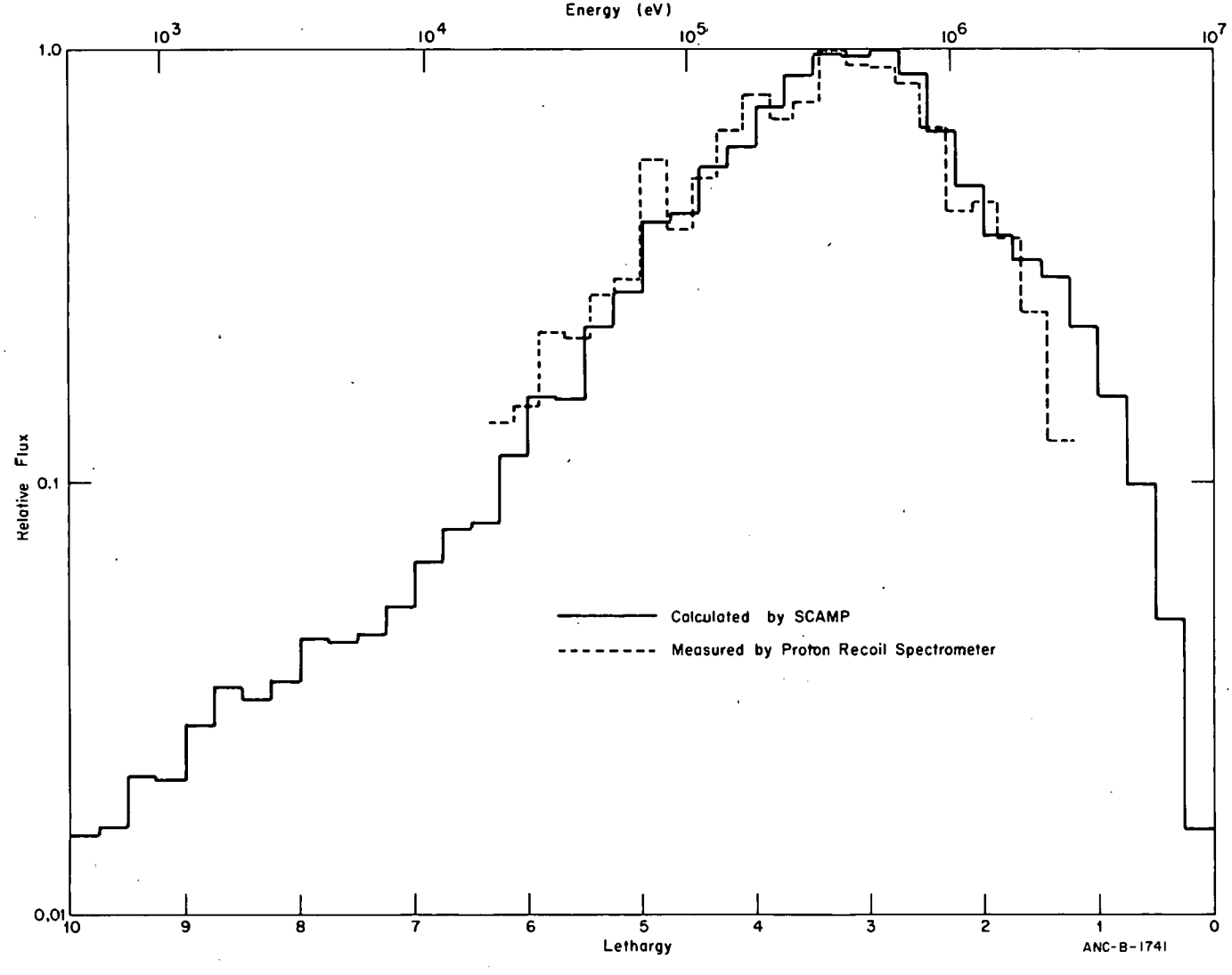

Figure 3 CFRMF Central Flux: A comparison of SCAMP calculation with proton-recoil measurement.

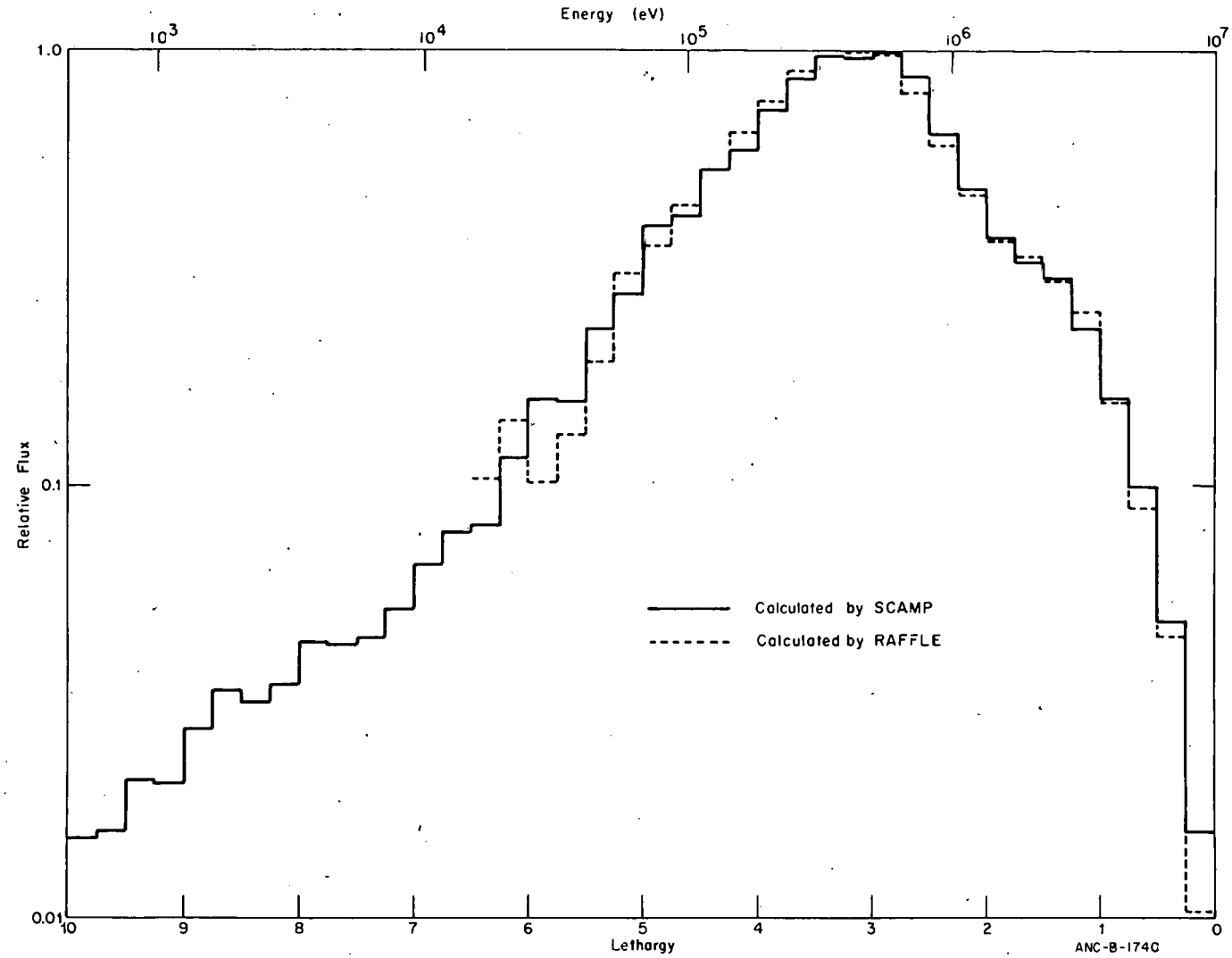

Figure 4 CFRMF Central Flux: A comparison of calculations by SCAMP and RAFFLE.

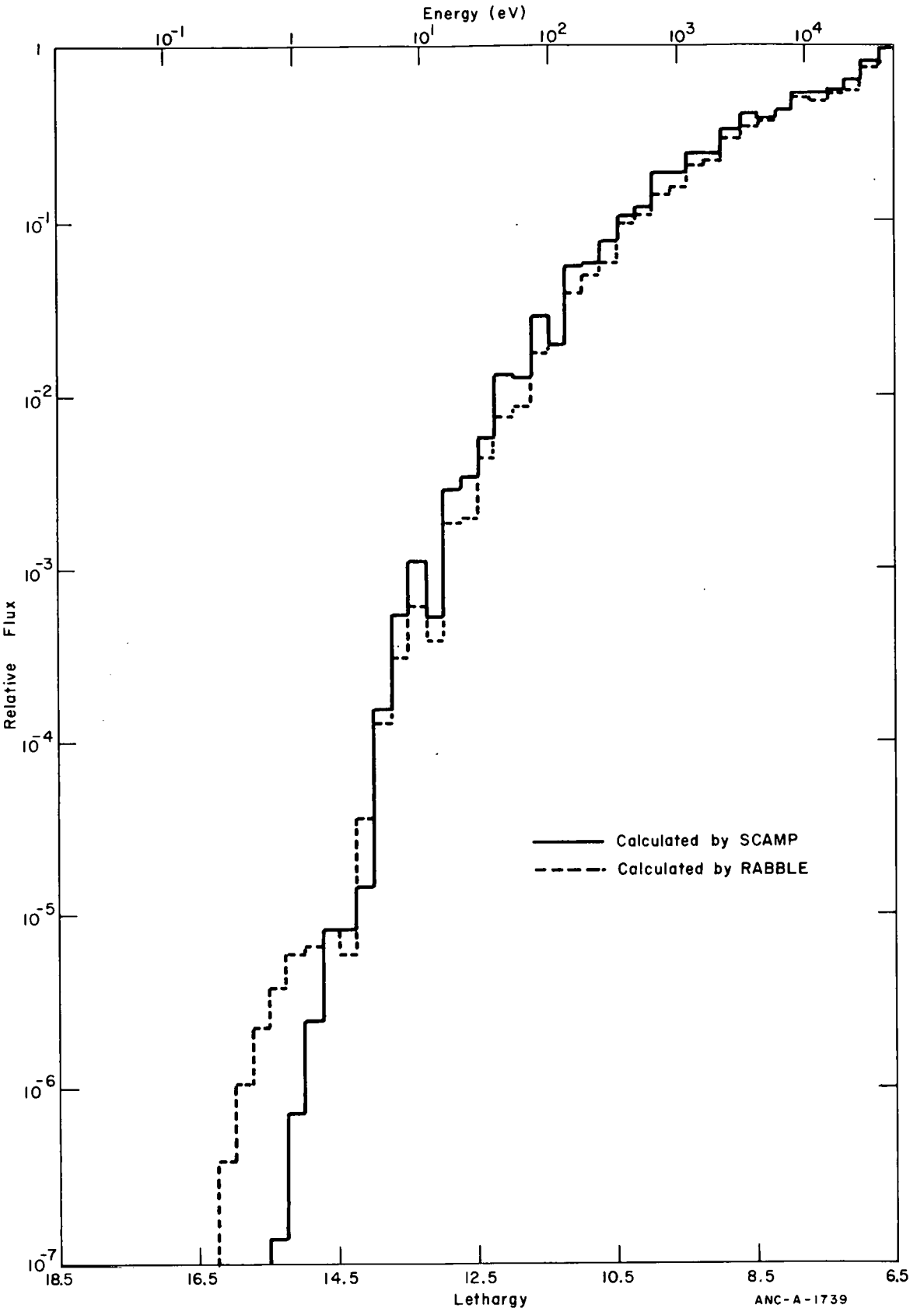

Figure 5 CFRMF Central Flux: A comparison of calculations by SCAMP and RABBLE.

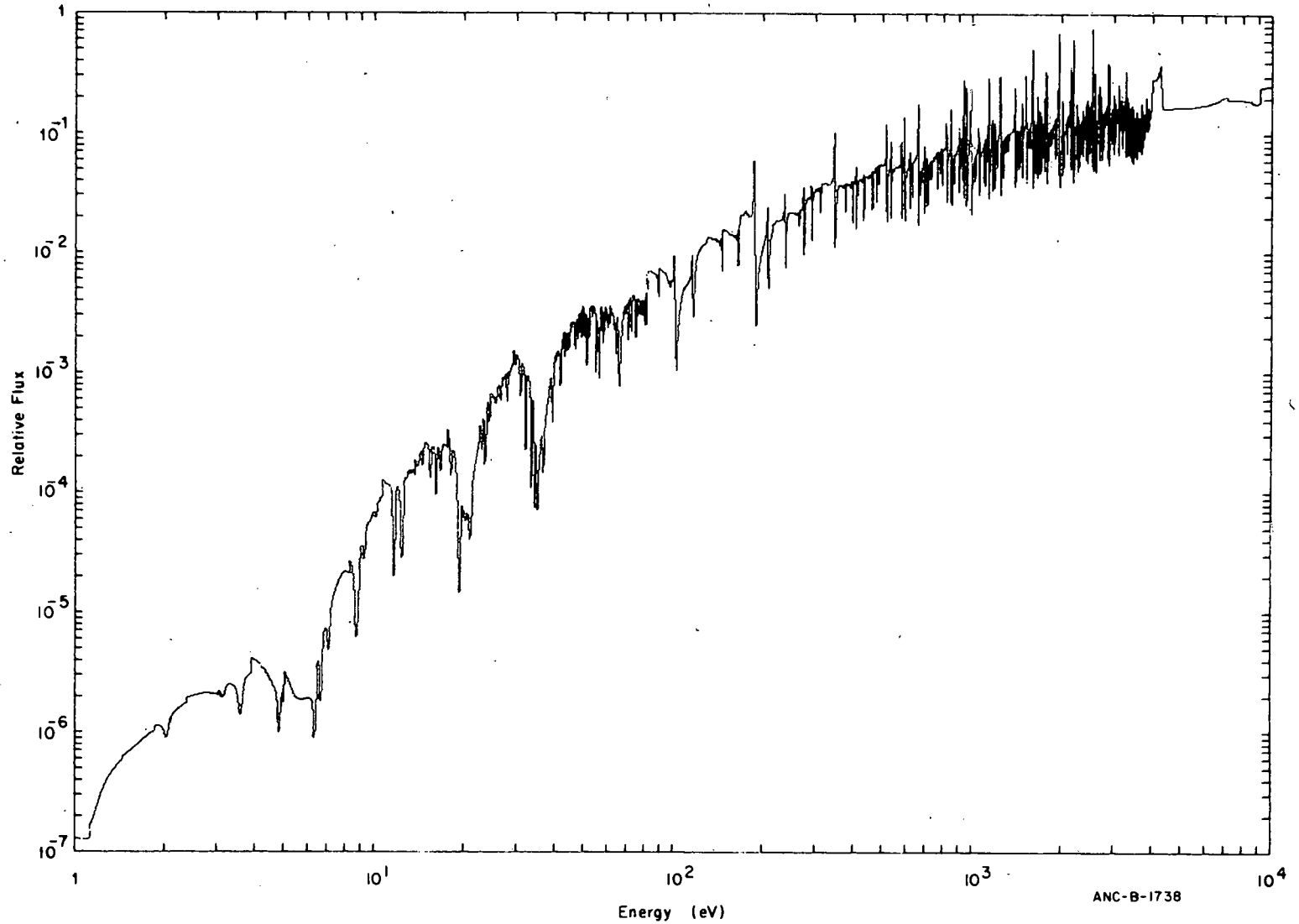

Figure 6 CFRMF Central Fine-Group Flux as Calculated by RABBLE.

FISSION PRODUCT ISOTOPE REACTIVITY MEASUREMENTS IN CFRMF

J. W. Rogers, I. E. Stepan

Reactivity measurements in the center of CFRMF have been made with fission product isotope samples of samarium, molybdenum and zirconium. These measurements were made to test cross section sets on an integral basis in the CFRMF neutron spectrum. The comparison of the measurements and calculations provides a check on all the nuclear reactions which produce reactivity effects and also checks the adequacy of calculational techniques. These tests on fission product isotopes are important because for most fission products only calculated cross sections exist in the energy range important to LMFBR's and have not been checked against any type of measurement. Correlative measurements have also been made with standard and control materials of gold, iodine, enriched uranium, boron and europium. Measurements were made with water which were necessary for correction purposes.

The isotopically enriched sample materials were obtained from the stable isotopes pool at ORNL and the standards and control materials were purchased commercially. Samples of these materials were prepared by vibra-compaction of the material into stainless steel capsules. These capsules are cylindrical shaped with a sample length of 14.2 cm and with inside diameters of 1.27 cm, 1.9 cm, 2.54 cm and 3.175 cm. These capsules, with volumes of 16.4 cm^3, 36.9 cm^3, 65.6 cm^3 and 102.5 cm^3, are designed to be self-positioning at the center of the CFRMF by having end caps of the appropriate diameter. The samples of different sizes were made so that the effects of sample size on reactivity could be investigated.

Most of the isotopically enriched samples were of the oxide form and due to the hygroscopic nature of oxides, moisture accumulation is common. Small portions of the samples used here have been checked by igniting them below volitization temperature and have been found to contain moisture. Table I lists the oxide samples, their enrichment and the percent weight loss due to ignition.

TABLE I

ISOTOPICALLY ENRICHED OXIDE SAMPLE MATERIALS

Material	% Enrichment	% Weight Loss
$^{90}ZrO_2$	97.85	2.39 (2.24)[a]
$^{91}ZrO_2$	89.31	0.37
$^{92}ZrO_2$	95.36	0.091
$^{94}ZrO_2$	96.07	0.21
$^{98}MoO_3$	97.30	0.084
$^{147}Sm_2O_3$	98.34	2.82
$^{149}Sm_2O_3$	97.72	0.874
$^{152}Sm_2O_3$	98.29	2.37
$^{154}Sm_2O_3$	98.69	4.08

[a] Determined at ORNL from the entire sample.

Because of the moisture contained in these samples it was necessary to either remove the moisture from the samples or to correct the reactivities for the effect due to moisture. Because of the problems of drying the samples and keeping them dry while loading them, corrections for the moisture were determined by measuring the reactivity effect of the moisture. This was accomplished by using SiO_2 as a carrier for amounts of moisture over the range contained by the samples to be corrected and measuring the reactivity effect of the moisture. The results of this "moisture calibration" are presented graphically in Figure 1. Tests also showed this calibration applicable to all sample sizes used in these measurements. Measurements to determine the reactivity effects of normal density water were also made and these results are shown in Figure 2. For normal density water the sample size effect is observed due to self-shielding.

Reactivity measurements have been made with materials being considered for standards. Gold was considered because of its well known cross-section and its frequent use as a standard, iodine because of its location on the atomic mass scale in relation to most fission products and its smooth shaped cross-section in the energy region of interest and ^{235}U because of its fuels standard recognition.

Gold metal powder (99.999% pure) and gold oxide powder (99.99% pure) were used as sample materials to get the reactivity effect of gold and oxygen. The gold oxide measurements had to be corrected for a moisture content of 2.36% by weight. Relative to the gold metal powder samples no reactivity effect due to the oxygen in the gold oxide samples was observed. Elemental iodine (99.9% pure) was used for the iodine samples. UO_2 powder with the uranium enriched to 93% was used for the ^{235}U samples and this material was not checked for moisture content. The results from the measurements of these samples are shown in Figure 3.

The measurements with the isotopically enriched samples have been corrected for moisture content as described above. To test the validity of these moisture corrections, two of the samples with different moisture concentrations were fired at 800°C and their changes in weights and reactivity worths were checked against the moisture calibration corrections determined from small portions of the sample material. The results were in excellent agreement in that they agreed well within the 2% uncertainties assigned to the results. Based on the gold oxide measurements, it is assumed that the oxygen contained in the oxide samples does not produce a measurable reactivity effect. The non-oxide samples have been assumed to be free of moisture. Table II summarizes these results along with the standards. The estimated combined uncertainties on the sample weights and the reactivity measurements are $\sim \pm 2\%$ for each sample. Where corrections are made for moisture in the samples, the uncertainties are estimated to be as much as ±5% where very large corrections are necessary. Most sets of samples of the same material show no statistically significant sample self-shielding but some show trends toward this effect. The ^{98}Mo solid metal sample has a density of 8.61 g/cm^3 where the ^{98}Mo in the oxide form has a density of only 0.534 g/cm^3 which may account for the disagreement between these samples.

Control materials of interest to LMFBR's have been measured to compare their reactivity worths in the CFRMF neutron spectrum. These measurements were made in the same manner as those mentioned above. Samples of enriched boron metal powder (99% pure) natural boron carbide (99.9% pure) and europium oxide (99% pure) were measured and the results are presented graphically in Figure 4 and are tabulated in Table III. The europium oxide results have been corrected for a moisture content of 3.49% by weight.

TABLE II

CFRMF REACTIVITY WORTHS OF FISSION PRODUCT ISOTOPES AND STANDARDS

Material	(% Enrichment)	Reactivity per Gram[a] of Four Sample Diameters (μk) 1.27 cm	1.9 cm	2.54 cm	3.175 cm
$^{90}ZrO_2$	(97.85)	-0.1125	-0.1113	-0.1194	-0,1157
$^{91}ZrO_2$	(89.31)	-0.2345	-0.2313		
$^{92}ZrO_2$	(95.36)	-0.2571	-0.2683		
$^{94}ZrO_2$	(96.07)	-0.2612	-0.2649		
^{95}Mo	(96.45)	-0.2375	-0.2399	-0.2368	-0.2338
^{96}Mo	(96.76)	-0.1847	-0.1877	-0.1837	-0.1822
^{97}Mo	(94.25)	-0.2642	-0.2673	-0.2647	-0.2614
^{98}Mo[b]	(98.30)			-0.1314	
$^{98}MoO_3$	(97.30)	-0.3232	-0.3200	-0.3317	-0.3283
^{100}Mo	(97.42)	-0.1993	-0.1954	-0.1964	-0.1921
$^{147}Sm_2O_3$	(98.34)	-0.3797	-0.3762		
$^{149}Sm_2O_3$	(97.72)	-0.6267	-0.6124	-0.5984	
$^{152}Sm_2O_3$	(98.29)	-0.1613	-0.1599	-0.1593	-0.1559
$^{154}Sm_2O_3$	(98.69)	-0.1519	-0.1438	-0.1492	-0.1396
^{197}Au		-0.3986	-0.3988	-0.3972	-0.3936
$^{197}Au_2O_3$		-0.410	-0.3856	-0.3857	-0.3850
$^{127}I_2$		-0.2336	-0.2322	-0.2281	-0.2244
$^{235}UO_2$	(93.12)	+1.008	+0.9952	+0.9930	+0.9839

[a] Grams of the metallic component of the sample material.
[b] Solid metal sample 2.159 cm diameter x 2.108 cm length.

TABLE III

REACTIVITY WORTHS OF CONTROL MATERIALS IN CFRMF

Material	(% Enrichment)	Reactivity per Gram of Four Sample Diameters (μk) 1.27 cm	1.9 cm	2.54 cm	3.175 cm
^{10}B	(92)	-8.742	-8.145	-7.681	
^{10}B	(85)	-8.404	-7.873	-7.359	
B_4C		-2.293	-2.256	-2.223	-2.181
Eu_2O_3		-0.7654	-0.7416	-0.7376	-0.7113

The estimated uncertainties on these reactivities are again ∿ ±2.0%. The sample size self-shielding effects are clearly observable in these results where cross-sections are much larger. In interpretation of these measurements relative to some other reactor environment, the relative results might be very different due to the neutron energy distribution and importance function (adjoint flux).

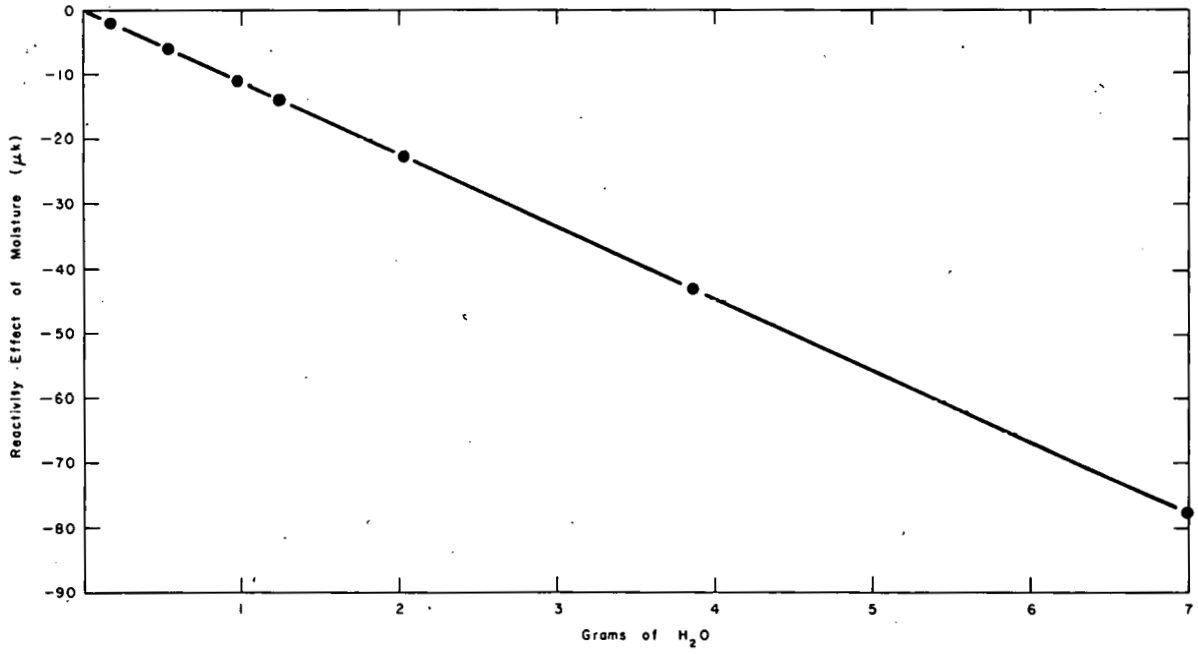

Figure 1 Measured reactivity effect of moisture in CFRMF.

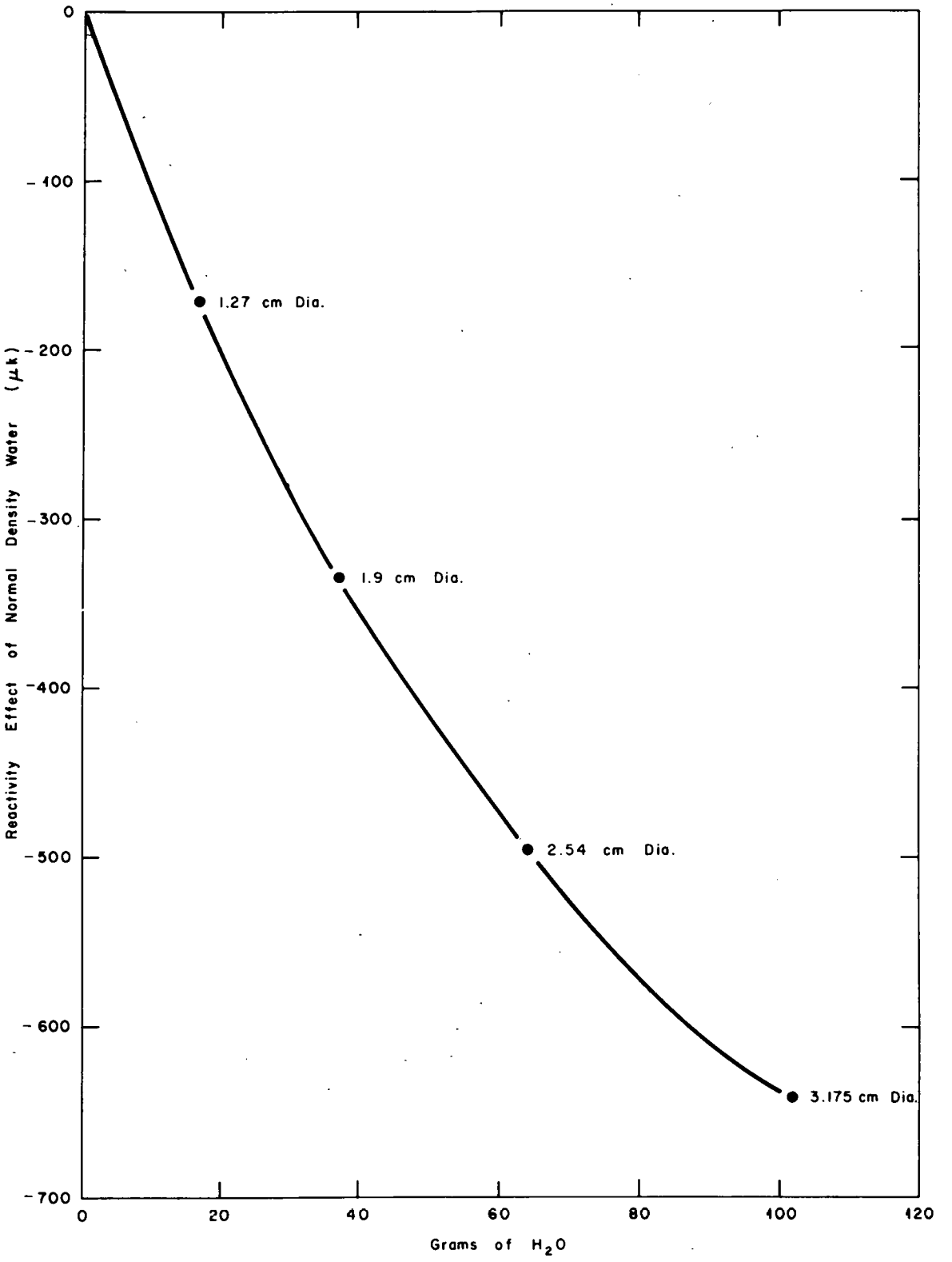

Figure 2 Measured reactivity effect of normal density water in CFRMF.

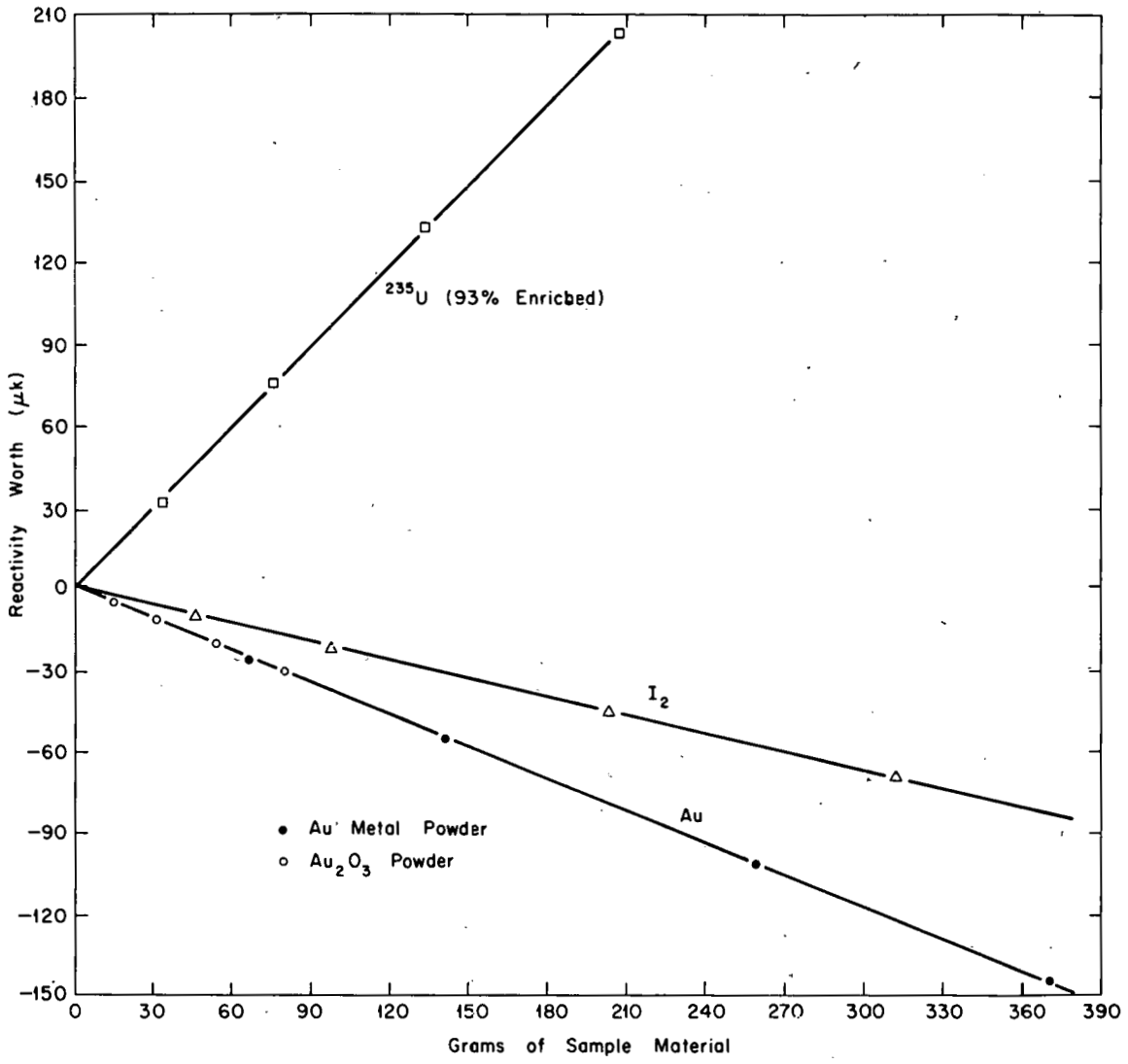

Figure 3 Measured reactivity effects of standard materials in CFRMF.

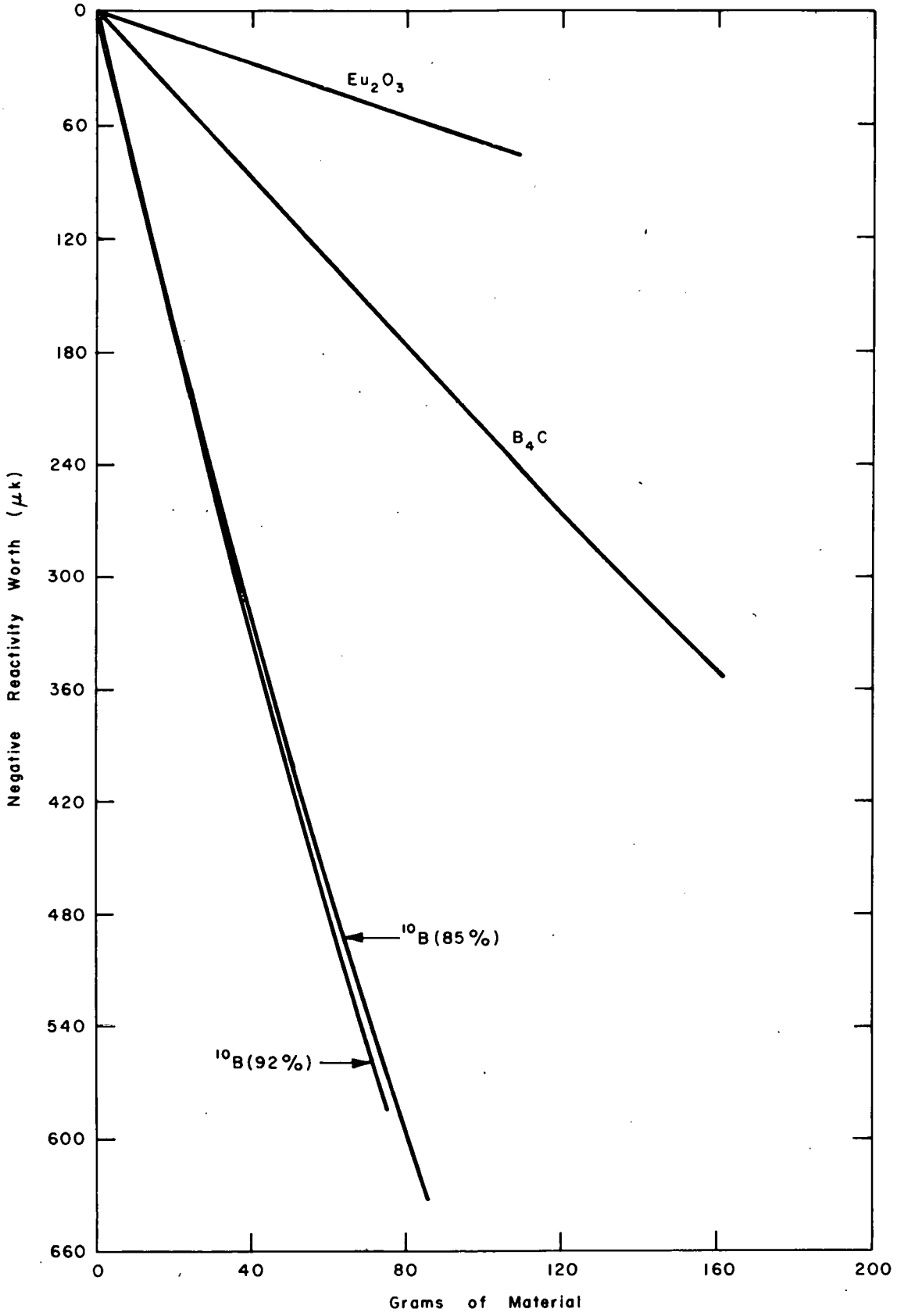

Figure 4 Measured reactivity effects of control materials in CFRMF.

DOSIMETRY REACTION RATE MEASUREMENTS IN CFRMF

J. W. Rogers

Reaction rates from foils of selected materials irradiated in the CFRMF neutron spectrum have been obtained by gamma-ray spectrometry measurements and activation analyses. This work was done in support of the Interlaboratory LMFBR Reaction Rate Program (ILRR) to compare activation analyses from various laboratories and to improve fast neutron induced reaction rate measurement techniques and accuracy. It is also intended to improve and perhaps standardize nuclear parameters involved in the measurement of neutron flux and spectra. This is important because of the reduction of uncertainties in design and analysis of reactors as these techniques are made more reliable.

The gamma-ray spectrometry measurements were made with a 7.62 cm x 7.62 cm NaI(Tℓ) crystal detector with a source-to-detector distance of 10 cm. A 1.024 g/cm^2 polystyrene absorber was used to stop the source beta radiation. The gamma-ray detection efficiency of the detector is that computed from its known characteristics. The system and techniques are checked against sources calibrated by different techniques and these tests over long periods of time have established the estimated uncertainty on the efficiency of the detector used to count these foils at ±1.0%. To avoid making high counting-rate corrections, most counts were made at decay times sufficiently long to yield optimum rates. When high counting rates were unavoidable and cascade gammas were present, corrections for random and coincident summing were made. Corrections have been made for gamma-ray attenuation within the foils. The foils were carefully weighed to ±0.00002 g following irradiation. The foils were counted several times each involving different decay periods for each count. Each count was handled individually to compute the saturated reaction rate and consequently all counting errors are represented in the uncertainties obtained from the span of the measurements except for the detector efficiency and decay scheme data. The decay scheme uncertainties are found elsewhere in this report. Reaction rates for three distinct groups of foils were obtained, power level monitor foils for normalizing the CFRMF flux levels, a package of foils for obtaining reaction rates sensitive to various neutron energy ranges and sets of foils with different thicknesses to determine self-shielding effects.

The monitor foils were 1.27 cm diameter 0.0508 mm thick gold metal and indium metal. A set of these foils (1 gold and 1 indium) from each ILRR-CFRMF test was counted. These foils were always positioned in a holding device 3.81 cm above the CFRMF center. Nominal power levels of 0.6 kW, 6.0 kW and 10 kW have been used in these tests. The 411.8-keV gamma ray from the decay of ^{198}Au from the ^{197}Au(n,γ)^{198}Au reaction was counted from the gold foils. In all measurements, more than 10^5 counts were collected in the photopeak. In order to have acceptable counting rates at 10 cm, decay times of 16 to 20 days were allowed for the higher exposure foils. A half-life of 2.696 days and a branching ratio of 0.9547 were used in the gold data reduction. The 335-keV gamma ray from the decay of ^{115m}In from the ^{115}In(n,n')^{115m}In reaction was

counted from the indium foils. In all measurements more than 10^4 counts were collected in the photopeak (in most cases, more than 10^5 counts). Decay times of between 20 and 28 hours were allowed so that good counting rates and a single photopeak spectrum were obtained. A half-life of 4.5 hours and a branching ratio of 0.47 were used in the indium data reduction. Table I summarizes the results from all the power monitor foils measured thus far. Some of these measurements were reported earlier but final corrections and analyses had not been made.

TABLE I

POWER LEVEL MONITOR FOILS REACTION RATES FROM CFRMF-ILRR TESTS

Test Identity	Foil	Mass (g)	Saturated Reaction Rate by NaI(Tℓ)	Number of Measurements[a]	Power Level[b] (kW)	Au/In
NBS Fission Chamber (2/2/72)	Au-AA	0.1216	3.225×10^{-15}	3 (.33%)	0.619	8.1316
	IN-2#1	0.04878	0.3966	1	0.599	
ANL SSTR 1, 2 & 3 (2/4/72)	Au-AC	0.1214	3.218	2 (.25%)	0.618	8.1883
	In-2#3	0.04802	0.3930	2 (.14%)	0.594	
NBS Fission Chamber (2/4/72)	Au-AE	0.1239	3.225	2 (.74%)	0.619	8.1584
	In-2#5	0.04909	0.3953	1	0.597	
ARHCO-I (2/8/72)	Au-AG	0.1234	49.51	3 (.26%)	9.506	7.9014
	In-2#7	0.04976	6.266	3 (1.04%)	9.470	
ANL-I (2/15/72)	Au-AI	0.1216	47.55	5 (.97%)	9.130	7.8362
	In-2#9	0.04848	6.068	3 (.27%)	9.171	
HEDL-I (2/16/72)	Au-AK	0.1220	47.12	6 (.53%)	9.047	7.7082
	In-2#11	0.04840	6.113	3 (.11%)	9.239	
ANC-I (2/29/72)	Au-AM	0.1221	48.12	8 (.49%)	9.239	7.8066
	In-2#13	0.04805	6.164	4 (.77%)	9.316	
AI-I (4/11/72)	Au-AO	0.1202	47.48	8 (.64%)	9.116	7.6717
	In-2#15	0.05010	6.189	8 (.54%)	9.354	
HEDL-V (11/6/72)	Au-AR	0.1220	29.84	4 (.17%)	5.729	7.8588
	In-2#17	0.05986	3.797	5 (.42%)	5.738	
HEDL-VI (11/7/72)	Au-AT	0.1213	29.94	4 (.90%)	5.748	7.841
	In-2#19	0.05020	3.812	5 (.84%)	5.761	

TABLE I (Contd.)

Test Identity	Foil	Mass (g)	Saturated Reaction Rate by NaI(Tℓ)	Number of Measurements[a]	Power Level[b] (kW)	Au/In
ANL-SSTR 4 (11/8/72)	Au-CA	0.1252	3.123×10^{-15}	3 (.60%)		7.8173
	In-2#21	0.04700	0.3995	3 (.60%)		
ANL SSTR 5 (11/8/72)	Au-CC	0.1223	3.136	4 (.54%)	0.600	7.9212
	In-2#23	0.04945	0.3959	3 (.91%)		
ANL SSTR 6 (11/8/72)	Au-CE	0.1237	3.118	4 (.38%)		7.8997
	In-2#25	0.04814	0.3947	3 (.51%)		
ANL SSTR 7&8 (3/7/73)	Au-CG	0.1201	3.188	3 (.53%)	0.599	8.0020
	In-2#27	0.04672	0.3984	3 (.60%)	0.602	
ANC-HEDL-ARHCO-SS-I (3/13/73)	Au-CI	0.1211	53.29	4 (.15%)	10.23	7.9478
	In-2#29	0.04880	6.705	5 (.76%)	10.13	
HEDL-SS-II (3/14/73)	Au-DA	0.1236	53.33	3 (.21%)	10.24	7.8507
	In-2#31	0.04887	6.793	3 (.41%)	10.27	
HEDL-SS-III (3/14/73)	Au-DC	0.1218	53.58	3 (.26%)	10.29	7.8945
	In-2#33	0.04988	6.787	3 (.35%)	10.26	
AI-B-3 (5/23/73 & 5/24/73)	Au-AE	0.1241	30.28	3 (.37%)	5.814	7.8793
	In-2#35	0.04843	3.843	3 (.47%)	5.810	

(a) The number in parentheses is the estimated percent standard deviation based on the span of the measurements and does not include uncertainties on efficiencies and decay data.

(b) Based on the average of the three ANL SSTR tests on 11/8/72 at the assumed 0.600 kW level.

The relative power level of the CFRMF has also been monitored with the NBS fission chamber located at the center of the reactor using ^{235}U and ^{238}U fission rates. By averaging the Au and In foils results and the ^{235}U and ^{238}U fission chamber results, these methods can be compared at different power levels. Table II summarizes the comparison of these measurements.

TABLE II

RELATIVE CFRMF POWER LEVELS BY FOILS AND FISSION CHAMBERS

Nominal Power	Foils	Fission Chambers
0.600 kW	1.000	1.000
6.0 kW	9.601 ± 0.031	9.66 ± 0.040
10.0 kW	17.06 ± 0.063	17.07 ± 0.004

In Table I the gold-to-indium ratio spectral index shows a statistically significant difference between the three 0.6 kW tests of 2/2/72 and 2/4/72 and all other tests. Upon examining the counting data for these foils, it was found that a systematically different way of subtracting the background activity was used for these data in comparison to the way used in all other tests. It is assumed that this is the cause for this discrepancy since it does not occur at the other 0.6 kW tests of 11/8/72 and 3/7/73.

The package of foils designated as ANC-I has been discussed and described in the previous annual report. Since final corrections and comparisons were not included in that reporting, they are summarized in Table III. The reaction rates from all laboratories were obtained from foils like those in the ANC-I foil set which were packaged and irradiated in the same orientation. The counting and analyses were done at each laboratory using the same decay scheme data.

Neutron self-shielding effects of certain reactions in individual foils irradiated in the CFRMF neutron field have been examined by irradiating foils of different thicknesses. These foils were then counted to determine their activities relative to their thicknesses. Foils of Au, Co, Cu, Sc and ^{235}U 0.00127 mm thick were irradiated in one package (ANC-SS-I) and their reaction rates determined. The Au and Co foils were counted bare and the Sc and ^{235}U were counted through the $\sim$ 0.2 mm Al wrapping. The Cu foil was sandwiched between 0.254 mm of unirradiated pure Cu to annihilate all the positrons. These results are summarized in Table IV. Sc and ^{235}U foils of the same and other thicknesses which were irradiated in other packages (HEDL-SS-I, II and III) at the same power level were also counted and analyzed. These results are summarized in Table V. For the $^{45}Sc(n,\gamma)^{46}Sc$ reaction, there may be about 2% self-shielding in the 0.254 mm foil. The $^{235}U(n,f)^{140}Ba$ shows no self-shielding and the 0.00127 mm foils from the HEDL and ANC tests are in agreement. There is disagreement between the HEDL and ANC 0.00127 mm Sc foils in excess of the known uncertainties which is being investigated.

TABLE III

CFRMF REACTION RATES FROM ANC-I FOIL SET PACKAGE

Foil	Mass (g)	Reaction	Saturated Reaction Rate by NaI(Tℓ)	Number of[a] Measurements	Saturated Reaction Rate From All Laboratories	% Standard[b] Deviation
Al-3	0.04720	$^{27}Al(n,\alpha)^{24}Na$	2.022×10^{-17}	4 (.81%)	2.042×10^{-17}	2.3
	0.04739	$^{27}Al(n,p)^{27}Mg$	1.137×10^{-16}	1	1.110×10^{-16}	
Au-2	0.03551	$^{197}Au(n,\gamma)^{198}Au$	5.238×10^{-14}	6 (.66%)	5.312×10^{-14}	1.8
In-3	0.04596	$^{115}In(n,n')^{115m}In$	6.311×10^{-15}	4 (.51%)	6.285×10^{-15}	0.9
Co-3	0.01473	$^{59}Co(n,\gamma)^{60}Co$	9.520×10^{-15}	3 (.44%)	9.477×10^{-15}	1.5
Co-2	0.01440	$^{59}Co(n,\gamma)^{60}Co$	8.922×10^{-15}	3 (.33%)	8.694×10^{-15}	1.5
Co-1	0.01439	$^{59}Co(n,\gamma)^{60}Co$	9.397×10^{-15}	3 (.92%)	9.374×10^{-15}	1.5
Ni-TC	0.19786	$^{58}Ni(n,p)^{58}Co$	3.084×10^{-15}	6 (.31%)	3.058×10^{-15}	1.1
Fe-A	0.002779	$^{58}Fe(n,\gamma)^{59}Fe$	7.692×10^{-16}	3 (1.56%)	7.673×10^{-16}	1.3
	0.04564	$^{54}Fe(n,p)^{54}Mn$	2.192×10^{-15}	3 (.77%)	2.213×10^{-15}	2.1
Al-2	0.04700	$^{27}Al(n,\alpha)^{24}Na$	2.000×10^{-17}	4 (1.04%)	2.037×10^{-17}	2.3
	0.4725	$^{27}Al(n,p)^{27}Mg$	1.133×10^{-16}	1	1.110×10^{-16}	
Au-1	0.00338	$^{197}Au(n,\gamma)^{198}Au$	5.365×10^{-14}	6 (.27%)	5.428×10^{-14}	2.0
In-2	0.04596	$^{115}In(n,n')^{115m}In$	6.332×10^{-15}	4 (.84%)	6.326×10^{-15}	0.9
Ti-N	0.012115	$^{46}Ti(n,p)^{46}Sc$	3.234×10^{-16}	2 (3.94%)	3.445×10^{-16}	6.4
	0.011364	$^{47}Ti(n,p)^{47}Sc$	5.264×10^{-16}	3 (2.14%)	5.348×10^{-16}	2.1
Ti-M	0.011998	$^{46}Ti(n,p)^{46}Sc$	3.262×10^{-16}	2 (1.50%)	3.369×10^{-16}	6.4
	0.011254	$^{47}Ti(n,p)^{47}Sc$	5.304×10^{-16}	3 (1.50%)	5.313×10^{-16}	2.1
Sc-1	0.04925	$^{45}Sc(n,\gamma)^{46}Sc$	2.944×10^{-15}	5 (.47%)	2.948×10^{-15}	0.4
^{235}U-1	0.23080	$^{235}U(n,f)^{140}Ba(5.8\%)$	2.045×10^{-13}	7 (1.62%)	2.051×10^{-13}	3.0
^{238}U-1	0.06439	$^{238}U(n,f)^{140}Ba(6.0\%)$	9.828×10^{-15}	7 (1.05%)	9.682×10^{-15}	2.7
In-1	0.04487	$^{115}In(n,n')^{115m}In$	6.349×10^{-15}	4 (.26%)	6.331×10^{-15}	0.9
Au-1	0.03733	$^{197}Au(n,\gamma)^{198}Au$	5.228×10^{-14}	6 (.69%)	5.290×10^{-14}	1.5
Al-1	0.04638	$^{27}Al(n,\alpha)^{24}Na$	2.028×10^{-17}	4 (1.10%)	2.078×10^{-17}	2.3
Au-Al	0.0001368	$^{197}Au(n,\gamma)^{198}Au$	5.326×10^{-14}	4 (.92%)	5.450×10^{-14}	2.3

(a) The number in parentheses is the standard deviation on span of measurements and does not include errors on efficiencies and decay scheme data.

(b) Deviation of the mean.

TABLE IV

ANC-SS-I FOIL REACTION RATES

Foil	Target Mass (mg)	Reaction	Saturated Reaction[a] Rate by NaI(Tℓ)
Au #1	6.918	$^{197}Au(n,\gamma)^{198}Au$	$5.979 \pm 0.020 \times 10^{-14}$
Co #1	1.646	$^{59}Co(n,\gamma)^{60}Co$	$1.408 \pm 0.012 \times 10^{-14}$
Cu #1	1.02	$^{63}Cu(n,\gamma)^{64}Cu$	$5.655 \pm 0.058 \times 10^{-15}$
^{235}U #1	3.100	$^{235}U(n,f)^{140}Ba$	$2.325 \pm 0.010 \times 10^{-13}$[b]
Sc #1	0.480	$^{45}Sc(n,\gamma)^{46}Sc$	$3.171 \pm 0.034 \times 10^{-15}$

[a]These uncertainties are the estimated standard deviation on span of measurements (does not include uncertainties on efficiencies and decay scheme data).

[b]Assuming a 5.8% yield.

TABLE V

REACTION RATES OF HEDL SELF-SHIELDING FOILS

Thickness	$^{235}U(n,f)^{140}Ba(5.8\%)$ Reaction	$^{45}Sc(n,\gamma)^{46}Sc$ Reaction
0.00127 mm	$2.312 \pm 0.04 \times 10^{-13}$	$3.307 \pm 0.04 \times 10^{-15}$
0.127 mm	$2.346 \pm 0.02 \times 10^{-13}$	$3.275 \pm 0.026 \times 10^{-15}$
0.254 mm	$2.337 \pm 0.02 \times 10^{-13}$	$3.246 \pm 0.044 \times 10^{-15}$

SPECTRUM DETERMINATIONS IN THE EBR-II

Y. D. Harker

In support of the irradiation programs being conducted in EBR-II by the Fast Breeder Reactor Physics Constants Project of ANC and the Burnup Methods for FBR Fuels Project of ACC, the multi-foil activation technique[1,2] has been utilized in measuring neutron spectra at various experimental positions in EBR-II. Foil activation spectrum techniques utilized in this manner are very powerful tools in the analyses of the integral measurements, primarily because the spectrum of the neutron environment is determined in the actual conditions of the irradiation. Interpretations of the integral results obtained are, therefore, aided by a more accurate picture of the neutronic conditions of the measurement. In addition, the foil packages are generally small in size and do not create perturbing effects on the neutron flux and are extremely adaptable to situations where direct access to the experiment cannot be maintained during the irradiation, such as is the case in EBR-II.

Spectra for seven positions traversing the vertical and horizontal axes of a B-7 assembly in row eight of EBR-II have been determined. An example of the measured spectrum and the comparison of the corresponding calculated to measured reaction rates are shown in Figure 1 and Table I, respectively. The ratios given in Table I indicate how well the resulting spectrum predicts the rates of the different dosimetry reactions and in this case, the agreement is quite satisfactory.

TABLE I

COMPARISON OF CALCULATED TO MEASURED REACTION RATES

Foil	Type	Calculated Activity	C/E
1	CO59(NG)CO60	0.32955810E 07	1.000
2	SC45(NG)SC46	0.11281354E 09	0.974
3	FE54(NP)MN54	0.47875550E 07	1.092
4	NI58(NP)CO58	0.21370320E 08	0.908
5	TI46(NP)SC46	0.24435230E 07	0.997
6	CU63(NHE)CO60	0.35169314E 04	0.999
7	NP237(NF)FP	0.45939943E 14	0.995
8	U235(NF)FPFAST	0.21782108E 15	1.033
9	U238(NF)FP	0.33959256E 13	0.988

The results of these seven determinations indicate a definite softening of the neutron flux for positions far removed from the mid-plane of the core and give evidence to the need for using foil activation packages at various locations within the experimental assembly.

The results, however, from equivalent measuring positions have demonstrated very satisfactory reproducibility.

From the foil packages handled to this date, it appears that the metal alloys[3] tested in these irradiations are not reliable and future foil packages will contain only separated elemental materials which can be processed and analyzed individually.

---

[1] D. A. Pearson, Nuclear Technology Branch Annual Progress Report for Period Ending June 30, 1970, IN-1407 (1970) p. 291.

[2] R. E. Narum, INSPECT - Interactive Computer Code for Unfolding Neutron Spectra from Activation Measurements, ANCR-1035 (1972).

[3] D. A. Pearson, Nuclear Technology Division Annual Progress Report for Period Ending June 30, 1971, ANCR-1016 (1971) p. 457.

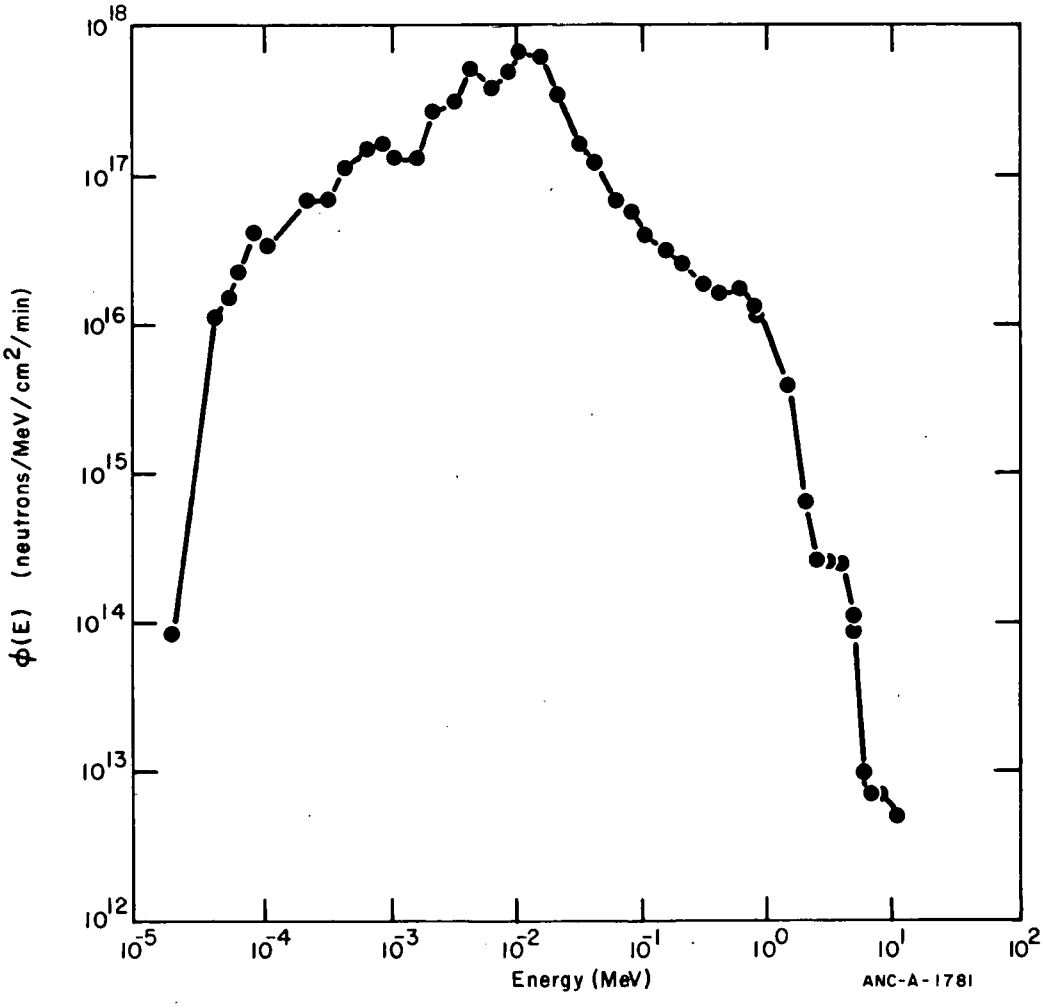

Figure 1 Neutron spectrum for EBR-II Row 8 near midplane.

FISSION PRODUCT DIFFUSION IN FUEL PINS

H. L. McMurry, E. F. Aber

This work was in response to an AEC request to provide data for an Aerojet project which aims at assessing the hazards of power reactor accidents. The results are to be used in evaluating hazards arising from the rupture of fuel pins in operating reactors. For this purpose calculated values are needed for the amount of fission products of various types which have diffused to the fuel-clad interface by the time of rupture.

A review of the literature relevant to calculation of fission product diffusion revealed much ambiguity as to the origins of the basic equations and their methods of application. Therefore, an early phase of this work was establishing the theoretical basis for fission product diffusion and deriving approximate equations for dealing with isotopes of Cs and Sr. Subsequently, various methods of finding asymptotic solutions and approximate solutions appropriate to different times and boundary conditions were examined. Finally, a method for numerically integrating the time dependent diffusion equation was developed. This material is being reported in three documents [1,2,3].

The specific calculations for this project were for releases to the fuel-clad interface of noble gases, and Cs and Sr isotopes from typical PWR and BWR reactors after 3 years of full power operation. The noble gas releases were calculated using methods developed by Yuill et al.,[4]. The ^{137}Cs, ^{90}Sr and some short lived Cs isotopes employed methods developed during the first phase of the project. However, the heats of transport needed in these calculations were from Yuill[4].

The results are presented in an internal report[5].

---

(1) H. L. McMurry, Theoretical Basis for Calculating Diffusion of Fission Products in Fuel Pins, ANCR-1126 (August 1973)

(2) H. L. McMurry, Comments on Solutions to the Equation for Diffusion of Fission Products in Fuel Pins, (in preparation).

(3) E. F. Aber, A Numerical Model Describing the Diffusion of Fission Products in Operating Fuel Pins, (in preparation).

(4) W. A. Yuill, V. F. Bason, and J. H. McFadden, An Analytical Model Describing the Behavior of Fission Products in Operating Fuel Pins, IN-1467, (June 1971).

(5) H. L. McMurry and E. F. Aber, Aerojet Nuclear Company Internal Report.

DEVELOPMENT OF CAPABILITIES FOR SHIELDING CALCULATIONS

T. E. Young

The general purpose Monte Carlo shielding code, MORSE, was obtained from the Radiation Shielding Information Center (RSIC) at ORNL and put into operation on the NRTS IBM-360. This code should be a valuable addition to the shielding calculation capabilities of the NRTS. The code can treat problems of very complex geometry for neutron or gamma-ray shielding. Combined neutron-gamma problems may also be solved, eliminating the need to use several codes to solve the problem of shielding against reactor-produced gamma rays. The main advantage of the code is, however, that it will permit solution of shielding problems which could not be solved accurately by previously available means.

SUPPORT TO ICPP

T. E. Young, J. W. Codding[1]

Work has been done on the XLACS code for the Idaho Chemical Processing Plant. This code was obtained from RSIC, and is to be used to produce a multigroup neutron cross section library for use with various neutronics codes at the NRTS. XLACS has been compiled, and data for several nuclides processed from the ENDF/B-III tapes.

---

[1] Member of the Analysis and Programming Branch, Technical Services Division, Aerojet Nuclear Company.

GAS CORE REACTOR NUCLEAR DESIGN

J. F. Kunze, P. J. Macbeth, J. H. Lofthouse, B. L. Rushton

The gas core nuclear rocket has long been considered the ultimate in specific impulse capability for space propulsion[1,2]. Figure 1 is a schematic of the concept. Recent considerations of the capabilities for this system[3] consider engines with specific impulses as high as 4400 seconds, with 6000 MW power and 10 lb/sec hydrogen propellant flow rates. Mass flow rate loss ratios of the nuclear fuel (^{235}U or ^{233}U) to that of the propellant are hoped to be in the range of 1% or less. Discharge temperatures through the nozzle of as high as 30,000°R are considered feasible[3] even though present-day chemical rocket discharges are only as high as 7500°R.

The gas core nuclear rocket concept will need to be tested at temperature in a test program on an earth-based "prototype" demonstration. Three possibilities exist for the demonstration test:

1. A loop-type (Mini-Cavity) test within a conventional test reactor driver core to test some but not all of the parameters of the full-scale reactor.

2. A small-scale full reactor test. A small cavity, nominally 4 ft in diameter, is envisioned which will allow a gaseous uranium core but at a reduced temperature from the full scale reactor. This test should allow testing of most parameters and extrapolation of the remainder to the full-scale reactor.

3. A full-scale, 10- to 12-ft-diameter cavity test, with all the characteristics of the rocket engine. This device would operate at a much higher total power than either of the other two devices.

It is the second approach that seems most reasonable. It will test the entire concept at less cost than the third approach. The question was, "How much less cost? What is the smallest sized reactor that will do the job?"

In performing the design, the large negative reactivity effect of hot hydrogen became apparent. This is a result of its ability to up-scatter neutrons, leaving them less effective in creating fissions and more vulnerable to leakage. The negative reactivity-temperature coefficient is in the range of $-7\%\Delta k$ per 1000°K of discharge propellant temperature. Furthermore, the larger the cavity the higher will be the system multiplication factor for given conditions of temperature, pressure, and radius ratio. Thus, for larger cavities, higher operating temperature and discharge temperature will be possible. The calculations were not done in sufficient number to create a family of curves of exhaust temperature vs cavity size for various fuel to cavity radius ratios. However, the work performed indicates that the temperature vs cavity radius coefficient is approximately as given above.

From the series of calculations performed for this study, the 70-cm radius (4-1/2-ft diameter) cavity size appears to provide satisfactory conditions. Further study could lead to systems of this size showing promise of attaining criticality through hydrogen perheating or reflector design modifications. However, the brief nature of this study precluded further investigation that would allow exactly specifying the needed cavity size. Several iterations between the nuclear and radiant heat transfer codes are required.

The thermalhydraulic design was based on a 4-ft-diameter cavity, as were the associated rough cost estimates. It appears that this size of reactor may be adequate for a useful demonstration test. There is little doubt, however, that the 4-ft-cavity diameter size is indeed marginal, and a somewhat larger size would be desirable.

Perhaps the most startling result from the study is that the pressure coefficient of reactivity is negative, at least for the conditions assumed in the study. This further illustrates that the hydrogen penalty is indeed severe, so much so that above 100 atm the addition of more fuel via an increase in pressure was more than counteracted by the negative effect of the corresponding increase in hydrogen. Certainly, the negative pressure

coefficient will not be true at all pressures and temperatures, and a more complete study appears warranted.

Finally, the effect of a change in radius ratio of fuel to cavity is much stronger than hitherto assumed. Measurements of the effect in a "cold" critical experiment[4] without hydrogen showed approximately a 6%Δk increase in reactivity as the fuel ball radius increased from 0.67 to 0.80 of the cavity radius. With hot hydrogen as a coolant surrounding the fuel ball, the identical change in radius ratio was calculated to be 22%Δk. The reasons for the difference are that with hot hydrogen, growth of the fuel ball not only has a positive geometric effect on reactivity but also displaces some of the extremely deleterious hydrogen coolant from the cavity. This net effect would appear to be a strongly positive contribution to the reactivity temperature coefficient. However, the larger fuel radius is probably unstable fluid-dynamically[5], and should quickly reduce back to its original size. Furthermore, the pressure and hydrogen temperature coefficients of reactivity are both negative. Thus, it would appear that overall the temperature effect on reactivity is negative.

---

[1] G. Safanov, The Criticality and Some Potentialities of Cavity Reactors, (abridged), RM-1835, The RAND Corporation (1955).

[2] F. E. Rom, Comments on the Feasibility of Developing Gas Core Nuclear Rocket, NASA TM-X 52644, Conference on Frontiers of Power Technology, (October 23, 1969).

[3] M. F. Taylor et al., The Open-Cycle Gas-Core Nuclear Rocket Engine--Some Engineering Considerations, 2nd Symposium on Uranium Plasmas: Research and Applications, Atlanta, Georgia (November 15-17, 1971), p. 179

[4] J. F. Kunze, G. D. Pincock, R. E. Hyland, Nucl Appl. 6, 104 (1969).

[5] J. F. Kunze et al., Flowing Gas, Non-Nuclear Experiment on the Gas Core Reactor, NASA CR-120824 (February 1972).

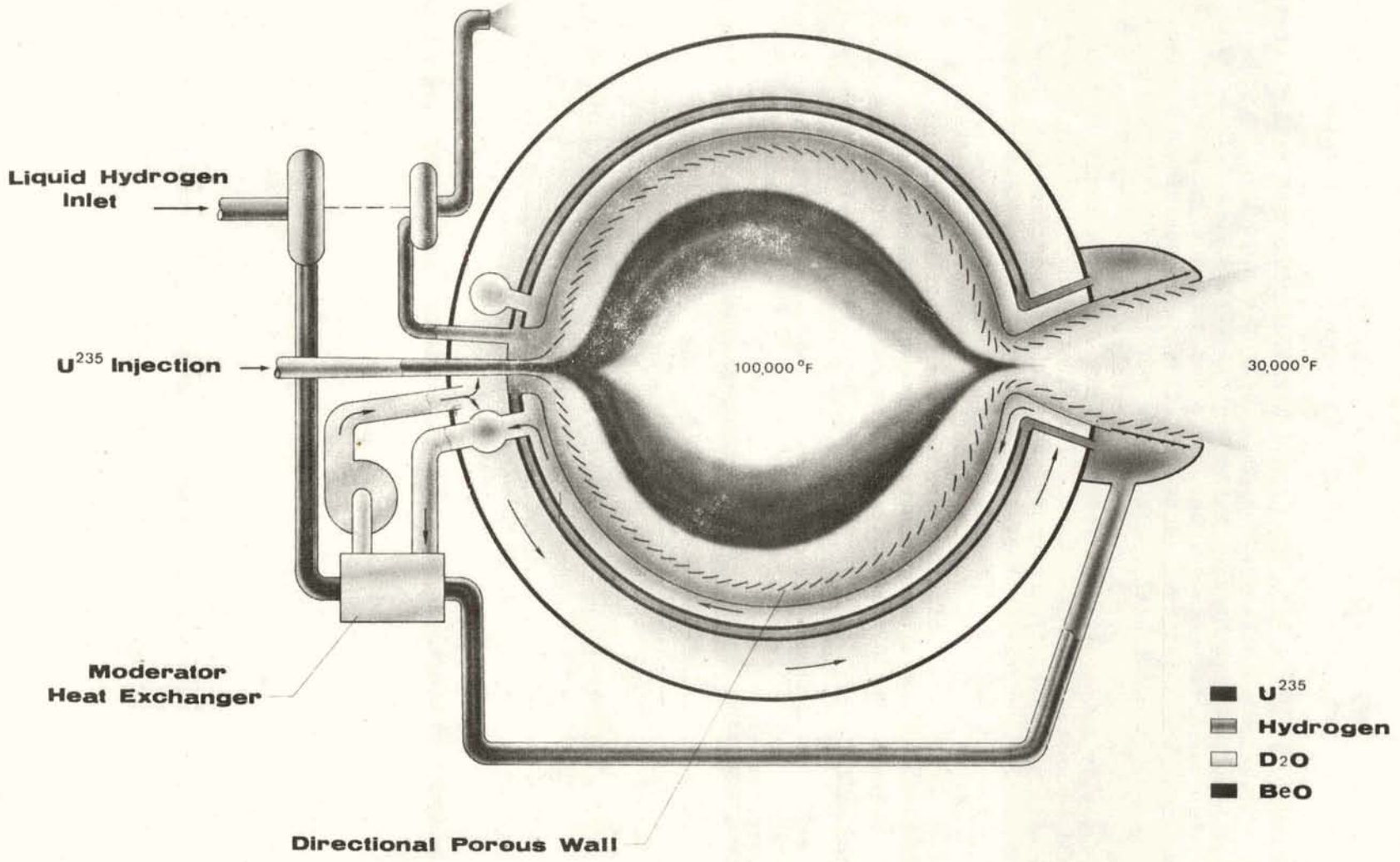

Figure 1 Schematic of the gas core nuclear rocket.

GAS CORE REACTOR FLOW STUDIES

J. F. Kunze, P. J. Macbeth, C. G. Cooper

The open cycle co-axial flowing gas core concept has been discussed in the preceding article. This concept has been studied experimentally in a number of laboratories. Patterns with high ratios of outer to inner gas flow rates were initially studied in cylindrical-geometry configurations[1,2]. Subsequent experiments concentrated on spherically shaped configurations, which would closely resemble conditions which would be achieved in actual high temperature operating engines and which gave the most clearly reactive configuration[3,4]. Critical experiments to study the reactor physics characteristics of a dilute gas core surrounded with hydrogen and a low absorption moderator (heavy water) have also been reported[5,6]. Since the ideal nuclear geometry is spherical, and since a gaseous fuel is to be used, nuclear considerations bear very heavily on the types of flow patterns which will be acceptable. In particular, the flow patterns must be capable of going critical within an engineering feasible operating pressure, which is generally assumed to be less than 1000 atm. These recent flow tests, conducted at Aerojet Nuclear Company, have concentrated on obtaining flow configurations which expand the central gas, simulating the fuel, into as large a volume as possible with as high as possible volume fraction. The goals for the conditions under which the system will be operated are: minimum cavity pressures, maximum propellant to nuclear fuel flow rate ratios, minimum reactor size, and more recently, overall low flow rates to correspond to the low thrust applications which are foreseen for nuclear rockets of the not too distant future.

The first phase of testing achieved flow configurations which gave high volume fractions for the inner gas, which simulated the fuel gas. Typically using air and air as the two gases, both simulating a propellant flowing around the outside and the fuel suspended in the center, volume fractions up to 35% in spherical configurations were obtained. The second phase of this work concentrated on improving the conditions when gases of different density were employed, the central gas being the heavier. Again, both two-dimensional (Figure 1) and three-dimensional (Figure 2) tests were run. In the two-dimensional cases, the round-shaped cavity was bounded by two flat walls on the viewing ends. The overall test apparatus is shown in Figure 3.

Since the largest tests were conducted on 3 ft diameter cavities, scaling up will be required to determine what the effects would be in the actual gas core rocket reactor which will have a cavity diameter of between 8 and 12 ft. The question of scaling from small models to larger sizes was investigated, using 18 in. and 36 in. diameter cavities. The results indicate that neither the Reynolds nor the modified Froude number are satisfactory scaling indicies. The most nearly equivalent flow patterns for different sizes of cavities generally resulted when a compromise was achieved between attempts to obtain a matching Froude number in one case, and a matching Reynold's number in another case.

Several difficult and unusual aspects of conditions in the flowing gas cavity were investigated. For instance, a dust injection test series was run. Such tests would simulate startup conditions in a cold reactor. Also, upside down arrangements, with the exhaust nozzle facing up were tested. This puts the inertial forces in the opposite direction from those in an accelerating space rocket. However, the upside down cases could be used in magnetohydrodynamic applications. In essence, containment of the heavy central gas was excellent in these upside down tests, with the principal problem being how to keep the central gas away from the walls of the cavity.

For the normal downfiring directions, one of the main considerations is the method of dispersing the heavy central gas so that it occupies a large volume of high density within the cavity before it "falls out" the exhaust nozzle. This results from the gravitational effect relative to the light propellant gas flowing around it. One mechanism that was found to be particularly effective was a strong upward recirculation pattern for the outer gas (Figure 4). Such a pattern could be generated by the convergence of the annular gas streams near the outlet nozzle. Such recirculation was most noticeable in the three-dimensional spherical configurations, and was undoubtedly dependent on the shape of the lower part of the cavity. The upward recirculation tended to prevent the heavy center gas from dropping straight to the exit nozzle, and also dispersed the central gas. Since the central gas simulated uranium fuel, this dispersal reduced the self-shielding and enhanced the nuclear reactivity of the system. This dependence of the shape of the lower portion of the cavity on containment that can be obtained with gases of different density is at variance with results reported in Phase I of the study. In those cases, principally two-dimensional studies were performed and mostly on gases of the same density, where the gravitational effect was not of concern.

---

[1] J. C. Bennett and B. V. Johnson, Experimental Study of One- and Two-Component Low-Turbulence Confined Axial Flows, NASA CR-1851 (June 1971).

[2] H. Weinstein et al, Turbulence in the Mixing Region Between Ducted Coaxial Streams, NASA CR-1335 (July 1969)

[3] J. F. Kunze et al., Phase I Topical Report, Flowing Gas, Non-Nuclear Experiments on the Gas Core Reactor, NASA CR-120824, ANCR-1032, Aerojet Nuclear Co. (February 1972).

[4] C. G. Lanzo, A Flow Experiment on a Curved-Porous-Wall-Gas-Core Reactor Geometry, Nuclear Applications and Technology, 8, p. 6 (1970)

[5] J. F. Kunze, G. D. Pincock, R. E. Hyland, Cavity Reactor Critical Experiments, Nuclear Applications, 6, p. 104 (1969)

[6] J. F. Kunze et al., Benchmark Gas Core Critical Experiment, Nuclear Science and Engineering, 47, p. 59 (1972).

Figure 1 Typical 18-in. two-dimensional test cavity configuration.